ON THE INERTIAL STABILITY OF COASTAL FLOWS

by

JAMES ALFRED HELBIG

M. Sc., University of British Columbia, 1977

A THESIS SUBMITTED IN PARTIAL FULFILLMENT OF

THE REQUIREMENTS FOR THE DEGREE OF

DOCTOR OF PHILOSOPHY

in

THE FACULTY OF GRADUATE STUDIES

(Department of Physics and Institute of Oceanography)

We accept this thesis as conforming

to the required standard

THE UNIVERSITY OF BRITISH COLUMBIA

November, 1978

In presenting this thesis in partial fulfillment of the requirements for an advanced degree at the University of British Columbia, I agree that the Library shall make it freely available for reference and study. I further agree that permission for extensive copying of this thesis for scholarly purposes may be granted by the Head of my Department or by his representatives. It is understood that copying or publication of this thesis for financial gain shall not be allowed without my written permission.

Institute of Oceanography and
Department of Physics

The University of British Columbia
2075 Wesbrook Place
Vancouver, British Columbia
V6T 1W5
Canada

Date 27 December 1978

Abstract

This thesis investigates two separate but related problems. In Part I a study is made of the propagation of continental shelf waves and barotropic Rossby waves in a steady, laterally sheared current of the form $V + \varepsilon W$, where W is a centred random function and $\varepsilon << 1$. If the correlation length of W is small compared with the characteristic horizontal length scale of the system; for example, the shelf width or a channel width, the waves are unstable. Their growth rate is largely determined by the magnitude of the correlation length, while the phase speed is given by the sum of weighted averages of the mean current V and the lateral gradient of potential vorticity. Application of the theory to the Brooks and Mooers (1977a) model of the Florida Straits yields wave parameters that are in accord with those measured by Düing (1975).

In Part II, an attempt is made to understand the dynamics governing observed low-frequency currents in the Strait of Georgia (GS). A simple two-layer model indicates that the mean currents in GS are probably baroclinically stable. A barotropic stability model implies that a shear instability might be of some importance. However, the analysis of current meter data shows that the velocity components of the fluctuations are either nearly in phase or close to 180° out of phase; this means that the motions are not due to the type of waves considered here. Analysis of the relationship between the winds and currents in both the frequency and time domains implies that the wind may play an indirect role in forcing GS motions.

It is conjectured that the wind and tide interact with the Fraser River outflow to modulate the estuarine circulation in the system and force low-frequency currents. Direct nonlinear interaction between tidal constituents produces a coherent fortnightly variation in the currents, but cannot account for the observations.

TABLE OF CONTENTS

LIST OF TABLES

Table

LIST OF FIGURES

ACKNOWLEDGEMENT

Many people contribute to a thesis. My foremost gratitude goes to Professor L. A. Mysak for his steady encouragement, persistent interest, proficient advice, and, most of all, his inordinate patience and kindness. I would also like to thank Professors G. L. Pickard, P. H. LeBlond, and G. S. Pond for their criticisms of an earlier version of this thesis. Each found a specific area that needed clarification or further development. My warmest appreciation extends to Dr. P. B. Crean for allowing me free access to the results of the numerical model of the Juan de Fuca-Strait of Georgia system; Mr. P. J. Richards was most helpful in making these results accessible to me. Dr. Crean also requires recognition for encouragement of a more moral nature. I would also like to thank Dr. J. A. Stronach for many useful conversations and for providing me with some results of his work. Mr. P. Y. K. Chang demands special thanks for allowing me use of his edited versions of wind and current data, and for providing me with enlarged copies of many of the figures in his thesis.

Above all, I must register my most heartfelt appreciation to my wife, Nelia, for her sacrifices during my long tenure as a graduate student and for her constant understanding and thoughtful advice. I want to thank her and my daughter Erika for the consideration extended to me during the final stages of this thesis. Finally, I express my gratitude to my parents for their constant faith in me.

Much appreciated financial support has been provided by the National Research Council of Canada and the University of British Columbia.

1. Introduction to Thesis

Two separate but related problems in physical oceanography are examined in this thesis. In Part I, the inertial instability of currents which contain a small, randomly fluctuating component is examined. While this is primarily a theoretical investigation, the theory is applied to observations made in the Florida Straits with encouraging results. The latter part of this thesis summarizes an attempt to understand the low-frequency currents observed in the Strait of Georgia. To this end, inertial instability, wind forcing, residual tidal flow, and modified estuarine circulation are considered. Separate, more detailed, introductions are provided for each part.

2. Introduction to Part I

Under certain conditions a planetary wave propagating through a region of mean current shear is capable of extracting energy from the flow. This was pointed out in the pioneering work of Kuo (1949) for Rossby waves in a zonal current. In particular, he showed that an extremum in the potential vorticity distribution was a necessary condition for the existence of unstable waves. Since then, numerous models of unstable flows on a β-plane have been considered, particularly for the atmosphere (see the review by Kuo, 1973). By comparison, scant attention has been paid to the study of the modification of another class of planetary motions, namely continental shelf waves (CSWs), by sheared mean flows, although the theory of CSWs in the absence of mean currents has been extensively investigated (see LeBlond and Mysak, 1977, for a review). Since mean coastal flows always exist, this represents a serious gap in our knowledge of continental shelf dynamics.

Niiler and Mysak (1971) considered a step-like continental shelf and a piecewise linear velocity profile and showed the existence of two classes of motions, modified CSWs and "shear" waves whose existence depends on the mean current shear. For a certain short wavelength range, the two modes coalesce into a single unstable wave travelling in the direction of the current. In a more formal study Grimshaw (1976) extended many of the results of barotropic instability theory to include unstable CSWs for quite general depth and velocity profiles. McKee (1977) has calculated the stable response of the continental shelf to travelling atmospheric disturbances and showed that it is comprised of a superposition of discrete

normal modes, a continuous set of transient solutions possessing phase speeds in the range of the mean current, and directly forced motions. Brooks and Mooers (1977a, hereinafter referred to as BrM), in a model of the Florida Straits, considered the effect of an intense, laterally sheared current on CSWs, but they evidently did not search for any possible unstable solutions. Thus they were limited to modified CSWs with phase velocities less than the minimum of the mean current velocity. It should be mentioned, though, that Schott and Düing (1976) found excellent agreement between BrM model predictions and observations in the Florida Straits for the 10-30-day wave period band.

In Part I we consider the barotropic stability of (1) an alongshore current and (2) a zonal flow with respect to CSW and Rossby wave perturbations, respectively. In each case the basic current is assumed steady and to be composed of a sheared mean component with a small, spatially random part superimposed upon it. Although this choice might seem to further complicate an already difficult mathematical problem, it turns out that the mathematics greatly simplifies, and the problem may be easily solved provided that the correlation length of the fluctuating current is sufficiently small. This approach was adopted by Manton and Mysak (1976) for the case of plane Couette flow, and Part I is an outgrowth of that work.

The rationale for choosing a random current is as follows. The small-scale features of the basic current are generally unknown and certainly vary in both space and time. Moreover, these features make the basic current profile so complicated as to render a description of the flow by a simple mathematical expression impossible. Thus it is reasonable to model the current by the sum of a smooth, deterministic profile and a small

irregular part. It is mathematically convenient to represent the irregular component as a random function. Thus we ignore the actual, small-scale structure of the current profile and concentrate on its statistical properties, in particular, its variance.

If this decomposition is to be physically realistic, it is necessary that the "random" features of the basic current be distinct from the motions predicted by the ensuing theory, since these motions are due, in large part, to the basic flow. This requires that the "waves" admitted by this theory be separated in both frequency and wavenumber space from the random component of the basic current. That is, there must be a spectral gap or rapid change in slope in the velocity spectra. Unfortunately, adequate data is not presently available to test validity of this representation.

As a first step in a more extensive study, we concentrate solely on the lateral spatial variations and henceforth ignore temporal fluctuations in the basic flow. In the case of the Florida Current, to which the theory developed here will be applied, the decomposition of the flow into deterministic and random components is especially appropriate, since in the region of the Florida Straits, the current is still adjusting to an almost 90° northward turn in its passage around the southern tip of Florida. This is a process which should introduce a large amount of noise into the flow.

The assumption that the superimposed wave field is barotropic in the frequency range of interest is supported experimentally by observations in both an intense western boundary current (Düing, 1975; Mooers and Brooks, 1977) and in a weak eastern boundary current (Huyer, et al., 1975; Kundu and Allen, 1976; Wang and Mooers, 1977). In a theoretical analysis,

Allen (1976) has shown that the continental shelf may support both barotropic and baroclinic motions, the latter trapped within an internal Rossby radius of deformation of the coast. We expect this assumption to be more questionable for Rossby waves in the open ocean where baroclinic instability is likely to be an important factor. Nevertheless, the present theory represents a first step in a study of combined barotropic-baroclinic instability in a randomly perturbed flow.

Two continental shelf models are considered, one in which the shelf is bounded by a wall parallel to the coast (channel model), and one in which it is not (shelf model). In both cases the BrM model of bottom topography and mean current is employed. Attention is primarily focused on the channel model since the observations to which the theory is to be compared were made in the Florida Straits. This model also has the added convenience of being less complex mathematically since the coastal trapped motion is isolated from the ocean interior and thus no coupling need be considered. A channel model is also assumed in the Rossby wave case.

Each of the two continental shelf models admits a class of unstable modified CSWs for long wavelengths provided that the horizontal correlation length of the fluctuating basic flow is sufficiently short compared with the shelf width. These waves may propagate in either direction along the coast depending on the strength of the mean current; their phase velocity is given by the weighted average of the difference between the mean velocity and the cross-stream gradient of potential vorticity. The growth rate is proportional to the amplitude of the random component of the current and inversely proportional to its correlation length. The fact that unstable solutions exist is especially important since the BrM velocity profile is almost certainly barotropically stable; that is, the

classical theory predicts the existence only of stable modified CSWs. Application of the channel model to the Florida Straits predicts wave parameters that are in good agreement with observations made by Düing (1975). The present theory may thus account, in part, for meanders observed in the Florida current.

The plan of Part I is as follows. In Section 3 the formal theory for modified CSWs in a channel is presented, and a complicated integro-differential equation is derived for the mass-transport stream function. Scaling arguments are employed to reduce this equation to a more manageable form. A more physical derivation of this equation based on the balance of vorticity in the system is given in Section 4. An energy equation is also derived. A perturbation solution is obtained in Section 5 for the BrM model, and the basic results for the growth rates and phase speeds are given. The results are applied to observations made in the Florida Straits. In Section 6, we briefly consider the continental shelf model, and in Section 7 the stability of a zonal flow on a β-plane to Rossby wave perturbations is examined. A summary is given in Section 8.

3. Formal Theory for Shelf Waves in a Channel

In this section the equations governing the propagation of small-amplitude, free, modified CSWs in a laterally sheared, barotropic current are derived. The basic current is assumed to flow along a continental boundary of infinite length and is composed of a sheared mean component and a small spatially random part. Only the channel model is treated here; consideration of the shelf model is deferred to Section 6.

The dynamics of CSWs derive from the conservation of potential vorticity, but rather than to proceed directly from the conservation law, it proves convenient for later purposes to begin with the equations of motion. It is also desirable to work in terms of nondimensional quantities and the following scale factors which are representative of continental shelf conditions are chosen: the shelf width L (which may be less than the channel width, see Figure 5.1) for the horizontal coordinates (x,y), the maximum channel depth H for z, a vertically averaged velocity U for the horizontal velocities (u,v), an advective time L/U, and fLU/g for the sea surface elevation. Here f is the Coriolis parameter and g is the acceleration due to gravity. A basic state which exactly satisfies the nonlinear, frictionless equations of motion is specified by the basic current $V_B(x)$ and is related to the basic sea surface slope by

$$V_B(x) = \eta_{Bx}(x). \tag{3.1}$$

The shallow-water equations of motion linearized about the basic state are:

$$Ro(u_t + V_B u_y) - v = -\eta_x \tag{3.2}$$

$$Ro(v_t + V_B v_y + uV_{Bx}) + u = -\eta_y \tag{3.3}$$

$$(hu)_x + h(v)_y = 0. \tag{3.4}$$

Here $h(x)$ is the nondimensional depth and $Ro = U/fL$ is the Rossby number for the basic flow and is not assumed small. To obtain (3.4) we invoked the nondivergent approximation, which is good to order f^2L^2/gH (10^{-3} in Florida Straits), and this allows the definition of a mass-transport stream function given by

$$\left.\begin{aligned} hu &= -\Psi_y \\ hv &= \Psi_x \end{aligned}\right\}. \tag{3.5}$$

In terms of Ψ the linearized potential vorticity equation is

$$Ro(\partial_t + V_B\partial_y)[h^{-1}\nabla^2\Psi - (h'/h^2)\Psi_x]$$

$$- \Psi_y[Roh^{-1}V''_B - (1 + RoV'_B)h'/h^2] = 0 \tag{3.6}$$

where a prime denotes differentiation with respect to x. For travelling wave disturbances of the form

$$\Psi = \Phi(x)e^{ik(y-ct)} \tag{3.7}$$

with positive k and possibly complex phase speed c, (3.6) reduces to

$$(V_B - c)\mathcal{D}\Phi - \hat{Q}_x\Phi = 0. \tag{3.8}$$

Here $\mathcal{D} = h^{-1}d^2/dx^2 - (h'/h^2)d/dx - h^{-1}k^2$ so that $\mathcal{D}\Phi$ is the relative vorticity of the perturbation and

$$\hat{Q} = (Ro^{-1} + V'_B)/h \tag{3.9}$$

is the basic state potential vorticity scaled by Ro. The boundary conditions are obtained by requiring that there be no flow through the sidewalls; hence

$$\Phi(x) = 0 \quad \text{at} \quad x = 0,\ell. \tag{3.10}$$

As the basic current is taken to be a stationary random variable, it may be separated into its mean and fluctuating parts as

$$V_B(x) = V(x) + \varepsilon W(x)$$

such that $E(V_B) = V$ and $E(W) = 0$ where E represents the average over an ensemble of realizations of W. The nondimensional parameter ε is assumed to be small and is related to the variances of V_B and W by

$$\varepsilon^2 = \text{var } V_B/\text{var } W. \tag{3.11}$$

In the present case we choose var W = 1 although a different choice will be made for the shelf model. Since the basic state is random and the disturbance interacts with it, it necessarily follows that the perturbation must also contain a random component; we decompose Φ as

$$\Phi(x) = \psi(x) + \varepsilon\phi(x) \tag{3.13}$$

with $E(\psi) = \psi$ and $E(\phi) = 0$. Although it is not necessary to scale the random part of Φ by ε, ψ will generally be large compared with $\varepsilon\phi$.

We are primarily concerned here with deriving a closed form equation for ψ. With these definitions the vorticity equation may be cast into the form

$$(L + \varepsilon M)(\psi + \varepsilon\phi) = 0, \tag{3.14}$$

where L and M are deterministic and random differential operators respectively defined by

$$L = (V - c)\mathcal{D} - Q_x \tag{3.15}$$

$$M = w\mathcal{D} - q_x \; ; \tag{3.16}$$

Q_x and q_x are the respective gradients of mean and fluctuating potential vorticity (scaled by Ro),

$$Q_x = h^{-1}V'' - (Ro^{-1} + V')h'/h^2 \tag{3.17}$$

$$q_x = h^{-1}W'' - W'h'/h^2. \tag{3.18}$$

The boundary conditions become

$$\left.\begin{aligned}\psi &= 0\\ \phi &= 0\end{aligned}\right\} \text{ at } x = 0,\ell. \tag{3.19}$$

Stochastic boundary value problems of the type defined by (3.14)-(3.19) have been investigated by a number of workers, and several techniques are available to deal with them (see Mysak, 1978, for a review). It proves useful to decompose (3.14) into its mean and fluctuating components. By ensemble averaging (3.14) and subtracting the resultant expression from it we obtain as follows:

$$L\psi + \varepsilon^2 EM\phi = 0 \tag{3.20}$$

$$L\phi + M\psi + \varepsilon[M\phi - E(M\phi)] = 0. \tag{3.21}$$

A formal solution of (3.20)-(3.21) was first given by Tatarskii and Gertsenshtein (1963) and is

$$L\psi = -\varepsilon EM \sum_{n=0}^{\infty} [-\varepsilon(1 - E)L^{-1}M]^{n+1}\psi. \tag{3.22}$$

Here 1 is the identity operator and L^{-1} is the operator inverse to L.

The sum in (3.22) is convergent provided that $\varepsilon\|L^{-1}M\| < 1$, where $\|(\cdot)\|$ denotes an appropriate operator norm. This clearly limits the amplitude of the fluctuating part of the basic flow, and it is henceforth assumed that $\varepsilon << 1$. In the present analysis we retain only the first term in (3.22) giving

$$L\psi = \varepsilon^2 E[ML^{-1}M]\psi. \tag{3.23}$$

This constitutes the "first-order smoothing" or "local Born" approximation and is equivalent to ignoring the bracketed terms in (3.21). Howe (1971) has given a clear physical interpretation of this approximation. Essentially, the neglected terms involve the interaction of the fluctuating component of the basic field with the random part of the perturbation at distances exceeding their mutual correlation length, whereas the other terms in (3.20)-(3.21) are determined by the local values of the two fields.

It is convenient to rewrite (3.13) in terms of the Green's function $G(x,\xi)$ for $(V - c)^{-1}L$ which satisfies

$$\mathcal{D}G(x,\xi) - (V - c)^{-1}Q_x G(x,\xi) = \delta(x - \xi)$$

$$G(0,\xi) = G(\ell,\xi) = 0. \tag{3.24}$$

Substitution of (3.15) and (3.16) into (3.23) and expression of L^{-1} in terms of $G(x,\xi)$ results in an integro-differential equation for ψ,

$$[(V - c)^2 - \varepsilon^2 R(0)]\mathcal{D}\psi - (V - c)Q_x\psi - \varepsilon^2 h^{-1}[(h'/h)R'(0)$$

$$- R''(0)]\psi = \varepsilon^2 Q_x \int_0^{\ell} (V - c)^{-1} G(x,\xi)[R(x - \xi)\mathcal{D}\psi$$

$$- (h'/h^2)R'(x - \xi)\psi - h^{-1}R''(x - \xi)\psi]d\xi$$

$$+ \varepsilon^2 (h'/h^2)(V - c) \int_0^{\ell} (V - c)^{-1} G(x,\xi)[R'(x - \xi)\mathcal{D}\psi$$

$$- (h'/h^2)R''(x - \xi)\psi - h^{-1}R'''(x - \xi)\psi]d\xi$$

$$- \varepsilon^2 h^{-1}(V - c) \int_0^{\ell} (V - c)^{-1} G(x,\xi)[R''(x - \xi)\mathcal{D}\psi$$

$$- (h'/h^2)R'''(x - \xi)\psi - h^{-1}R^{iv}(x - \xi)\psi]d\xi. \qquad (3.25)$$

Here the correlation function $R(\xi)$ is defined as $R(\xi) = E[W(x)W(x + \xi)]$. This equation also holds for the shelf model if the upper limit of integration is extended to infinity. For the channel model we assume that W is a homogeneous random function so that $R'(o)$ vanishes; further, we choose $R(o) = 1$ and define $\sigma^2 = - R''(o)$. Then $1/\sigma$ is representative of the nondimensional correlation length L_c/L of the fluctuating current. (In fact, $R''(o) = - 2/\lambda^2$ for a Gaussian process described by $R(\xi) = \exp(-\xi^2/\lambda^2)$.)

Certainly, (3.25) is much too complex to be dealt with directly, and, indeed, $G(x,\xi)$ will generally be unknown analytically, expressing our inability to solve the associated deterministic problem. Hence some approximate analysis must be adopted, and it clearly would be advantageous

to eliminate the integral terms in (3.25). We will presently demonstrate that the rhs of (3.25) is an order of magnitude smaller than the lhs and thus, to a first approximation, may be ignored. It is shown in Appendix A that all the integrals in (3.25) are of $O(1)$ provided that $R(x)$ and its derivatives are also $O(1)$. Hence, away from the singular points of the equation where $V = c \pm \varepsilon$, the rhs of (3.25) is $O(\varepsilon^2)$ and is thus negligible compared with the lhs which contains terms of $O(1)$ (and also terms of $O(\varepsilon^2)$). Near the singular points, however, the analysis is considerably more complicated, but we claim that either Q_x or that both ψ and $G(x,\xi)$ are $O(\varepsilon)$ there and hence that the rhs of (3.25) may be safely neglected. To see this, consider the limiting case of $\varepsilon = 0$ for which (3.25) reduces to

$$(V - c)\mathcal{D}\psi - Q_x\psi = 0. \tag{3.26}$$

Since (3.26) must hold pointwise it follows that there are two possibilities at points x_c where $V(x_c) = c$ which must be considered. Either the gradient of potential vorticity Q_x or the cross-stream velocity ψ vanishes there. We disregard the third possibility of solutions with singular derivatives (that is, those corresponding to a vortex sheet at $x = x_c$) for two reasons. First, McKee (1977) has demonstrated for stable mean velocity profiles that, in this case, c belongs to the continuous part of the eigenvalue spectrum of L and the corresponding eigenfunction represents only a transient component of the complete solution. McKee's arguments are readily extended to cases with unstable velocity profiles. Second, and more importantly, Lin (1961) has elegantly demonstrated that the inclusion of a small amount of (molecular or eddy) viscosity precludes

the existence of a continuous spectrum. That is, in the limit of vanishing friction, the singular solutions of the inviscid theory are not obtained as limits of viscid solutions.

Now if ε is sufficiently small, it follows that at a distance ε away from $V = c$, either Q_x or ψ is of $0(\varepsilon)$. A similar argument shows that in the latter case $G(x,\xi)$ is also $0(\varepsilon)$: at $x = x_c$ and away from $\xi = x_c$, the rhs of (3.24) vanishes and hence so does $G(x_c,\xi)$ since Q_x is nonzero by assumption. As $G(x,\xi)$ is a continuous function of x and ξ, it follows that $G(x_c, x_c) = 0$. We again argue that at a distance ε from $x = x_c$, $G(x, \xi)$ is $0(\varepsilon)$. (The above comments concerning the continuous spectrum of L also imply that we may exclude the possibility of $G(x,\xi)$ having singular derivatives at $x = x_c$, $\xi \neq x_c$; see McKee, 1977.)

Consider the first case in which $Q_x = 0(\varepsilon)$; then the terms on the lhs of (3.25) are all $0(\varepsilon^2)$ while those on the rhs are $0(\varepsilon^3)$. In the second case, where ψ and G are $0(\varepsilon)$, the first three terms on the lhs are $0(\varepsilon^2)$ and all the remaining terms in (3.25) are $0(\varepsilon^3)$. Hence in all cases the lhs contains terms at least $0(\varepsilon^{-1})$ greater than the rhs which may thus be ignored. An entirely analogous argument holds if c is complex with a small imaginary part. We are therefore led to the consideration of the simplified equation

$$[(V - c)^2 - \varepsilon^2]\mathcal{D}\psi - (V - c)Q_x\psi - \varepsilon^2\sigma^2 h^{-1}\psi = 0, \tag{3.27}$$

which is subject to the boundary conditions (3.19). A more physical derivation of (3.27) is given in the next section.

In the analysis presented in the following sections, approximate

solutions are obtained for the case of large σ. Thus one of the assumptions made in the preceding scaling argument is violated, namely that $R(x)$ and its first four derivatives are all $O(1)$. An evaluation of the relative sizes of the terms in the analogue of (3.25) for a zonal random flow on a β-plane is made in Appendix C. It turns out that the integral terms are generally smaller than the other terms, although in some cases they are of similar magnitude for certain regions of the channel. As k increases and σ decreases, the neglect of these terms is better justified. Thus σ must be large enough to permit a perturbation expansion but not so large that the integral terms become overly significant. In the latter case, the solutions obtained in this thesis are best regarded as approximations to the first iterative solution of the full integro-differential equation. Of course, if σ is not large, then the integral terms may be safely ignored to a good approximation.

Comparison of (3.27) with the corresponding equation for the deterministic case (3.26) shows that the randomness of the basic current manifests itself in two ways. First, the single critical point of (3.26) at $V = c$ is bifurcated into the pair $V = c \pm \varepsilon$. In any given realization of V_B, there would no doubt exist numerous points at which $c = V + \varepsilon W$ (provided that c is real), and this is expressed, in the mean, by the existence of two points each removed by the rms value of εW from $V = c$. The second effect appears in the term $\varepsilon^2\sigma^2 h^{-1}\psi$ and depends not only on the strength of the fluctuating current but also on its correlation length. The physical significance of this term is more fully discussed in the next section where the vorticity balance is considered.

4. The Vorticity and Energy Balances

In this section the various vorticity and energy balances present in the system are examined. Consider first (3.20) and (3.21) rewritten in a more explicit form.

$$(V - c)\mathcal{D}\psi - Q_x\psi + \varepsilon^2 E[W\mathcal{D}\phi] - \varepsilon^2 E[q_x\phi] = 0 \tag{4.1}$$

$$(V - c)\mathcal{D}\phi - Q_x\phi + W\mathcal{D}\psi - q_x\psi = -\varepsilon(W\mathcal{D}\phi - E[W\mathcal{D}\phi]). \tag{4.2}$$

To an observer moving with the wave speed, the terms in (4.1) correspond respectively to: (1) alongshore advection of mean disturbance vorticity $\mathcal{D}\psi$ by the mean basic flow, (2) cross-stream advection of mean basic vorticity by the mean disturbance, and the correlated parts of (3) advection by the fluctuating basic flow of the random disturbance vorticity $D\phi$, and (4) the cross-stream advection of random basic vorticity by the fluctuating disturbance. Similarly, the terms in (4.2) are interpreted as: (1) advection by the mean basic flow of fluctuating disturbance vorticity, (2) advection of mean basic vorticity by the random disturbance, (3) advection of mean disturbance vorticity by the random basic flow, (4) cross-stream advection by the mean disturbance of fluctuating basic vorticity, and (5) the alongshore advection of random disturbance vorticity by the fluctuating basic current. The last term in (4.2) is the only one quadratic in the random fields and thus might be expected to be small. In fact, it consists of the difference of the total advection of $\mathcal{D}\phi$ by W and that part of $W\mathcal{D}\phi$ which is correlated. Since it primarily involves

the interaction of the two fields at distances exceeding their mutual correlation length, it plays an insignificant role in the vorticity balance expressed by (4.2) and is henceforth neglected.

We now consider the relative magnitudes of the various terms in (4.1) and (4.2) and give a heuristic derivation of (3.27). Substitution of $\mathcal{D}\phi$, as determined by (4.2), into (4.1) yields the analogue of (3.25),

$$(V - c)\mathcal{D}\psi - Q_x\psi - \varepsilon^2(V - c)^{-1}\mathcal{D}\psi - \varepsilon^2\sigma^2 h^{-1}(V - c)^{-1}\psi$$

$$+ \varepsilon^2 Q_x(V - c)^{-1}E[W\phi] - \varepsilon^2 h^{-1}E[W''\phi] + \varepsilon^2(h'/h^2)E[W'\phi] = 0. \quad (4.3)$$

In order to determine the magnitudes of ϕ and $\mathcal{D}\phi$, we use the expression

$$\phi(x) = -\int_0^{\ell} (V - c)^{-1} G(x,\xi)[W\mathcal{D}\psi - q_x\psi]d\xi \quad (4.4)$$

which is obtained from (3.21) in the local Born approximation. Consider now the cases examined in the preceding section corresponding to $(V - c) = O(1)$ and $V - c = O(\varepsilon)$. (If c is complex with small imaginary part, then the latter case is equivalent to $V - c_r = O(\varepsilon)$, and $c_i = O(\varepsilon)$.) The results are summarized in Table I. In the first case the random fields play an insignificant role in the balance of mean vorticity, and $\mathcal{D}\psi$ exceeds $\varepsilon\mathcal{D}\phi$ by an order of magnitude. On the other hand, the alongshore advection of fluctuating disturbance vorticity by the random basic flow (4.1, term 3) is important in the last two cases, but the cross-stream advection of the random background vorticity by the fluctuating disturbance (4.1, term 4) remains unimportant. Near the critical point the random component of

Table I. Order of magnitude estimates of terms in the vorticity balance equations. The rhs of (4.2) is neglected, and the magnitudes of ϕ and $\mathcal{D}\phi$ are calculated from (4.4).

A. $V - c = O(1)$	(4.1)	1	1	ε^2	ε^2			
$\mathcal{D}\psi, \psi = O(1)$	(4.2)	1	1	1	1			
$\mathcal{D}\phi, \phi = O(1)$	(4.3)	1	1	ε^2	ε^2	ε^2	ε^2	ε^2
B. $V - c = O(\varepsilon)$								
$Q_x = O(\varepsilon)$	(4.1)	ε	ε	ε	ε^2			
$\mathcal{D}\psi, \psi, \phi = O(1)$	(4.2)	1	ε	1	1			
$\mathcal{D}\phi = O(1/\varepsilon)$	(4.3)	ε	ε	ε	ε	ε^2	ε^2	ε^2
C. $V - c = O(\varepsilon)$								
$\psi, \phi = O(\varepsilon)$	(4.1)	ε	ε	ε	ε^3			
$\mathcal{D}\psi = O(1)$	(4.2)	1	ε	1	ε			
$\mathcal{D}\phi = O(1/\varepsilon)$	(4.3)	ε	ε	ε	ε^2	ε^2	ε^3	ε^3

disturbance vorticity $\varepsilon\mathcal{D}\phi$ is the same order of magnitude as the mean component, although $\varepsilon\phi$ remains small. Thus the fluctuating vorticity tends to concentrate near points where $V - c$ is small. In all cases, the last three terms in (4.3) may be disregarded, and hence (4.3) reduces to (3.27). Note that neglect of these terms in no way requires the correlations between ϕ and its derivatives to be small, as suggested by Manton and Mysak (1976).

An energy equation for the mean component of the perturbed field is now derived. It is easiest to proceed directly from the nonaveraged equations of motion (3.2) - (3.4) and then to average the resulting expression. In the usual fashion we take the scalar product of the momentum equations with $\underline{u}$ to obtain

$$(h/2)(u^2 + v^2)_t + (h/2)V_B(u^2 + v^2)_y$$

$$= - V'_B huv - Ro^{-1}h(u\zeta_x + v\zeta_y). \tag{4.5}$$

An integration over the region R defined by the channel width and one wavelength in the y-direction with application of the boundary conditions and the assumed periodic nature of the disturbance gives

$$(\partial/\partial_t) \int_R (h/2)(u^2 + v^2) = \int_0^{\ell} V'_B(x)\tau_{12}dx. \tag{4.6}$$

Here the Reynolds stress τ_{12} is defined by

$$\tau_{12} = - \int_y^{y+\lambda} huvdy. \tag{4.7}$$

Thus if a wave is unstable, the Reynolds stress must extract kinetic energy from the shear of the basic current.

By expressing the real quantities u, v and τ_{12} in (4.6) in terms of the deterministic and random components of the stream function (3.7), and by ensemble averaging the resultant expression we find,

$$\Omega \int_0^{\ell} h^{-1}(|\psi'|^2 + k^2|\psi|^2)dx$$

$$+ \varepsilon^2\Omega \int_0^{\ell} h^{-1}(|\phi'|^2 + k^2|\phi|^2)dx$$

$$= + k \int_0^{\ell} h^{-1}V'F(\psi_R,\psi_I)dx + \varepsilon^2 k \int_0^{\ell} h^{-1}V'E[F(\phi_R,\phi_I)]dx$$

$$+ \varepsilon^2 kE \int_0^{\ell} h^{-1}W'\mathrm{Im}F(\psi^*,\phi)dx. \qquad (4.8)$$

Here the subscripts R and I (or r and i) refer to the real and imaginary parts of a quantity, $\Omega = kc_i$ is the growth rate of the disturbance, and $F(f,g) = fg' - f'g$ is the Wronskian of f and g. The full Reynolds stress assumes the form

$$\tau_{12} = (k/2h)[F(\psi_R,\psi_I) + F(\phi_R,\phi_I) + \mathrm{Im}F(\psi^*,\phi)]. \qquad (4.9)$$

The interpretation of (4.8) is direct and is not pursued here; however, we note that it is not energy conserving since no provision was made for the modification of the basic field which therefore acts as an infinite reservoir of energy for the disturbance.

It is not clear how to approximate (4.8) in order to obtain an equation consistent with (3.27); i.e., it is difficult to transfer scaling

arguments from the vorticity domain to the energy domain. To avoid this problem we form another energy equation from (3.27) rewritten as

$$(V - c)\mathcal{D}\psi - \varepsilon^2(V - c)^{-1}\mathcal{D}\psi - Q_x\psi - \varepsilon^2\sigma^2 h^{-1}(V - c)^{-1}\psi = 0. \qquad (4.10)$$

Multiplication of (4.10) by ψ^* and integration over the channel width yields an expression whose imaginary part is

$$\Omega \int_0^{\ell} h^{-1}(|\psi'|^2 + k^2|\psi|^2)dx = k \int_0^{\ell} h^{-1}V'F(\psi_R,\psi_I)dx$$

$$+ \varepsilon^2 k \int_0^{\ell} \frac{[(V - c_r)^2 - c_i^2]}{h|V - c|^4} V'F(\psi_R,\psi_I)dx$$

$$+ \varepsilon^2\Omega \int_0^{\ell} \frac{(V - c_r)V'|\psi'|^2}{h|V - c|^4} dx + \varepsilon^2\sigma^2\Omega \int_0^{\ell} \frac{|\psi|^2}{h|V - c|^2} dx$$

$$- \varepsilon^2\Omega \int_0^{\ell} \frac{|\psi'|^2 + k^2|\psi|^2}{h|V - c|^2} dx. \qquad (4.11)$$

A careful comparison of (4.8) and (4.11) with particular regard to the form of ϕ as given by (4.4) reveals that terms 1 and 2 in (4.11) correspond exactly to terms 1 and 3 in (4.8), and that terms 3 and 4 and terms 5 and 6 in (4.11) represent terms 4 and 5 in (4.8), respectively. In the case of large σ, which will be considered later, it is clear from (4.11) that the energy source for the unstable perturbation is the shear of the random part

of the basic flow.

One could proceed, at this point, to derive the equivalents of the formal relationships developed by Grimshaw (1976). These concern necessary conditions for instability and bounds to growth rates and phase speeds. It is sufficient here to derive only a generalized Rayleigh condition for instability. Rather than use the techniques employed by Grimshaw, since they are tedious in the present case, we proceed from the unaveraged Rayleigh condition

$$c_i \int_0^{\ell} \left| \frac{\Phi}{V_B - c} \right|^2 \hat{Q}_x dx = 0. \tag{4.12}$$

This relationship is the imaginary part of the expression obtained by multiplying (3.26) by $\psi^*/(V - c)$ and integrating over the channel width. If a system is unstable $(c_i \neq 0)$, the integral must vanish. This implies that $\hat{Q}_x$ must vanish at least once in the interval $(0,\ell)$. To generalize (4.12), we express Φ in terms of ψ and ϕ and expand $(V_B - c)^{-1} = (V - c + \varepsilon W)^{-1}$ in a binomial series. Ignoring triple correlations in the ensemble average of the resultant expression we obtain to $0(\varepsilon^3)$

$$c_i \int_0^{\ell} Q_x \left| \frac{\psi}{V - c} \right|^2 dx$$

$$+ \varepsilon^2 c_i \int_0^{\ell} \left\{ \frac{Q_x}{|V - c|^2} E[|\phi|^2] - \frac{2Q_x(V - c_r)}{|V - c|^4} E[W\mathrm{Re}(\psi\phi)] \right.$$

$$\left. + \frac{E[W''\mathrm{Re}(\psi\phi)]}{h|V - c|^4} + \frac{2\sigma^2|\psi|^2(V - c_r)}{h|V - c|^4} \right\} dx = 0. \tag{4.13}$$

In the limit of large σ (i.e., $\varepsilon^2\sigma^2 = 0(1)$), this reduces to

$$c_i \int_0^{\ell} \left|\frac{\psi}{V - c}\right|^2 \left\{Q_x + \frac{2\varepsilon^2\sigma^2(V - c_r)}{|V - c|^2}\right\} dx = 0 \qquad (4.14)$$

Equation (4.14) shows that instability does not demand that the mean potential vorticity distribution vanish, since the random part of the basic flow may possess sufficient relative vorticity to render the basic flow unstable. In this sense, the instability described more fully in the next section is essentially a shear instability. In more physical terms, the random component introduces local extrema into the potential vorticity distribution (i.e., points at which $\hat{Q}_x = 0$). Lin (1945) has demonstrated that the existence of such points is necessary for instability; otherwise a particle displaced from its equilibrium position will always be subject to a net restoring force. As σ increase, the relative vorticity associated with the random flow increases and therefore so does the likelihood of finding local maxima and minima in $\hat{Q}$.

If $c_i \neq 0$ and $Q_x > 0$ everywhere, (4.14) implies that $(V - c_r) < 0$ somewhere and hence that c_r must lie in the range of the mean current. However, if $Q_x < 0$ everywhere then $(V - c_r) > 0$ somewhere and c_r is simply bounded above by the maximum value of V; unstable waves could then, in principle, propagate against the mean flow.

5. The Channel Model

The boundary value problem defined by (3.27) and (3.19) encompasses all and more of the difficulties inherent in a deterministic, barotropically unstable system, for not only does (3.27) have variable coefficients but it also possesses a pair of singular points at $V(x) = c \pm \varepsilon$. Since $\varepsilon \ll 1$, an obvious approach to (3.27) would be to attempt a perturbation solution in ε. However, the resulting equations would contain all the mathematical difficulties of the nonrandom problem, and the solutions, as interesting as they might be, would represent small deviations from the deterministic solutions. We are interested in a different class of solutions to (3.27) which does not exist in the nonrandom case. If the parameter σ is large (i.e., if the correlation length of W is small) then we may try a perturbation expansion in the limit of $\sigma \to \infty$; we shall show that the resulting solutions are unstable. Hence even though classic barotropic instability theory may indicate a given system to be stable, unstable waves may still exist if there is sufficient "noise" in the mean current.

In order to make the following results more specific, we adopt the Brooks and Mooers (1977a) model of the Florida Straits (Figure 5.1):

$$V = xe^{1-x} \tag{5.1}$$

$$h = \begin{cases} e^{2b(x-1)} & 0 \le x \le 1 \\ 1 & 1 \le x \le \ell, \end{cases} \tag{5.2}$$

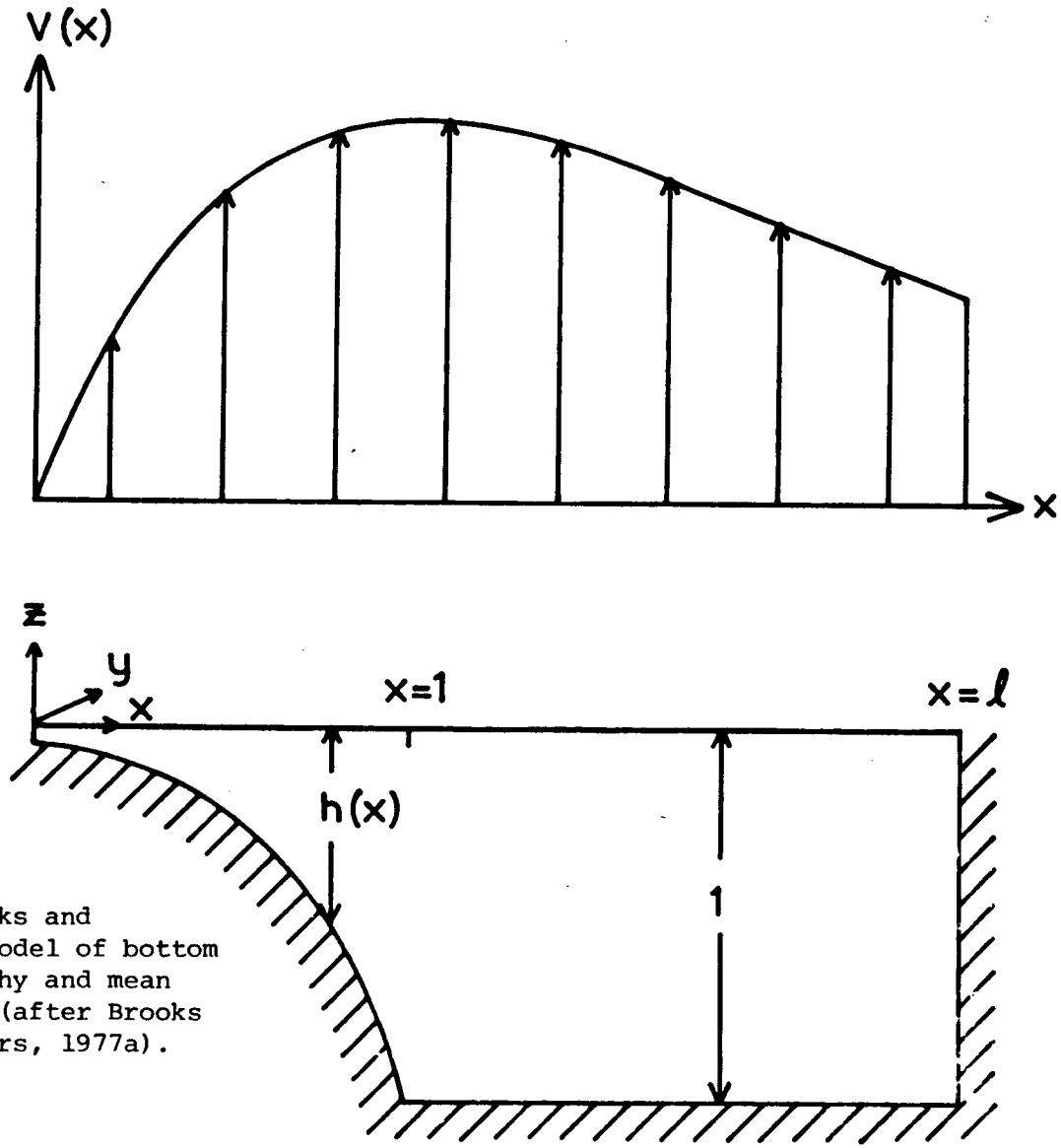

Figure 5.1 The Brooks and Mooers model of bottom topography and mean current (after Brooks and Mooers, 1977a).

with the parameters $b = 1.385$, $\ell = 2.5$ and $Ro = 0.3$. This model is chosen since it employs nontrivial but realistic velocity and bathymetric profiles, and since we wish to apply our results to the Florida Straits. Although V satisfies all the necessary conditions for instability, it is extremely unlikely that this model is unstable as the subsequent argument shows. The Rayleigh condition (4.12) requires that

$$c_i \int_0^{\ell} Q_x |\psi|^2 / |V - c|^2 dx = 0. \tag{5.3}$$

This requirement is usually stated in the form: if $c_i \neq 0$, then Q_x must vanish at least once in the interval $(0,\ell)$. In fact, Q_x does vanish at $x = 2$, but this is not sufficient to ensure that (5.3) is satisfied. A plot of Q_x (Brooks and Mooers, 1977a, Figure 2) shows that it is extremely small in the interval $(2,\ell = 2.5)$ compared with the interval $(0,2)$. This means that $|\psi|$ must be extremely large in the former interval which is not likely as the boundary conditions require $\psi(\ell) = 0$. That is, if (5.3) were satisfied with $c_i \neq 0$, very large alongshore currents trapped against the outer wall would be necessary. With respect to application of the present theory to the Florida Straits, we note, however, that a more realistic bathymetric profile results in a potential vorticity distribution that is probably unstable (Brooks and Mooers, 1977a). Unfortunately, Brooks and Mooers apparently did not search for unstable solutions.

If a perturbation expansion of (3.27) is to lead to nontrivial results, the term $\varepsilon^2\sigma^2 h^{-1}\psi$ must be balanced by another term. For fixed k this requires that c be $0(\sigma)$. It might appear that this could lead

to a contradiction of the semicircle theorem (Grimshaw, 1976) which states that for each realization of the basic flow V_B ,

$$[c_r - 1/2(V_{BM} + V_{Bm})]^2 + c_i^2 \leq [1/2(V_{BM} - V_{Bm}) - 1/2\ c_w]^2$$

where V_{BM} and V_{Bm} are, respectively, the algebraic maximum and minimum values of V_B , and c_w is the phase speed of the first mode CSW in the case of $V_B = 0$. Thus if W is bounded, c is bounded above independent of σ. Hence, once again the magnitude of σ is limited. Nevertheless, we assume that σ is large enough to permit its use as an expansion variable. On the other hand, the values of c_i and c_r computed in this section fall well within the bounds of the semicircle theorem. Moreover, it turns out that successive corrections to c_r and c_i diminish as σ^{-2} not σ^{-1}.

In the following development it is convenient to expand both the real and imaginary parts of c separately; we take

$$\psi = \sum_{m=0}^{\infty} \sigma^{-m}\psi_m \qquad c_r = \sum_{m=0}^{\infty} \sigma^{-m}c_{rm} \qquad c_i = \sigma \sum_{m=0}^{\infty} \sigma^{-m}c_{im}\,. \tag{5.4}$$

The choice of either $c_r = 0(\sigma)$, $c_i = 0(1)$ or $c_r, c_i = 0(\sigma)$ leads only to trivial solutions. The boundary conditions (3.19) become

$$\psi_m = 0 \quad \text{at} \quad x = 0, \ell.$$

If the system under consideration contains discontinuities in the gradient

of potential vorticity, then the equations must be solved in each region and matched across the point of discontinuity. In general, the matching conditions are

$$[\psi] = 0$$

$$[\{(V - c)^2 - \varepsilon^2\}\psi'/h] - [(V - c)Q\psi] = 0 \tag{5.6}$$

where $[(\cdot)]$ represents the jump in $(\cdot)$. Physically, these conditions ensure the continuity of mass flux and sea surface elevation across the discontinuity. Their validity requires that V be continuous. Both h and Q are continuous in the present case and (5.6) reduces to

$$\left.\begin{aligned}[\psi] &= 0\\ [\psi'] &= 0\end{aligned}\right\} \text{ at } x = 1. \tag{5.7}$$

The three lowest order equations are

$$\mathcal{D}\psi_0 + h^{-1}(\varepsilon/c_{i0})^2\psi_0 = 0 \tag{5.8}$$

$$\mathcal{D}\psi_1 + h^{-1}(\varepsilon/c_{i0})^2\psi_1$$

$$= - c_{i0}^{-1}\{2[c_{i1} + i(V - c_{r0})]\mathcal{D}\psi_0 - iQ_x\psi_0\} \tag{5.9}$$

$$\mathcal{D}\psi_2 + h^{-1}(\varepsilon/c_{i0})^2\psi_2 = c_{i0}^{-2}\{(V - c_{r0})^2 - 2c_{i2}c_{i0} - c_{i1}^2 - \varepsilon^2$$

$$- 2i[(V - c_{r0})c_{i1} - c_{i0}c_{r1}]\}\mathcal{D}\psi_0$$

$$- 2c_{i0}^{-1}[c_{i1} + i(V - c_{r0})]\mathcal{D}\psi_1$$

$$- c_{i0}^2 Q_x[(V - c_{r0}) - ic_{i1}]\psi_0 + ic_{i0}^{-1}Q_x\psi_1 \ . \qquad (5.10)$$

The zeroth order equation (5.8) defines a Sturm-Liouville problem for which an infinite number of solutions $\psi_0^{(n)}$ exist such that the nth mode has exactly n zeros, and the corresponding eigenvalues $(\varepsilon/c_{i0}^{(n)})^2$ are ordered and tend to infinity as $n \to \infty$. The superscript (n) is henceforth dropped.

Solutions to (5.8) satisfying both the boundary and jump conditions are given by:

$$\psi_0 = A_0 \begin{cases} e^{b(x-1)} \sin \lambda x/\sin \lambda & 0 \le x \le 1 \\ \sin \alpha(x - \ell)/\sin \alpha(1 - \ell) & 1 \le x \le \ell \end{cases} \qquad (5.11)$$

$$\lambda^2 = \varepsilon^2/c_{i0}^2 - k^2 - b^2 \qquad (5.12)$$

$$\alpha^2 = \varepsilon^2/c_{i0}^2 - k^2 = \lambda^2 + b^2 \qquad (5.13)$$

provided that λ and α satisfy

$$b + \lambda/\tan \lambda = \alpha/\tan \alpha(1 - \ell). \tag{5.14}$$

If λ^2 is negative, the solutions over the shelf are hyperbolic and are obtained by replacing λ with $i\lambda$. For a given choice of k, b, and ℓ, the admissible values of ε/c_{i0} are determined implicitly by (5.14) together with either (5.12) or (5.13). A graphical solution of (5.14) is shown in Figure 5.2 for a case in which hyperbolic solutions are found. The growth rates of the hyperbolic modes, if they exist, exceed those of the trigonometric solutions. For the values of b and ℓ appropriate to the Florida Straits only trigonometric modes are found.

Further information may be extracted from (5.8)-(5.10) without actually solving for ψ_1 and ψ_2. Since these equations all have identical homogeneous parts, the Fredholm alternative implies that ψ_0 must be orthogonal to the respective inhomogeneous terms. We thus obtain

$$c_{i0}^2 = \varepsilon^2/(\lambda^2 + k^2 + b^2) \tag{5.15}$$

$$c_{r0} = \langle V \rangle + (c_{i0}^2/2\varepsilon^2)\langle hQ_x \rangle \tag{5.16}$$

$$c_{i1}, c_{r1} = 0 \tag{5.17}$$

$$c_{i2}c_{i0} = -(3/2)\langle (V - c_{r0})^2 \rangle - \varepsilon^2/2 - (c_{i0}^2/2\varepsilon^2)\langle (V - c_{r0})hQ_x \rangle \tag{5.18}$$

$$- ic_{i0}\langle (V - c_{r0})|\psi_1 \rangle - i(c_{i0}^3/2\varepsilon^2)\langle hQ_x|\psi_1 \rangle$$

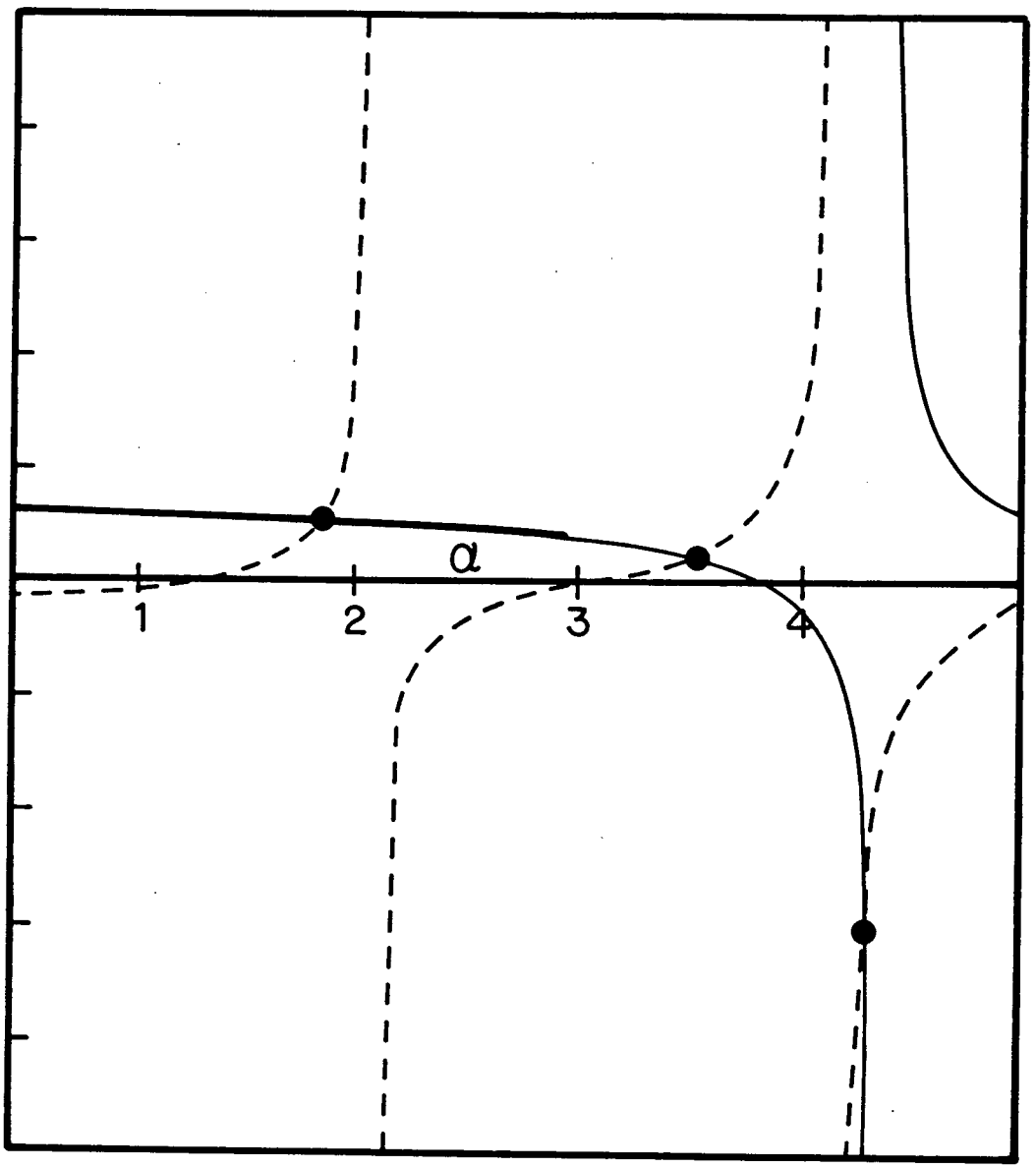

Figure 5.2 Graphical solution of (5.14) for $b = 3.0$ and $\ell = 2.5$. The (light, heavy) solid line is the locus of $b + \lambda/\tan\lambda$ for (real, imaginary) λ, while the dotted line represents $\alpha/\tan\alpha(1 - \ell)$. Intersections with the (light, heavy) line correspond to (trigonometric, hyperbolic) solutions. For Florida Strait parameters ($b = 1.385$, $\ell = 2.5$) the first three solutions are $\alpha_1 = 1.650$, $\alpha_2 = 2.809$, and $\alpha_3 = 3.891$.

where

$$\langle f(x) | g(x) \rangle = \int_0^{\ell} h^{-1}\psi_0(x) f(x) g(x)\,dx \Big/ \int_0^{\ell} h^{-1}\psi_0^{\,2}(x)\,dx \tag{5.19}$$

and

$$\langle f(x) \rangle \equiv \langle f(x) | \psi_0(x) \rangle \tag{5.20}$$

are weighted cross-channel averages. These results are completely general and are not limited to the BrM model. For this model, however, c_{r0} may be rewritten as

$$c_{r0} = \langle V \rangle + \langle hQ_x \rangle / 2(\lambda^2 + k^2 + b^2) \tag{5.21}$$

which is strikingly similar to the expression for a CSW in a constant current $\overline{V}$ over an exponential shelf,

$$c = \overline{V} - 2b/(\lambda^2 + k^2 + b^2) \equiv \langle \overline{V} \rangle + \langle hQ_x \rangle / (\lambda^2 + k^2 + b^2) \tag{5.22}$$

where $hQ_x = -2b$ (cf. Buchwald and Adams, 1968, for the case $\overline{V} = 0$). We see that the weighted average $\langle V \rangle$ replaces $\overline{V}$, while the potential vorticity term in (5.21) is diminished by 1/2. This means that the speed of the Doppler shifted wave $c_{r0} - \langle V \rangle$ is reduced by the presence of random irregularities in the basic current. The explanation is clear: the disturbance must traverse a longer path length in travelling from one point to another since it is buffeted about and scattered by the fluctuating current. This phenomenon is common to wave propagation in random media

(Howe, 1971).

In order to determine c_{i2} it is necessary to first evaluate ψ_1. This is a straightforward, although tedious task, and the complete results are summarized in Appendix B. The solutions in the onshore and offshore regions take the form

$$\psi_1 = \begin{cases} A_{11}\psi_0 + iA_0P_1 & 0 \le x \le 1 \\ A_{12}\psi_0 + iA_0P_2 & 1 \le x \le \ell \end{cases} \tag{5.23}$$

where P_1 and P_2 are particular solutions that satisfy the boundary conditions; the factor of i ensures that P_1 and P_2 are real. These solutions must be matched across $x = 1$, and the matching conditions (5.7) in matrix form are

$$M \begin{bmatrix} A_{11} \\ A_{12} \end{bmatrix} = iA_0 \begin{bmatrix} P_2 - P_1 \\ P'_2 - P'_1 \end{bmatrix} \equiv P \tag{5.24}$$

where

$$M = \begin{bmatrix} \sin\lambda & -\sin\alpha(1-\ell) \\ b\sin\lambda + \lambda\cos\lambda & -\alpha\cos\alpha(1-\ell) \end{bmatrix}, \tag{5.25}$$

and all quantities are evaluated at $x = 1$. However, M is singular,

since in matching the zeroth order solutions we required that $\det M = 0$. If a solution to (5.24) is to exist, it is necessary that P be orthogonal to each linearly independent solution of the associated homogeneous adjoint equation,

$$M^{\dagger}\begin{bmatrix} a_1 \\ \\ a_2 \end{bmatrix} = 0. \tag{5.26}$$

Since M is of rank one, there is only one independent solution of (5.26), and it leads to the auxiliary condition

$$P_2 - P_1 = \alpha^{-1} \tan \alpha(1 - \ell)(P'_2 - P'_1). \tag{5.27}$$

The fulfillment of this restriction was used as a check of the numerical results presented in Figures 5.3-5.7. The one independent equation represented by (5.24) serves to fix A_{12},

$$A_{12} = A_{11} \sin \lambda / \sin \alpha(1 - \ell) - iA_0(P_2 - P_1)/\sin \alpha(1 - \ell), \tag{5.28}$$

but A_{11} remains indeterminate. A careful examination of (5.10) reveals that the part of ψ_1 proportional to ψ_0 does not contribute to c_{i2} and we choose $A_{11} = 0$. Alternatively, A_{11} could be chosen so that ψ_0 and ψ_1 were orthogonal. Similar considerations apply to the higher order eigenfunctions and eigenvalues. Finally, although it is not immediately obvious, one finds that c_{r2n+1} and c_{i2n+1} vanish and that ψ_{2n}/A_0 and ψ_{2n+1}/A_0 are purely real and imaginary quantities, respectively. This

means that successive corrections to c_r and c_i diminish by $O(1/\sigma^2)$.

We now examine the results illustrated in Figures 5.3-5.7 which were computed for the parameters characteristic of the Florida Straits. The dependence of the growth rate $\Omega_1 = k(\sigma c_{i0} + \sigma^{-1} c_{i1})$ on σ for the first mode is shown in Figure 5.3. As σ increases, Ω_1 increases and the wave number range over which it is nonzero widens. There is a threshold value of σ above which unstable waves exist. For mode 1 it lies between $\sigma = 3$ and $\sigma = 4$; for a given k this value decreases with increasing mode number. Figure 5.4a exhibits the dependence of Ω_1 on k for the first three modes. It is particularly interesting that the regions of instability overlap and that for short wavelengths the higher modes may be the more unstable. We note, however, that for large wavenumbers, higher order terms which are neglected here may be significant. The frequencies and phase speeds as functions of k are plotted in Figures 5.5a and 5.6a, respectively, for modes 1-3. The most striking feature in them is the existence of points where the curves intersect, which implies the possible existence of a "resonance" interaction (this potentially was also inherent in the Couette flow model of Manton and Mysak, 1976, for which the phase speed was constant and equal for all modes; see Section 7). It has been documented in the literature (see Mysak, 1978) for a variety of physical systems, that modes which are uncoupled in the deterministic case may become coupled when randomness is introduced into the problem. Here, however, we are dealing with disturbances which do not exist in the deterministic case; moreover, it is clear that the higher order terms in the perturbation expansion will not lead to mode coupling. Hence a more careful analysis of (3.27) is required to resolve this point, perhaps using ψ_0 and ψ_1 as a basis set for the real and imaginary parts of ψ. We also note the

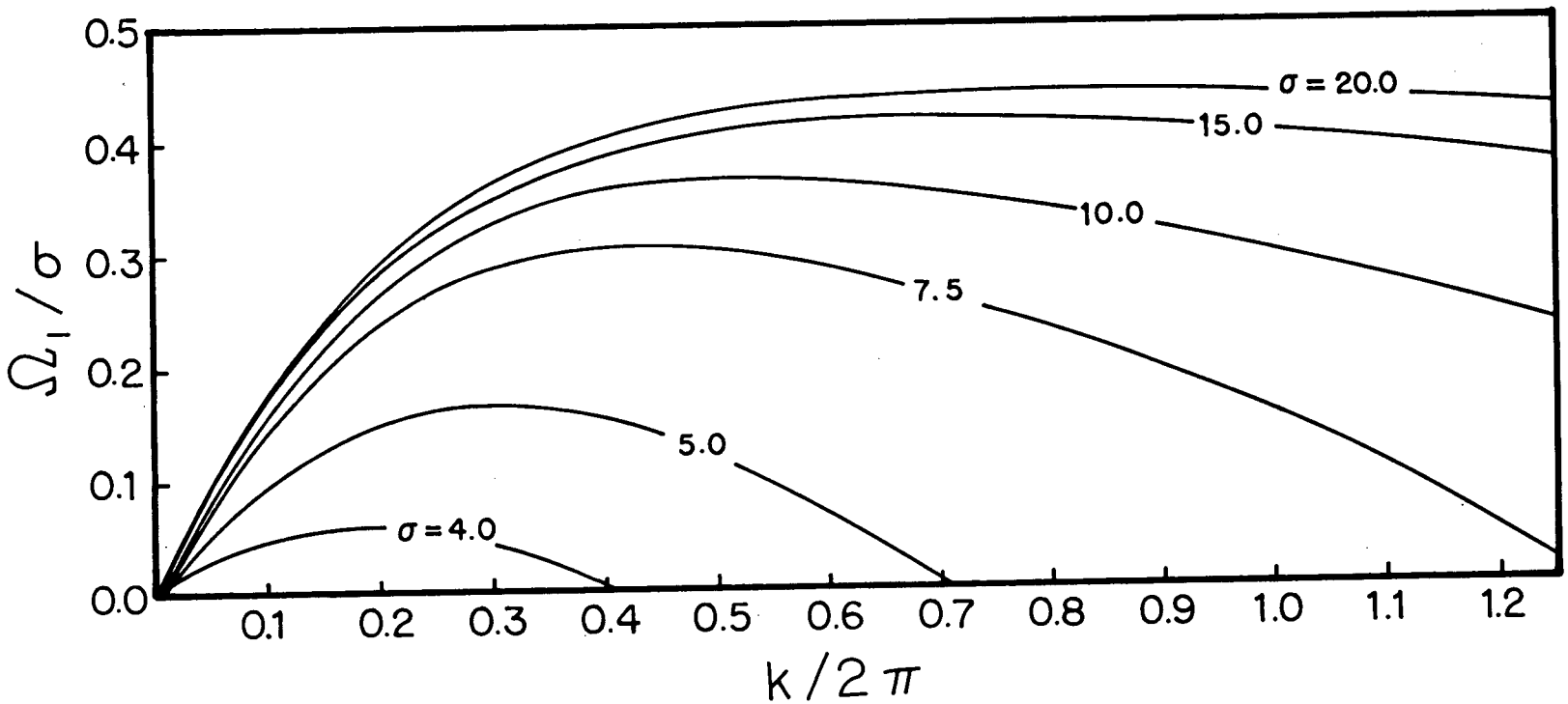

Figure 5.3 Behaviour of the first mode nondimensional growth rate Ω_1 as a function of σ and k. The dimensional values given correspond to Florida Strait parameters (b = 1.385, ℓ = 2.5, Ro = 0.3). The curves are labeled by the value of σ.

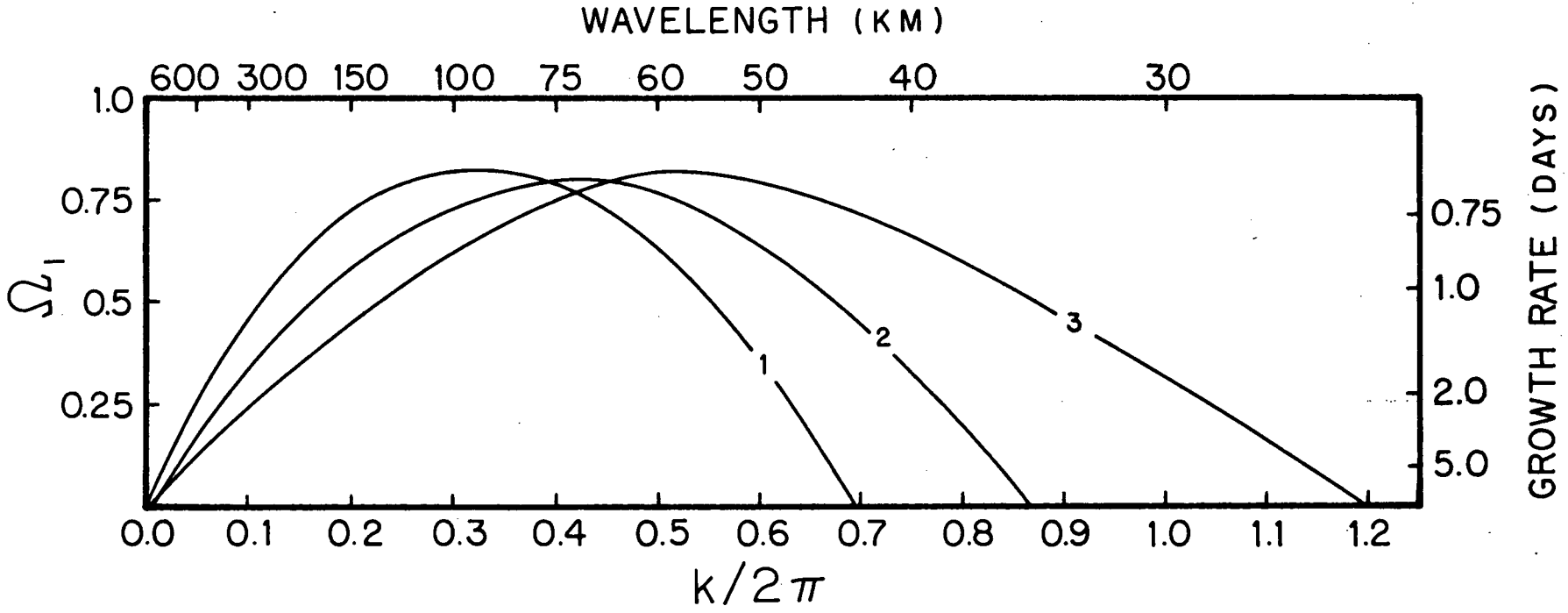

Figure 5.4A Behaviour of the nondimensional growth rate Ω_1 as a function of k for the first three modes for $\sigma = 5$ and $\varepsilon = .5$; (A) channel model (b = 1.385, ℓ = 2.5, Ro = 0.3), (B) shelf model (b = 1.385, μ = 1.0, Ro = 0.3).

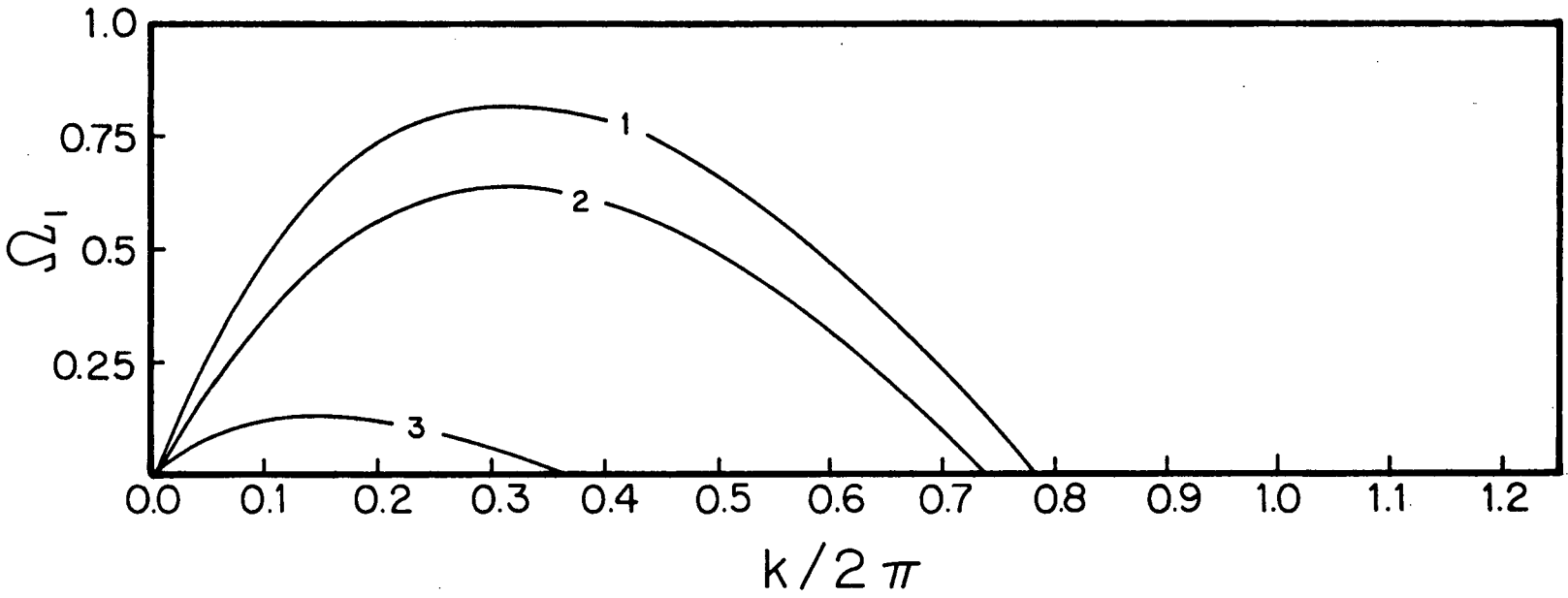

Figure 5.4B

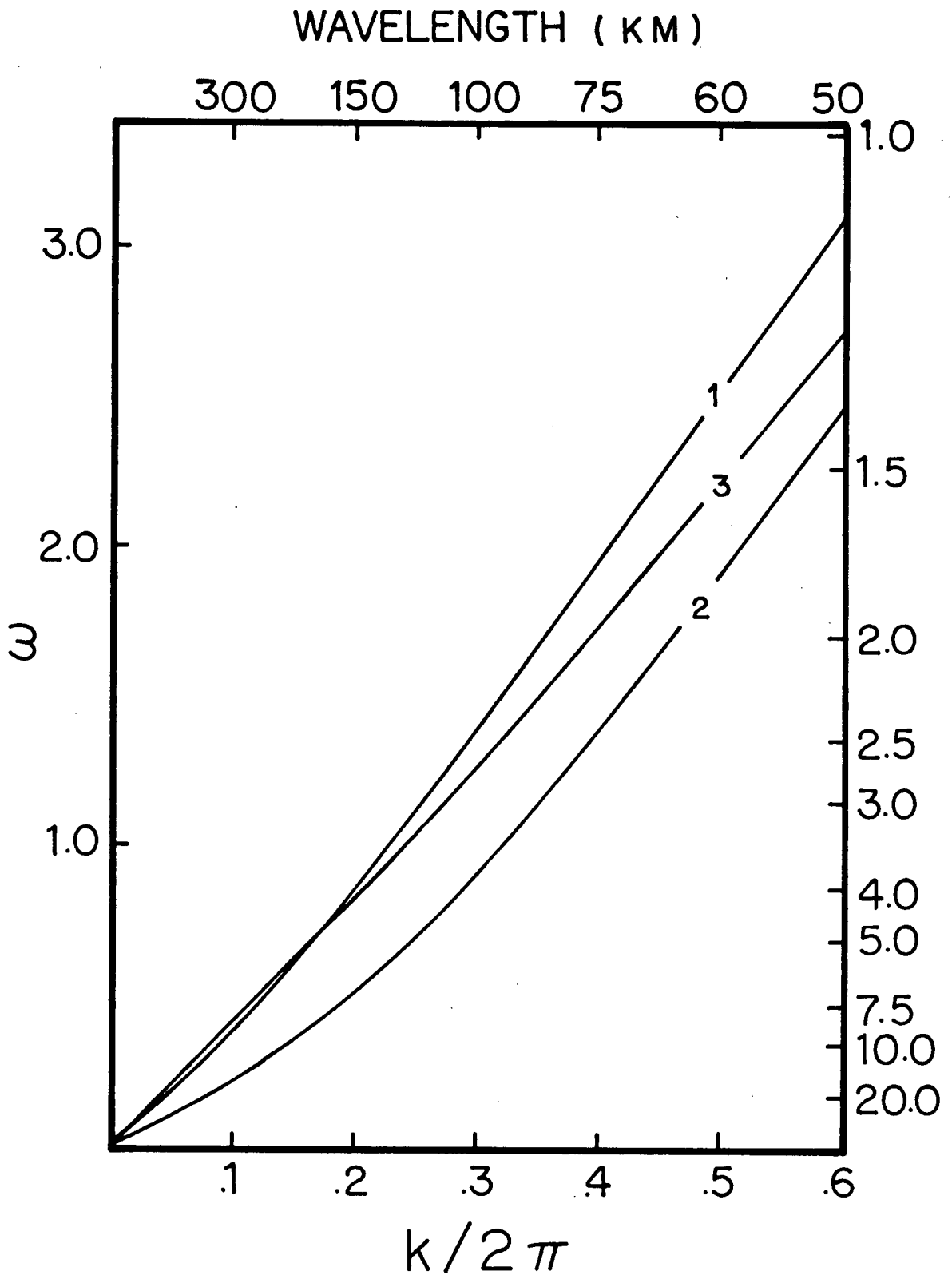

Figure 5.5A Dispersion curves for the first three modes, (A) channel model, (B) shelf model. Beyond $k/2\pi = 0.6$ the curves are essentially linear.

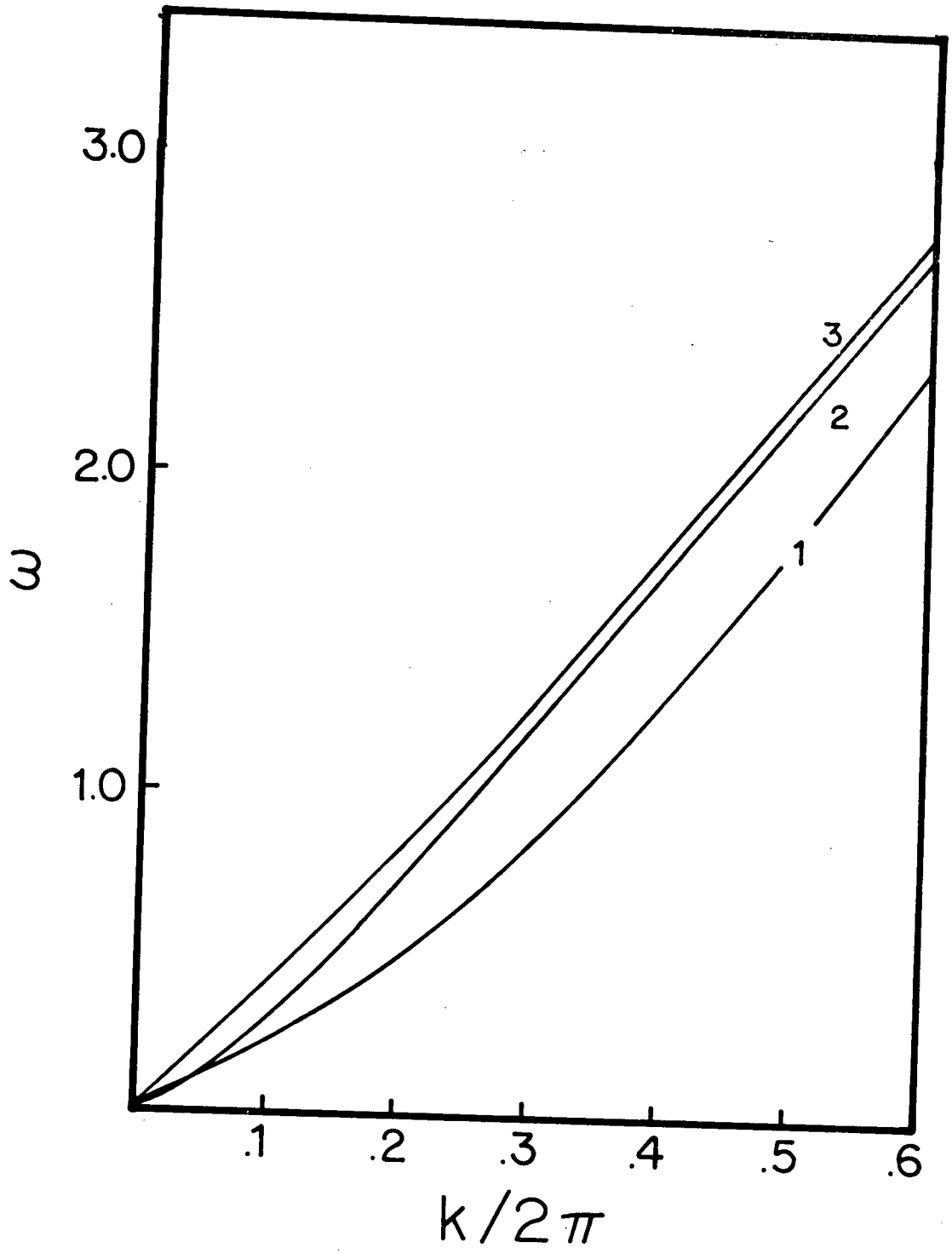

Figure 5.5B

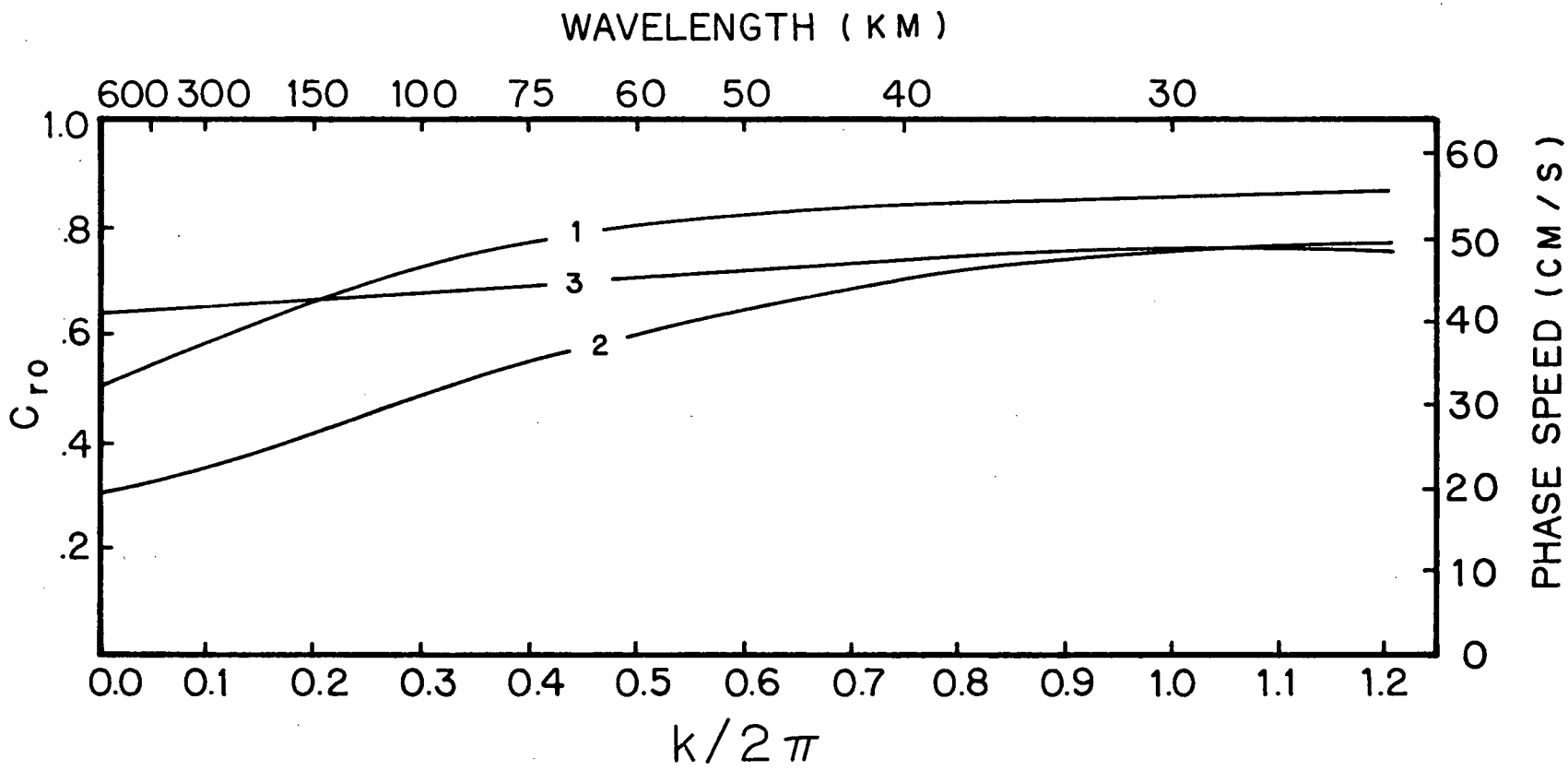

Figure 5.6A Behaviour of the nondimensional phase speed as a function of k for the first three modes, (A) channel model, (B) shelf model.

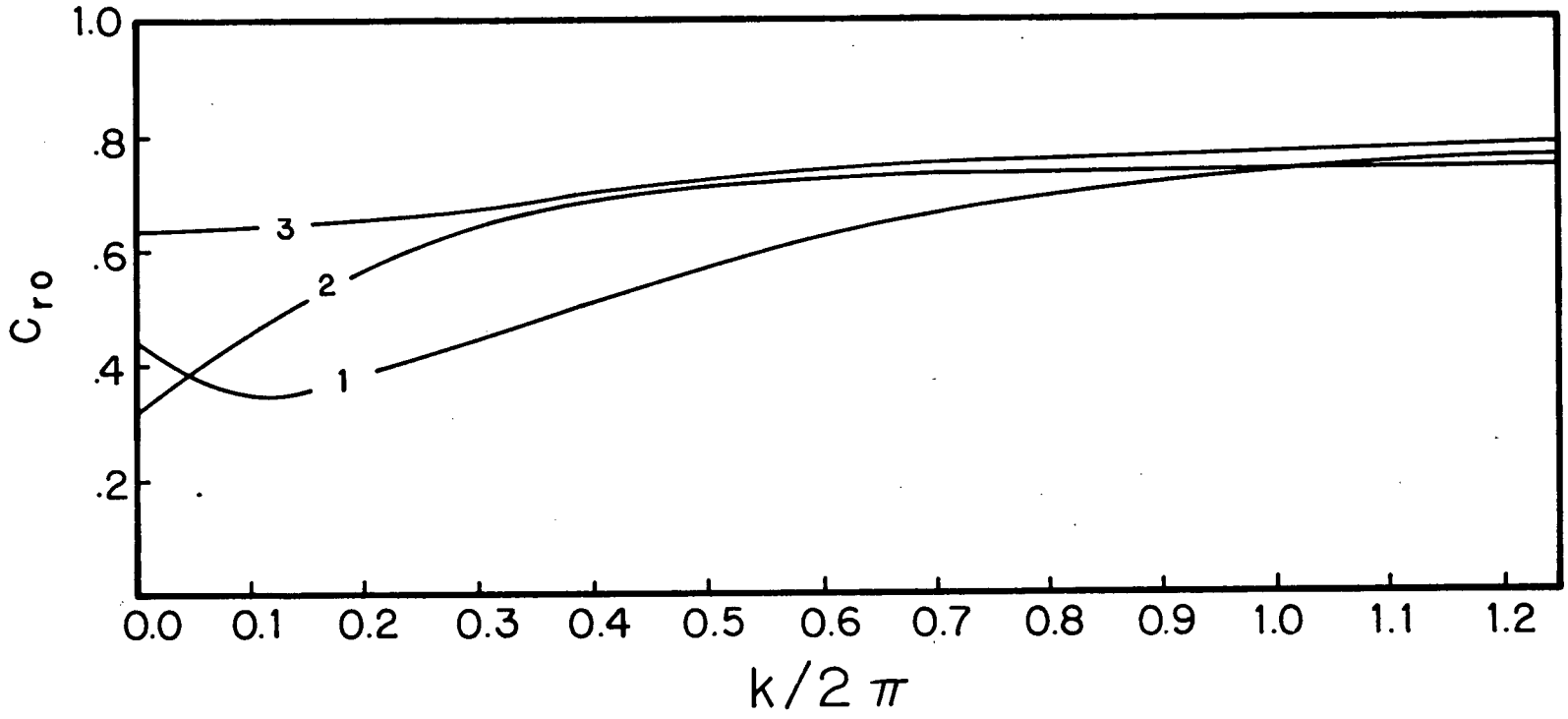

Figure 5.6B

related study by Allen (1975) of coastal trapped waves in a stratefied ocean where it was shown that CSWs may be coupled to internal Kelvin waves.

Figure 5.6A indicates that the phase speed is positive for all k and thus that the waves propagate northward; i.e., in the direction of the mean flow. However, if the Rossby number were small enough, the vorticity term in (5.16) would predominate, and the disturbances could travel southward. (Consider, for example, the case of $V = 0$, $hQ_x = -2b$.) This is in marked contrast to the stable CSW's admitted by the BrM model which propagate only southwards.

From the slopes of the dispersion and phase speed curves, we infer that the group velocity is positive and exceeds c_{r0} for all k. Finally, we note that $c_{r0} \to \langle V \rangle$ as $k \to \infty$ and thus that the waves are simply advected by the mean current in this limit.

Contour plots of the mass transport stream function for the first three modes are shown in Figure 5.7. An important feature is the tilting of the gyre axes toward the coast since it is related to the sign of the mean disturbance Reynolds stress $\overline{\tau}_{12} = (k/2h)F(\psi_R,\psi_I)$. In terms of the phase $\theta = k(x - c_r t)$, the stream function is given by $\psi = \psi_R \cos\theta - \psi_I \sin\theta$. The line along which it vanishes is determined by $\tan\theta = \psi_R/\psi_I$, with slope $d\theta/dx = -(\cos^2\theta/\psi_I^2)F(\psi_R,\psi_I)$. Hence $\overline{\tau}_{12} \alpha - d\theta/dx$ and Figure 5.7 shows that it is everywhere negative. Since $V' \gtrless 0$ for $x \gtrless 1$, (4.11) reveals the rather surprising result that over the shelf, $\overline{\tau}_{12}$ acts to remove energy from the nonrandom part of the disturbance and to strengthen the mean shear. This is in concert with the finding of Niiler and Mysak (1971) that the continental shelf acts as a stabilizing factor. Of course, the largest source term in (4.11) is the one proportional to σ^2 which shows that the disturbance energy is extracted primarily from the fluctuating part of the basic current.

Plots of the mass transport stream function are of limited value

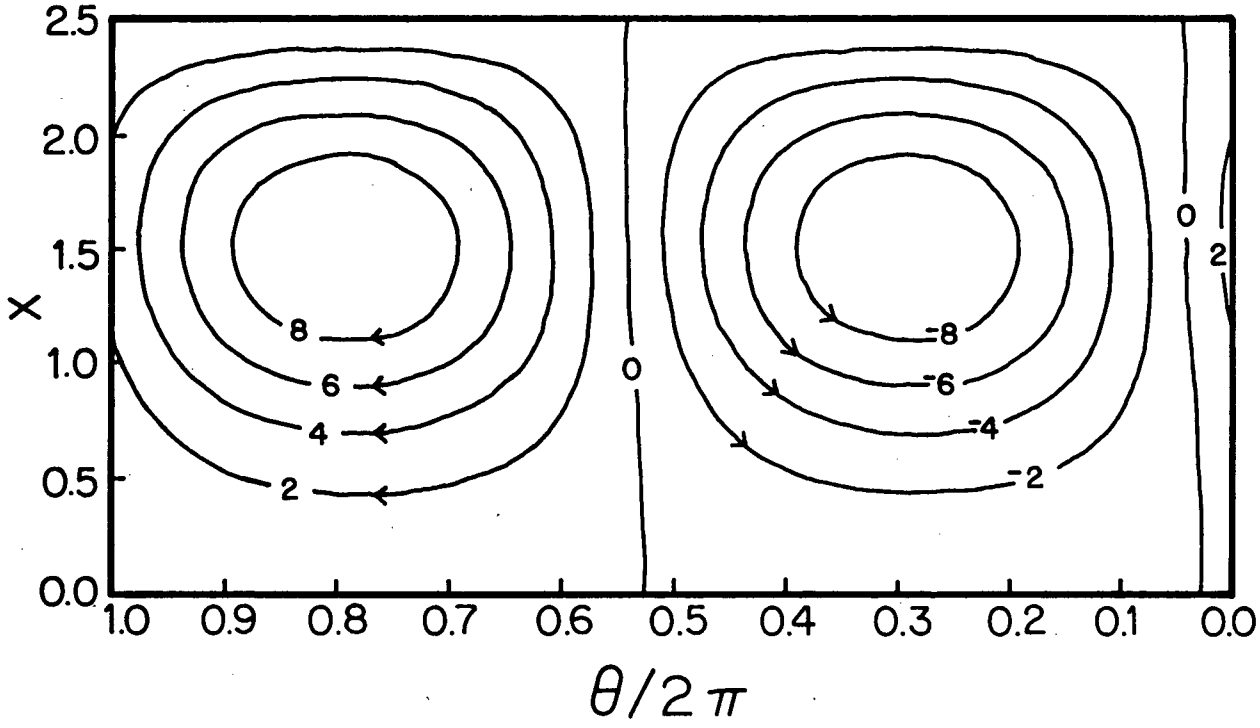

Figure 5.7A The mass transport stream function for (A) channel mode 1, (B) channel mode 2, (C) channel mode 3, (D) shelf mode 1, (E) shelf mode 2, (F) shelf mode 3. Here $\theta = k(y - c_{rt})$. The amplitude is arbitrary.

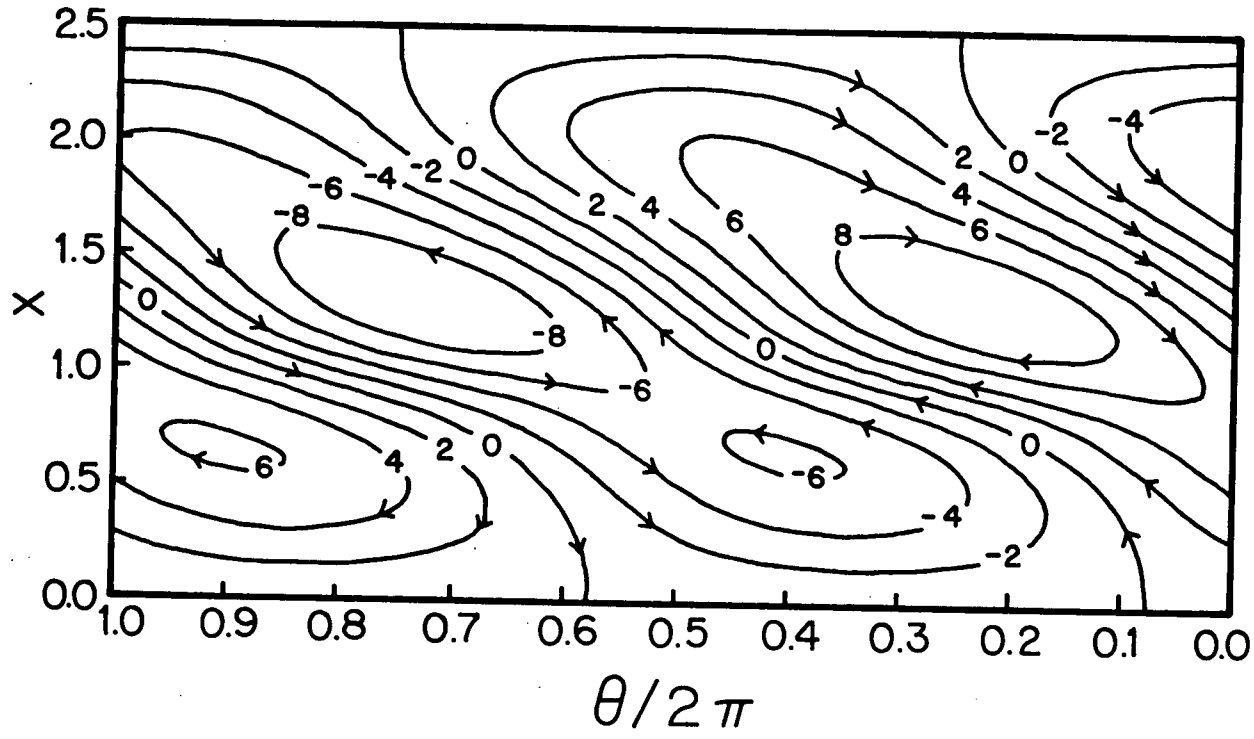

Figure 5.7B

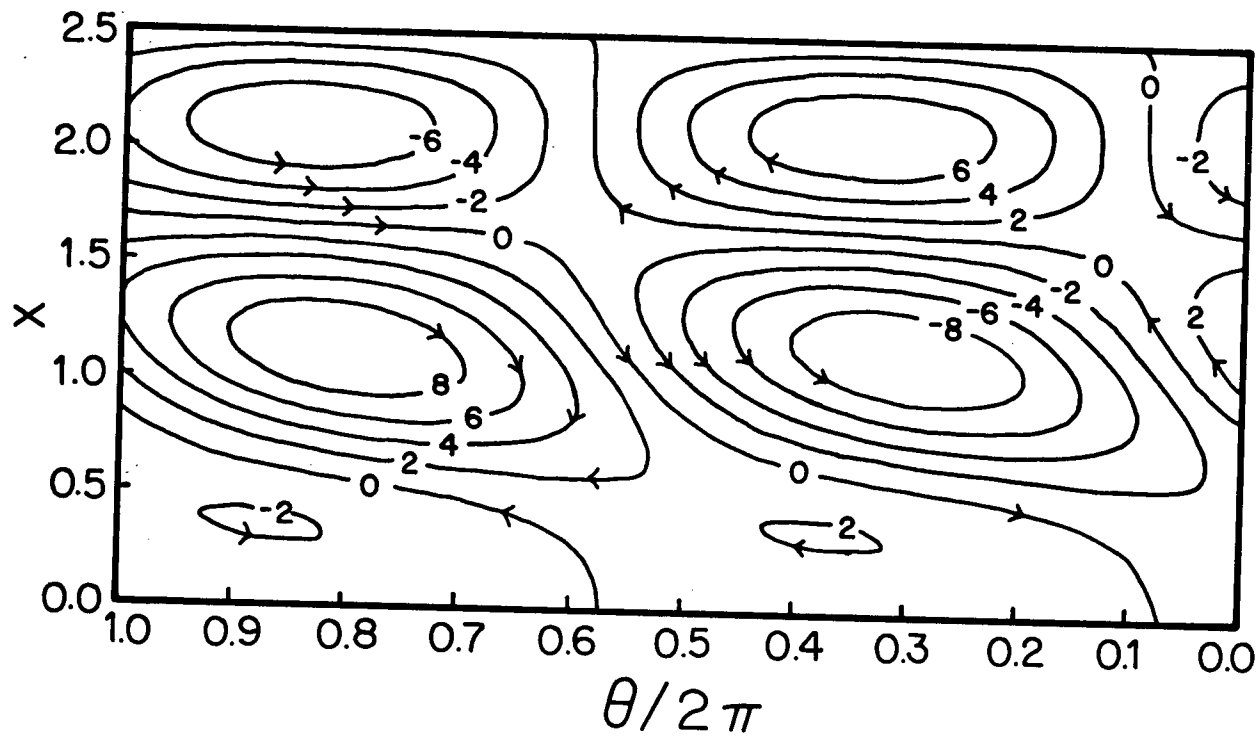
2.5
2.0
1.5
1.0
0.5
0.0
X
1.0 0.9 0.8 0.7 0.6 0.5 0.4 0.3 0.2 0.1 0.0
θ/2π
-6
-4
-2
0
6
4
2
0
-2
0
-2
-6
-4
-8
2
8
6
4
2
0
-2
0
2

Figure 5.7C

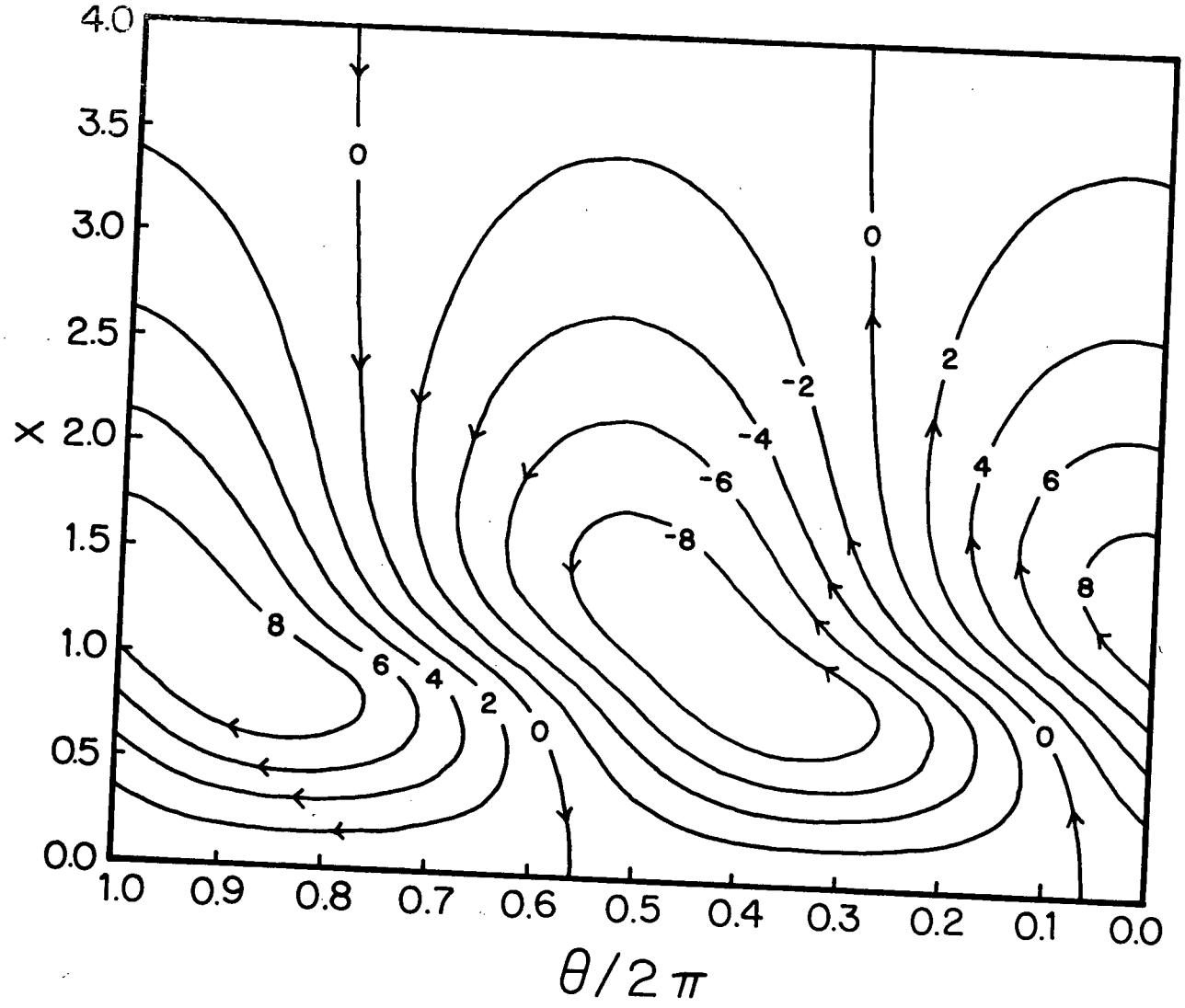
4.0
3.5
3.0
2.5
X 2.0
1.5
1.0
0.5
0.0
1.0 0.9 0.8 0.7 0.6 0.5 0.4 0.3 0.2 0.1 0.0
θ/2π
0
-2
-4
-6
-8
2
4
6
8

Figure 5.7D

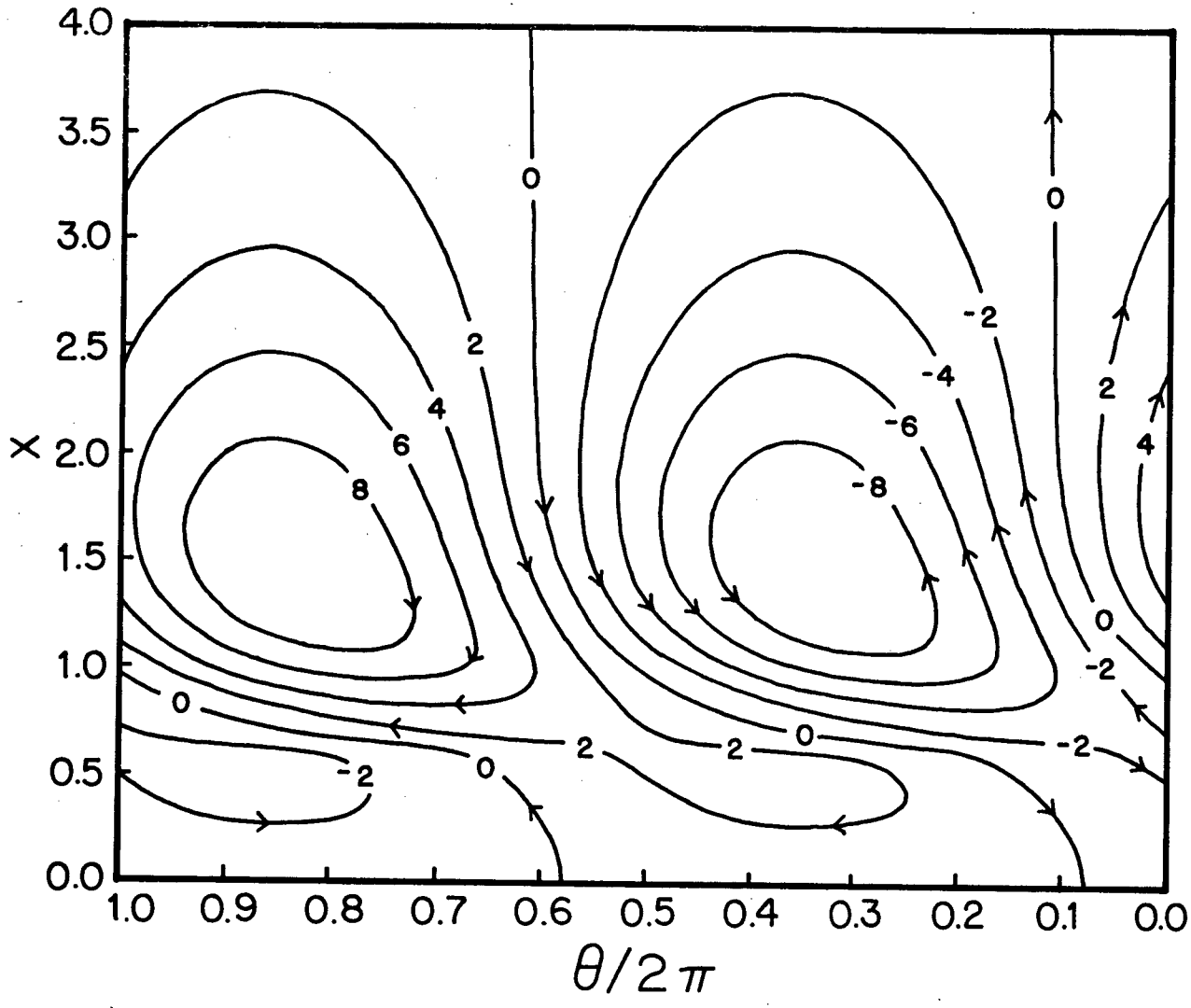
4.0
3.5
3.0
2.5
X 2.0
1.5
1.0
0.5
0.0
1.0 0.9 0.8 0.7 0.6 0.5 0.4 0.3 0.2 0.1 0.0
θ/2π
0
2
4
6
8
-2
-4
-6
-8

Figure 5.7E

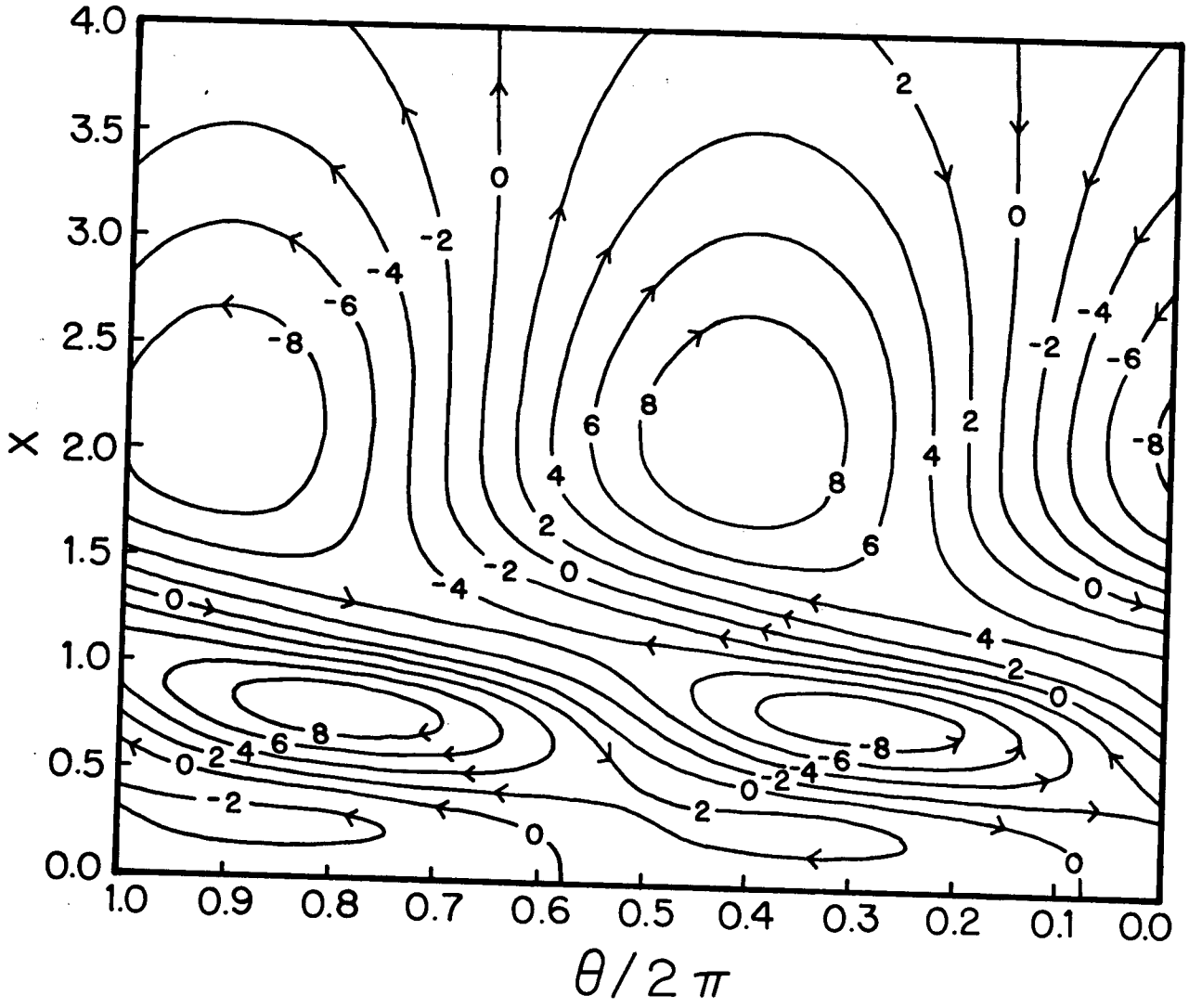

Figure 5.7F

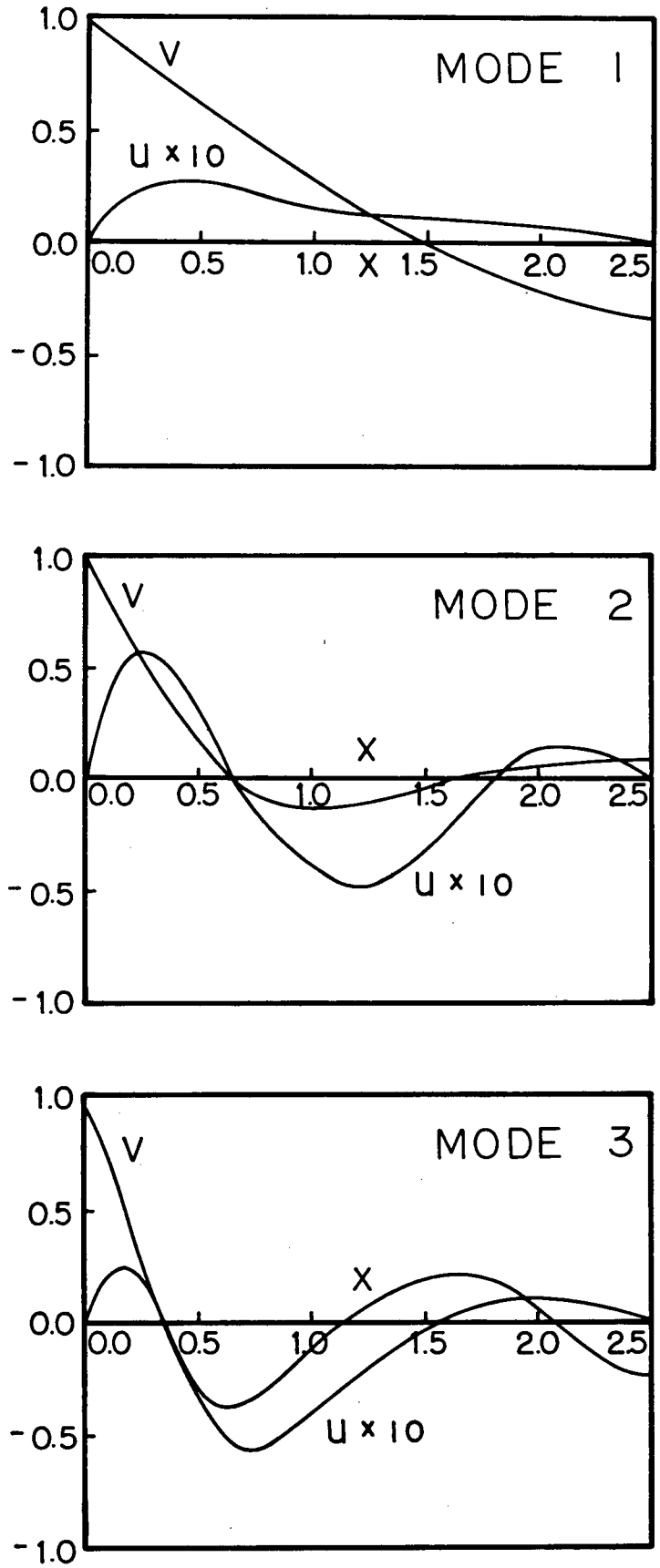

Figure 5.8 Profiles of u and v for: (1) channel mode 1 taken along the line $\theta/2\pi = 0.8$ in Fig. 7a, (2) channel mode 2 taken along $\theta/2\pi = 0.9$, and (3) channel mode 3 taken along $\theta/2\pi = 0.37$. In each case the values are normalized by $V(x = 0)$.

in visualizing the velocity structure over the shelf. Figure 5.8 shows selected profiles of u and v corresponding to Figure 5.7. In all cases the motion is trapped against the coast.

These results are now compared with observations made in the Florida Straits. The occurrence of fluctuations in the Florida Current with periods ranging from a few days to several weeks is well known, and the following review is not intended to be exhaustive; the reader is referred to the papers referenced here for a more extensive discussion. A plan view of the Florida Straits is shown in Figure 5.9. It reveals the channel-like topography and illustrates the sharp turn the Florida Current must make on its northward passage. Cross sections of σ_t and alongshore velocity are presented in Figure 5.10. In addition to showing the highly baroclinic nature of the mean flow, it also indicates some of the longitudinal variations in bathymetry and in the density and velocity fields. The stratification is compressed over the shelf, and a typical value of the Brunt-Väisälä frequency in the pycnocline is 2×10^{-2} rad s^{-1} (Mooers and Brooks, 1977).

In a marked contrast to low-frequency motions in the open ocean that are characterized by a red spectrum, there appears to be a spectral gap between motions with periods of about 25 days and 1 year (Brooks and Niiler, 1977; Düing et al., 1977; Wunsch and Wimbush, 1977). Düing et al. (1975) estimate from mid-channel velocity measurements that approximately 80% of the nontidal variance occurs at periods exceeding 8 days. In general, the low-frequency motions may be broken into three time scales, 8-25 days, 4-5 days, and 2-3 days (Düing et al., 1977) each of which is treated separately here. Seasonal fluctuations in the Florida Current have also been observed (Niiler and Richardson, 1973).

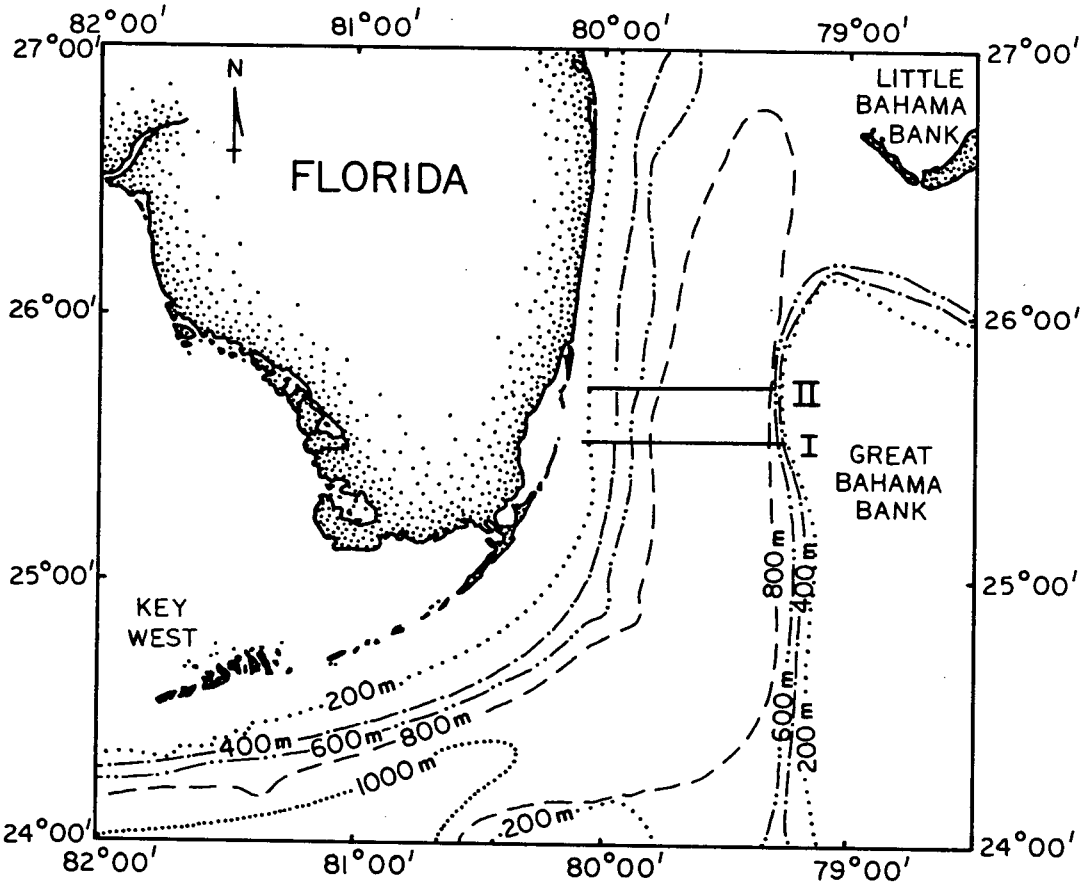

Figure 5.9 Plan view of the Florida Straits showing lines I and II along which the sections in Fig. 5.10 are taken (from Mooers and Brooks, 1977).

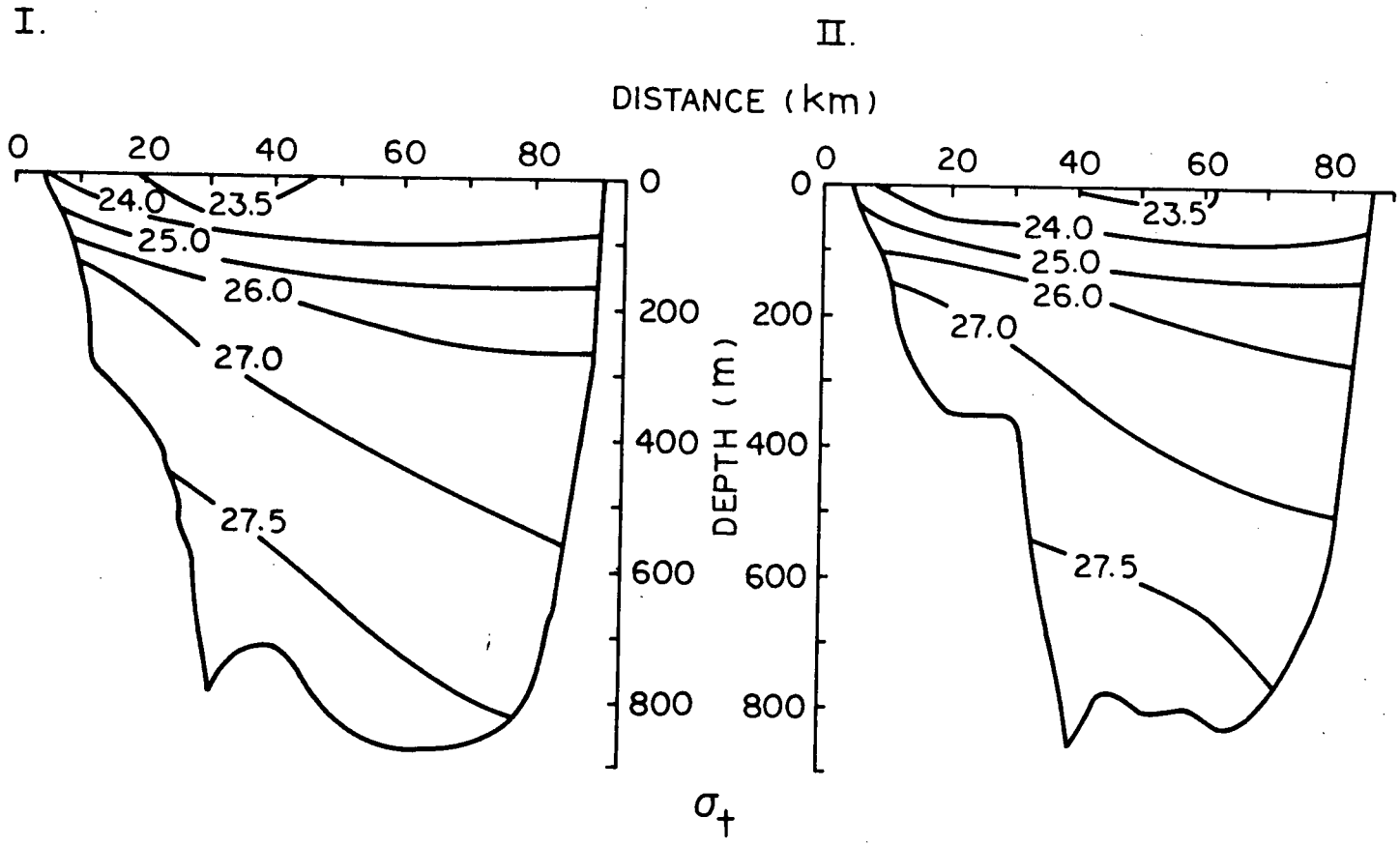

Figure 5.10A Sections along lines I and II of (A) σ_t and (B) alongshore velocity (from Mooers and Brooks, 1977).

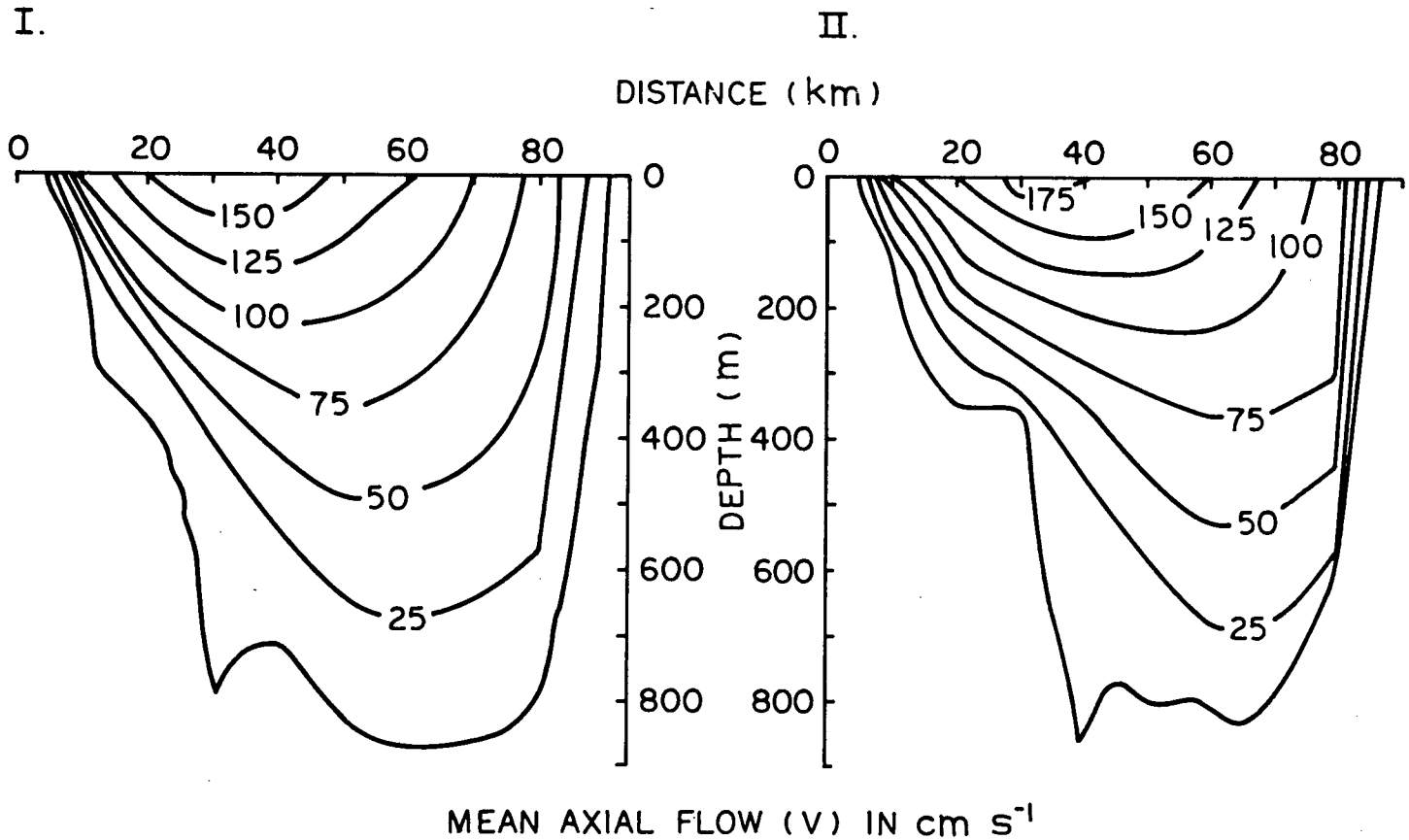
I.
II.
DISTANCE (km)
0
20
40
60
80
150
125
100
75
50
25
175
DEPTH (m)
200
400
600
800
MEAN AXIAL FLOW (V) IN cm s⁻¹

Figure 5.10B

The 8-25-Day Band

From the analysis of year-long records of sea level, sea temperature, and atmospheric pressure, Brooks and Mooers (1977b) demonstrated the existence of southward travelling waves with periods of 7-10 days in winter and 12-14 days in summer and speeds of 100 cm s^{-1} or greater. Strong coherence between sea level and temperature and the atmospheric variables showed that these disturbances were wind generated; a fit of the BrM CSW model to these observations was only partially successful as the model predicts wave speeds less than 50 cm s^{-1}. Schott and Düing (1976) applied a single barotropic wave model to the results obtained from the analysis of 65 days of current measurements taken concurrently at stations separated in the alongshore direction and found a statistically significant fit for the 10-13-day wave period band and a marginal fit for the 7-10-day band. In the former case they calculated a wavelength of 270 km, a southward phase speed of 17 cm s^{-1}, and an amplitude of 14 cm s^{-1}, values which are in excellent agreement with the BrM model. The wave parameters were similar for the 7-10-day band. Düing et al. (1977) concluded that 9-20-day oscillations possessed amplitudes ranging from 15-25 cm s^{-1}; they also showed that disturbances in the 10-14-day band occurred intermittently as phase-coherent wave packets consisting of 4-6 cycles. Since high coherence was observed between the velocities and the atmospheric variables, especially the wind stress curl, it appears likely these motions are, initially at least, atmospherically forced and represent stable, modified shelf waves.

The 4-5-Day Band

In the 4-5-day wave period band, Düing (1975) described a nearly

barotropic wave, 160-240 km in length, that propagates northward with a mean speed of 45 cm s^{-1}, and an amplitude of about 10 cm s^{-1}. An interesting manifestation of this disturbance is the reversal of the baroclinic mean flow at depth on the western side of the channel that accompanies its passage. Based on the analysis of six months of current, temperature, and bottom pressure measurements taken in 1974, Wunsch and Wimbush (1977) have also described a northward travelling 4-7-day wave about 60 km in length. Düing et al. (1977) showed that like the 10-14-day motion, a 4-5-day disturbance occurs intermittently as a wave packet of about 4 cycles and that it is significantly correlated with the wind stress curl and other atmospheric variables. No indication of the direction of wave propagation was given.

The 2-3-Day Band

Lee (1975) and Lee and Mayer (1977) have documented the existence of wave-like meanders of the mean flow and the transient occurrence of cyclonic "spin-off" eddies in the 2-3-day band. These eddies are trapped against the continental boundary, have a lateral length scale of about 10 km and a longitudinal one 2 to 3 times greater. They occur at approximately weekly periods, propagate northward at speeds ranging between 20-40 cm s^{-1} and persist for up to 3 weeks. A kinematical model of a pair of vortices superimposed on the mean flow gave a good representation of the observed near-surface current. The meanders also propagate northward but at speeds between 65 and 100 cm s^{-1}.

It is for the motions in the 4-5-day band that the present theory might offer a possible explanation. Indeed, barotropic instability of the

mean flow has been suggested by Düing (1975) as a likely mechanism for these motions. We should note, however, that Brooks and Niiler (1977) determined that, in the mean, the Florida Current is in an equilibrium state and that the net interchange of energy between the mean current and the fluctuations superimposed upon it is extremely small. Of course, this does not rule out the possibility that disturbances in some frequency ranges may extract energy from the mean flow. Furthermore, it has been shown that the primary source of energy for the motions described in this paper is the small, sheared, fluctuating component of the basic current. Nevertheless, Brooks and Niiler's work indicates that along-stream variations in the flow, as well as its baroclinic nature, may be significant.

For the parameters appropriate to the Florida Straits, Figure 5.6a indicates phase speeds of about 40 cm s^{-1} for modes 1 and 3, and 25 cm s^{-1} for mode 2 for the wavelength range of 160-240 km. These results are independent of ε and σ. However, the corresponding growth rates are strong functions of these factors as is illustrated in Table II. In general, the higher modes are more unstable, and in particular, it is seen that the third mode could grow significantly within one wave period for a wide range of values of ε and σ. Düing's (1975) plots of the eastward velocity component imply the existence of a second or third (or higher) mode; unfortunately, his measurements extend only over 2/3 of the channel width. Wunsch and Wimbush (1977) have calculated velocity cross-spectra, and the phase difference at 5 days between northward velocities measured at the continental boundary and the shelf break, and at the shelf break and the eastern wall is approximately 180° in each case. This is consistent with a third mode unstable wave but not a second mode disturbance. On the basis of these results we conclude that a mode 3 fluctuation as described by the

Table II. The characteristic growth times $\tau = 1/\Omega_{dim}$ for a 200-km wave $(k/2\pi = .15)$. The threshold values σ_T are also given.

	Mode 1			Mode 2			Mode 3		
ε	.1	.25	.50	.1	.25	.50	.1	.25	.50
σ_T	16.0	6.60	3.50	13.0	5.50	3.30	5.0	3.30	3.00
σ					τ (days)				
3.0	-	-	-	-	-	-	-	-	4.40
4.0	-	-	2.40	-	-	2.60	-	7.00	2.50
5.0	-	-	.86	-	-	1.20	-	3.20	1.40
7.5	-	-	.37	-	2.64	.56	5.5	1.50	.72
10.0	-	-	.25	-	.78	.38	3.1	1.00	.50

present theory provides a possible explanation of Düing's observations. It is particularly intriguing that the mode 1 and mode 3 dispersion curves cross in the range of interest, but it would be improper to draw any conclusions from this observation.

It is interesting to speculate that some relationship might exist between a mode 3 wave in the 2-3-day band and the spinoff eddies described by Lee. The propagation speeds are similar and the "inner gyre" illustrated in Figure 5.7 is approximately the same size as the observed eddies. (Although Figure 5.7 corresponds to $k/2\pi = .15$, its form changes relatively little as k is increased.)

6. The Continental Shelf Model

We now turn to the continental shelf model mentioned in the introduction. In order to examine a coastal phenomenon such as the modification of CSWs by a mean current, it is necessary that any mechanisms capable of altering the potential vorticity distribution be localized with respect to the coast. In all studies of CSWs in the absence of a basic flow, the gradient of the background potential vorticity, h'/h^2, has always died out away from the coast so that this requirement was automatically fulfilled. If one includes a sheared mean current, however, the potential vorticity gradient becomes $h^{-1}V'' - (Ro^{-1} + V')h'/h^2$, it is no longer sufficient that only h'/h^2 decay as $x \to \infty$. Niiler and Mysak (1971) avoided this problem by employing a piecewise linear current that became constant at a small distance offshore. McKee (1977) and Brooks and Mooers (1977a) have avoided this problem by adopting a channel model, although Brooks and Mooers briefly discussed a continental shelf model utilizing an exponentially decaying current. Grimshaw (1976) also required the mean current to diminish exponentially.

Our approach is to require V_B to be bounded away from the shelf edge. Specifically, we choose

$$V(x) = s(x)v(x)$$
$$W(x) = s(x)w(x) \qquad (6.1)$$

where $s(x)$ is a deterministic function that satisfies $s(x) \to 0$ as $x \to \infty$, and we assume $w(x)$ is a homogeneous random function. In terms of

the correlation function $r(\xi) = E[w(x)w(x + \xi)]$ one finds that

$$R(o) = s^2 r(o)$$

$$R'(o) = s^2 r'(o) + ss'r(o) \tag{6.2}$$

$$R''(o) = ss''r(o) + 2ss'r'(o) + s^2 r''(o).$$

With the choice of $r(o) = 1$ and $\sigma^2 = - r''(o)$ we find the equation equivalent to (3.27) to be

$$[(V - c)^2 - \varepsilon^2 s^2]\mathcal{D}\psi - (V - c)Q_x\psi$$

$$- \varepsilon^2 h^{-1}[s^2\sigma^2 - ss'' + ss'h'/h]\psi = 0. \tag{6.3}$$

The boundary conditions are

$$\psi(x) = 0 \quad \text{at} \quad x = 0$$

$$\psi(x) \to 0 \quad \text{as} \quad x \to \infty. \tag{6.4}$$

The interpretation of (6.3) is identical to that of (3.27), but we note that the term corresponding to $\varepsilon^2\sigma^2$ in (3.27) is more complex here and involves a contribution from $R'(0)$.

The appropriate matching conditions are

$$[\psi] = 0$$

$$[\{(V - c)^2 - \varepsilon^2 s^2\}\psi'/h] - [(V - c)Q\psi] - \varepsilon^2[ss'\psi/h] = 0. \tag{6.5}$$

The general form of the BrM model is retained and we choose

$$V(x) = s(x)v(x) = \begin{cases} x\, e^{1-x} & 0 \le x \le 1 \\ x\, e^{\mu(1-x)} & x \ge 1 \end{cases} \tag{6.6}$$

$$s(x) = \begin{cases} 1 & 0 \le x \le 1 \\ e^{\mu(1-x)} & x \ge 1 \end{cases} \tag{6.7}$$

$$h(x) = \begin{cases} e^{2b(x-1)} & 0 \le x \le 1 \\ 1 & x \ge 1 \end{cases} \tag{6.8}$$

where μ is positive.

As before, we seek a perturbation solution of the form (5.4). The three lowest order equations are

$$\mathcal{D}\psi_0 + h^{-1}(\varepsilon s/c_{i0})^2\psi_0 = 0 \tag{6.9}$$

$$\mathcal{D}\psi_1 + h^{-1}(\varepsilon s/c_{i0})^2\psi_1 = -c_{i0}^{-1}\{2[c_{i1} + i(V - c_{r0})]\mathcal{D}\psi_0 - iQ_x\psi_0\} \tag{6.10}$$

$$\begin{aligned}\mathcal{D}\psi_2 + h^{-1}(\varepsilon s/c_{i0})^2\psi_2 = {} & c_{i0}^{-2}\{(V - c_{r0})^2 - 2c_{i2}c_{i0} - c_{i1}^2 - \varepsilon^2 s^2 \\ & - 2i[(V - c_{r0})c_{i1} - c_{i0}c_{r1}]\}\mathcal{D}\psi_0 - 2c_{i0}^{-1}[c_{i1} + i(V - c_{r0})]\mathcal{D}\psi_1 \\ & - c_{i0}^{-2}\{Q_x[(V - c_{r0}) - ic_{i1}] - \varepsilon^2 h^{-1}ss'' + \varepsilon^2 ss'h'/h^2\}\psi_0 \\ & + ic_{i0}^{-1}Q_x\psi_0 \,.\end{aligned} \tag{6.11}$$

For $x < 1$, (6.9)-(6.11) are identical with (5.8)-(5.10). The zeroth order solution satisfying both the boundary and matching conditions is:

$$\psi_0 = A_0 \begin{cases} e^{b(x-1)} \sin \lambda x / \sin \lambda \\ \\ J_\nu(\rho\zeta)/J_\nu(\rho) \end{cases} \tag{6.12}$$

$$\lambda^2 = \varepsilon^2/c_{i0}{}^2 - k^2 - b^2 \tag{6.13}$$

$$\nu = k/\mu \qquad \rho = \varepsilon/\mu c_{i0} \qquad \zeta = e^{\mu(1-x)} \tag{6.14}$$

provided that

$$b + \lambda/\tan \lambda = - k + (\varepsilon/c_{i0}) J_{\nu+1}(\rho)/J_\nu(\rho) . \tag{6.15}$$

If λ^2 is negative, the solutions are hyperbolic over the shelf and may be obtained by replacing λ with $i\lambda$. The graphical solution of (6.15) closely resembles that of (5.14), but note that (6.15) must be solved separately for each choice of ε, μ, and k. This solution is not valid for $k = 0$ since J_0 cannot satisfy the boundary condition at $x = \infty$ (i.e., at $\zeta = 0$).

The first order solution is of the form

$$\psi_1 = \begin{cases} A_{11}\psi_0 + iA_0P_1 \\ \\ A_{12}\psi_0 + iA_0P_2 \, , \end{cases} \tag{6.16}$$

and the particular solutions are specified in Appendix B. In order for ψ_1 to satisfy the matching conditions, the consistency condition (5.27) must again be satisfied; it was used as a check on the numerical results derived here, and it proved extremely sensitive to the accuracy of the roots of (6.15). We again choose $A_{11} = 0$ and A_{12} is specified by (5.28).

Application of the Fredholm alternative to (6.9)-(6.11) implies that

$$c_{r0} = \langle V \rangle + (c_{i0}^2/2\varepsilon^2)\langle hQ_x/s^2 \rangle \tag{6.17}$$

$$c_{i1}, c_{r1} = 0 \tag{6.18}$$

$$\begin{aligned} c_{i2}c_{i0} = &- (3/2)\langle (V - c_{r0})^2 \rangle - (\varepsilon^2/2)\langle s^2 \rangle \\ &- (c_{i0}^2/2\varepsilon^2)\langle (V - c_{r0})hQ_x/s^2 \rangle - (c_{i0}^2/2)\langle s''/s \rangle \\ &+ (c_{i0}^2/2)\langle h's'/hs \rangle - ic_{i0}\langle (V - c_{r0}) \mid \psi_1 \rangle \\ &- i(c_{i0}^3/2\varepsilon^2)\langle hQ_x/s^2 \mid \psi_1 \rangle \end{aligned} \tag{6.19}$$

where

$$\langle f(x) \mid g(x) \rangle = \int_0^\infty h^{-1}s^2\psi_0(x)f(x)g(x)dx \Big/ \int_0^\infty h^{-1}s^2\psi_0^2(x)dx \tag{6.20}$$

and

$$\langle f(x) \rangle \equiv \langle f(x) \mid \psi_0(x) \rangle \tag{6.21}$$

by comparison with (5.17)-(5.19), we see that the terms involving the potential vorticity gradient are emphasized since $s < 1$ off the shelf. Otherwise the interpretation of (6.17)-(6.19) remains unchanged.

A comprehensive study of the dependence of the various results on μ was not carried out, and the choice $\mu = 1$ was made to facilitate comparison with the channel mode. The dependence of Ω_1 on σ is similar to that shown in Figure 5.3, and is not shown here. The threshold values of σ are smaller for modes 1 and 3 and larger for mode 2 than they are for the corresponding channel modes. Plots of Ω_1 and c_{r0} as functions of k are illustrated in Figures 5.4b and 5.6b and a detailed comparison with their channel counterparts reveals nearly as many differences as similarities. Two general conclusions may be drawn, however. As either k or the mode number increases, the disparities between the two models increase for Ω_1 and decrease for c_{r0}. This is physically reasonable since as k or the mode number increases, the effective wavelength decreases; thus, the wave should become less sensitive to the outer boundary and more sensitive to the basic current profile. Now Ω_1 depends intimately on this profile and so the two models should be increasingly disparate at small wavelengths. Similarly, the wave frequency does not depend on the details of the basic current but it certainly depends strongly on the position of the channel wall. Hence the phase speeds predicted by the two models should differ for long wavelengths. We also note that the growth rates for the different models no longer overlap. Figure 5.5b shows that the group velocity is always positive, and from the slope of the curves in Figure 5.6b we see that, with the exception of the first mode at small wavenumbers, it exceeds the phase velocity. Finally, the mass transport stream function is shown in Figure 5.7; it generally resembles its channel counterpart although the axis tilt is increased.

7. Rossby Waves in a Random Zonal Flow

In this section we examine the interaction of small-amplitude, nondivergent, free barotropic Rossby waves with a stochastic, sheared zonal current. For convenience we assume that the flow is confined to an infinitely long channel with side walls at $y = 0,L$. The theory is also applicable to topographic Rossby waves provided that the bottom slope α is small enough so that $\alpha L/H$ is of the order of the Rossby number. The following analysis is entirely analogous to that of the preceding sections, and it is therefore presented in as succinct a fashion as possible. We note the related study of Keller and Veronis (1969) who examined the propagation of Rossby waves in a weak random current on an infinite β-plane. For a zonal flow of zero mean they found that the waves were damped and the wave speed reduced.

In terms of the velocity stream function defined by

$$\left.\begin{aligned} u &= -\Psi_y \\ v &= \Psi_x \end{aligned}\right\} \tag{7.1}$$

the nondimensional, linearized vorticity equation is

$$(\partial_t + U_B\partial_x)\nabla^2\Psi + \Psi_x(\beta - U''_B) = 0 \tag{7.2}$$

where the zonal current $U_B(y)$ defines the basic state. As scale factors we choose an average current U for (u,v), the channel width L for

(x,y), and L/U for the time; β is nondimensionalized by L^2/U so that the dimensionless Coriolis parameter is $f = 1 + Ro\beta y$. For a travelling wave solution of the form

$$\Psi = \Phi(y)e^{ik(x-ct)} \tag{7.3}$$

(7.1) reduces to

$$(U_B - c)(\Phi'' - k^2\Phi) + (\beta - U''_B)\Phi = 0 \tag{7.4}$$

which is precisely the equation first considered by Kuo (1949). The boundary conditions require no flow normal to the channel wall, hence

$$\Phi(y) = 0 \quad \text{at} \quad y = 0,1. \tag{7.5}$$

We decompose U_B into its mean and fluctuating components as

$$U_B = U(y) + \varepsilon W(y) \tag{7.6}$$

where $E(U_B) = U$ and $E(W) = 0$, and we choose $E(W^2) = 1$. Then application of the theory developed in Section 3 leads to an equation for the mean part of Φ,

$$[(U - c)^2 - \varepsilon^2]F\psi + (U - c)Q_y\psi - \varepsilon^2\sigma^2\psi = 0. \tag{7.7}$$

Here $F = d^2/dy^2 - k^2$, $\sigma_2 = - R''(0)$, and $Q_y = (\beta - U'')$.

A perturbation expansion of the form (4.4) leads to the following

results,

$$c_{i0} = \varepsilon^2/K^2 \tag{7.8}$$

$$c_{r0} = \langle U \rangle + \langle Q_y \rangle/2K^2 \tag{7.9}$$

$$c_{i1}, c_{r1} = 0 \tag{7.10}$$

$$c_{i2}c_{i0} = -(3/2)\langle (U - c_{r0})^2 \rangle - \varepsilon^2/2 + (1/2K^2)\langle (U - c_{r0})Q_y \rangle - ic_{i0}\langle (U - c_{r0}) \mid \psi_1 \rangle + i(c_{i0}/2K^2)\langle Q_y \mid \psi_1 \rangle \ . \tag{7.11}$$

Here

$$\langle f(y) \mid g(y) \rangle = \int_0^1 \psi_0(y) f(y) g(y) dy / \int_0^1 \psi_0^2(y) dy \tag{7.12}$$

and

$$\langle f(y) \rangle = \langle f(y) \mid \psi_0(y) \rangle \tag{7.13}$$

where $\psi_0 = A_0 \sin(n\pi y)$ and $K^2 = k^2 + n^2\pi^2$. Again one finds that c_{2n+1} vanishes and that ψ_{2n}/A_0 and ψ_{2n+1}/A_0 are real and imaginary quantities respectively.

These expressions are generalizations of those found by Manton and Mysak (1976) for plane Couette flow; their results may be recovered by putting $U = y$ and $Q_y = 0$. In particular, they showed that all modes travelled with the same constant phase speed; the inclusion of a nonzero

vorticity gradient in the present model serves to separate the dispersion curves as is revealed by (7.9). Somewhat more specific results are given in Appendix C for a parabolic flow model, $U = \beta y(y - 1)/2$.

Finally, we note that the present theory is not in conflict with the study of Keller and Veronis which predicts wave damping. Their results require two-dimensional, translational invariance of the basic state (Keller, 1967), a condition which cannot be satisfied by a system with a sheared mean current or by one confined to a channel. Hence their results do not apply to the present system, even in the limiting case of $U = 0$.

8. Summary and Concluding Remarks to Part I

It has been demonstrated that shelf and Rossby waves propagating through a region of basic sheared current of the form $V_B = V + \varepsilon W$ where W is a centred random function may be unstable if the lateral correlation length of W is small compared to the characteristic length scale of the problem. This is true whether or not V satisfies the well-known necessary conditions for barotropic instability. The growth rate of these disturbances is principally determined by the inverse of the correlation length. The phase speed is the sum of weighted cross-stream averages of the mean current and the mean gradient of potential vorticity. Depending on the Rossby number of the system, the waves may travel with or against the mean flow.

When this theory is applied to a model of the Florida Straits, unstable CSWs are found with properties that are in good agreement with observations made by Duing (1975). It may, therefore, offer an explanation for some of the observed meanders of the Florida Current.

The present theory could obviously be extended in many ways. A detailed comparison is needed with an intrinsically unstable system in order to compare growth rates. One could also introduce a small, random cross-stream velocity into the basic flow. The problem of mode-coupling has yet to be resolved as does the effect of temporal or along-shore variations in the basic current. Of course, the present theory represents only a first step in a more comprehensive examination of the effects of random potential vorticity distributions on barotropic-baroclinic instabilities.

9. Introduction to Part II

The waters lying between Vancouver Island, the mainland coast of British Columbia, and the State of Washington (see Figure 9.1) are important from economic, environmental, navigational, and recreational points of view. Oceanographically it is a complex estuarine system. In addition to the major influences of tides, fresh water inflow, topography, Coriolis force, winds and other atmospheric variables, one must consider the intense mixing that occurs in the channels that separate the Strait of Georgia (GS) from Juan de Fuca Strait in the south, and Queen Charlotte Sound in the north.

Part II of this thesis represents an attempt to understand some of the results presented by Chang et al. (1976; see also Chang, 1976). From the analysis of 18 months of current records collected along line H in GS (see Figure 10.1), Chang showed that nearly one-half of the kinetic energy associated with horizontal motions is contained in broad-banded, low-frequency current fluctuations characterized by periods ranging from 4 to over 200 days. No forcing mechanisms were evident from Chang's analysis as the coherences between the currents and the wind, atmospheric pressure, sea level, and water temperature were all calculated to be very small.

In an earlier attempt to understand the low-frequency dynamics of GS, Helbig and Mysak (1976) constructed an analytic model that included both bottom topography and density stratification. This model admits northward-travelling topographic planetary waves with periods that lie in the observed range, but it incorrectly predicts the vertical distribution of horizontal energy. Helbig and Mysak (1976) suggested that baroclinic instability of the mean flow was a likely mechanism to account for observed fluctuations, and it is from this premise that the present study commenced.

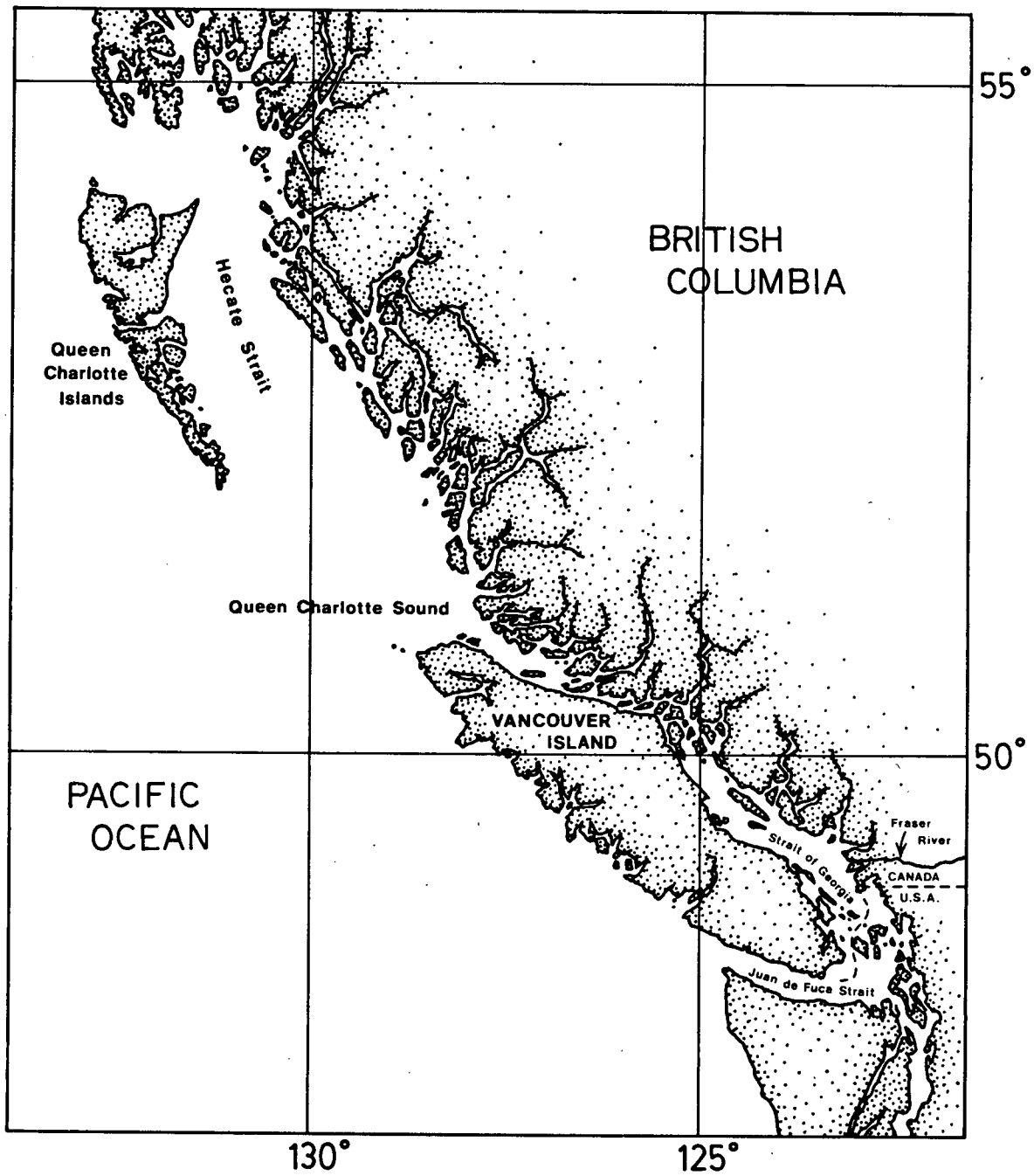

Figure 9.1 Plan view of the west coast of British Columbia and adjoining waters.

As it turns out, this conjecture is probably incorrect as the anlysis presented in Sections 11 and 12 shows. Two simple stability models were constructed of a purely baroclinic and barotropic system, respectively. For the baroclinic system the results indicate that the mean flow is unstable for only a narrow band of wave numbers. An unstable shear wave exists at all wavelengths in the barotropic system and for a 15-day period, has an e-folding time of about 8 days. However, as is shown in Section 12, the observed Cartesian velocity components are generally in phase indicating that the motions are not composed of the types of waves studied here. These results imply that inertial instability plays only a minor role, at most, in the dynamics of GS.

Additional current data collected by the Canadian Hydrographic Service at points not along line H (see Figure 10.1) were also examined. Since these records were of limited length (about 30 days) their analysis is subject to severe statistical limitations. It indicates, however, that during the observation period an anticyclonic gyre existed in the southern half of GS. Interestingly, this circulation was of the opposite sense to that postulated by Waldichuck (1957).

The longer-term records investigated by Chang were also reexamined with the object of gaining fresh insights. In particular, Chang calculated rotary spectra which yield no direct information about the individual Cartesian velocity components. As mentioned, the present results indicate the motion is not comprised of simple waves. Cross-spectra between the currents and wind stress were computed. While generally low coherence was found, a consistent phase pattern seemed to emerge. In the frequency range of interest, the along-channel currents are 180° out of phase with the wind. The conjecture is made that the forcing of the low-frequency motions is not

direct but rather that the winds interact nonlinearly with the tides and Fraser River outflow to modulate the estuarine circulation of the system. An examination in the time domain of winds and currents suggests that the water column responds most directly to the wind along the eastern side of GS with a lag of about five days. The response elsewhere is not clear.

Residual tidal currents were calculated from the time series of barotropic tidal streams generated from the numerical model of the Juan de Fuca-Strait of Georgia system developed by Crean (1976, 1978). A coherent pattern of residuals that varied with the fortnightly tidal cycle was found. These currents were insufficiently large and of the wrong direction to explain the observations, however.

The outline of Part II is as follows. A brief description of the physical oceanography of GS is given in Section 10 and includes a discussion of the possible character of the observed low-frequency currents and an enumeration of various forcing mechanisms that might be important. Two simple inertial instability models are considered in Section 11, while the data analysis is presented in Section 12. In Section 13, tidal residuals are calculated, and a brief development of the concept of modulated estuarine flow is given. In Section 14, the key points of Part II are summarized.

10. Physical Oceanography of the Strait of Georgia

Although the physical oceanography of GS has received comprehensive treatment elsewhere (cf. Waldichuck, 1957), it is important to summarize here some of its principal features to provide a motivation for the following study. Some parts of this description are abstracted from Helbig (1977).

A plan view of GS is shown in Figure 10.1. It reveals that the average width of GS is about 30 km while its length is slightly less than 250 km. Thus, the aspect ratio of channel length to width is approximately 8:1. Bathymetric sections along the lines 1-10 are presented in Figure 10.2, and were extracted from a topographic map of GS compiled by Dr. P. B. Crean (personal communication) giving average depths over 2-km squares throughout the Strait. Even though small-scale features are implicitly smoothed, the bathymetry exhibits great irregularity, particularly in the northern sector. In general, extremely steep slopes characterize GS along its western boundary, while slopes nearly as steep (exceeding 10^{-2}) are common along the east. North of line 4, two channels exist: a narrow one to the east of Texada Island and a much wider one on the western side. South of line 4 the topography becomes progressively smoother; lines 7 and 8 illustrate the marked effect of Fraser River sedimentation as extensive banks on the east. The longitudinal section 10 reveals that although the axial bathymetry is somewhat smoother than the transverse bathymetry, it still possesses a high degree of irregularity and exhibits slopes that often exceed 10^{-2}.

Figure 10.3 shows longitudinal sections of density for winter and summer. In the upper 50 metres near line 7 (see Figure 10.1) there exists a strong seasonal variation which is associated with the outflow of fresh

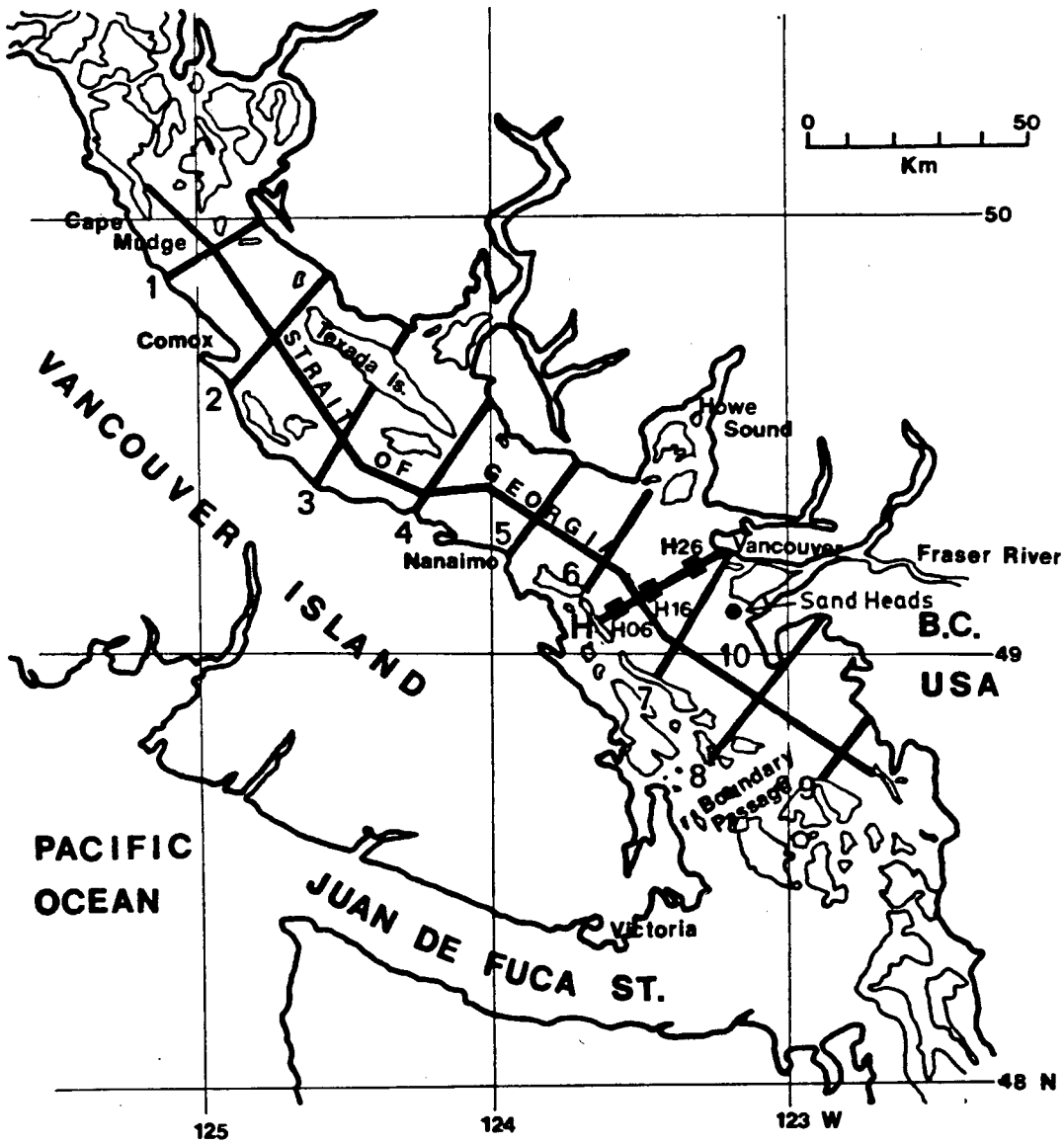

Figure 10.1 Plan view of the Strait of Georgia showing lines of topographic cross sections (1-10) presented in Fig. 10.2.

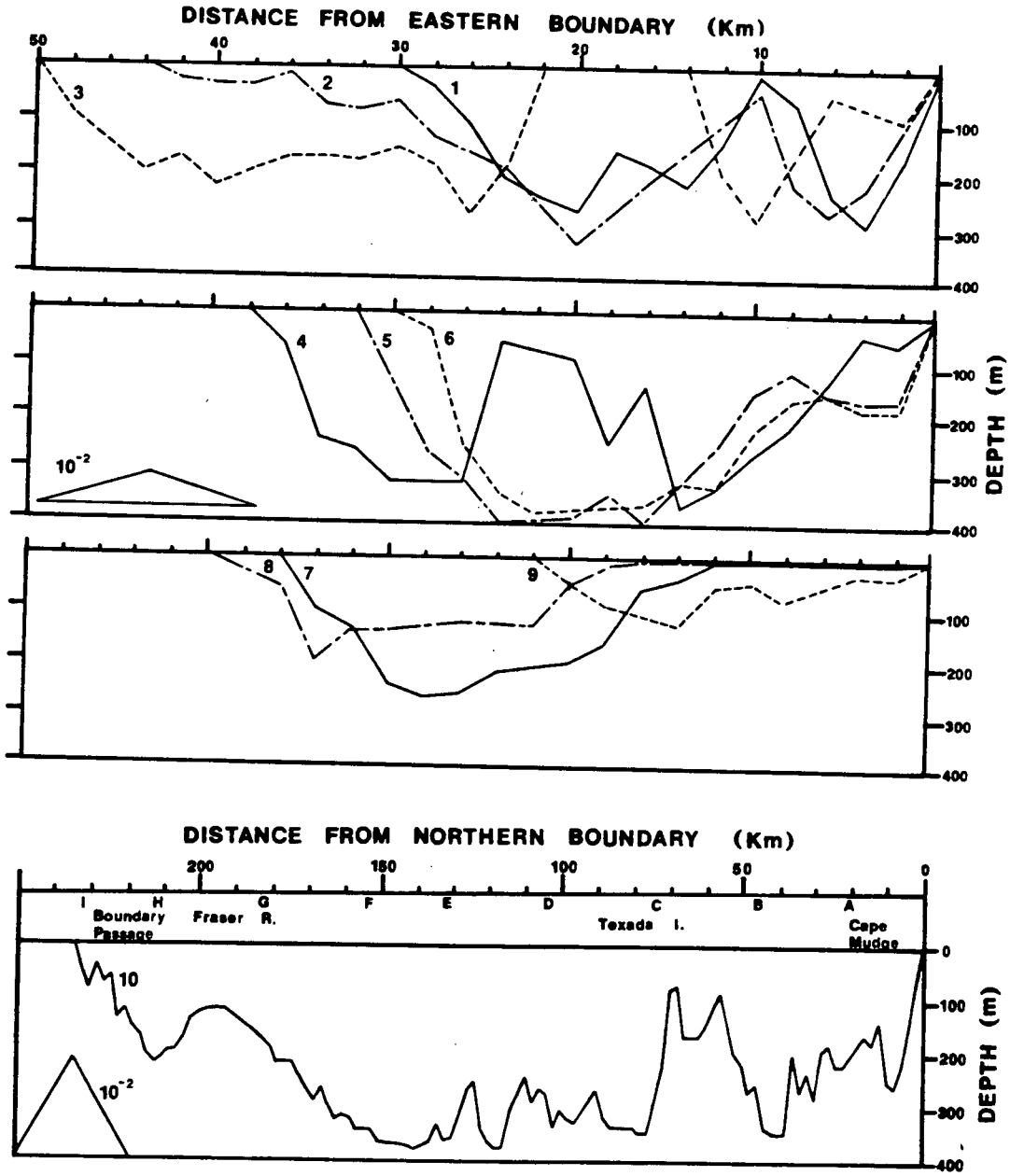

Figure 10.2 Topographic cross sections: (A) Upper panels: 1-9; (B) lower panel: 10. The vertical exaggeration is 30:1 in (A) and 150:1 in (B). The insets indicate slopes of 10^{-2}.

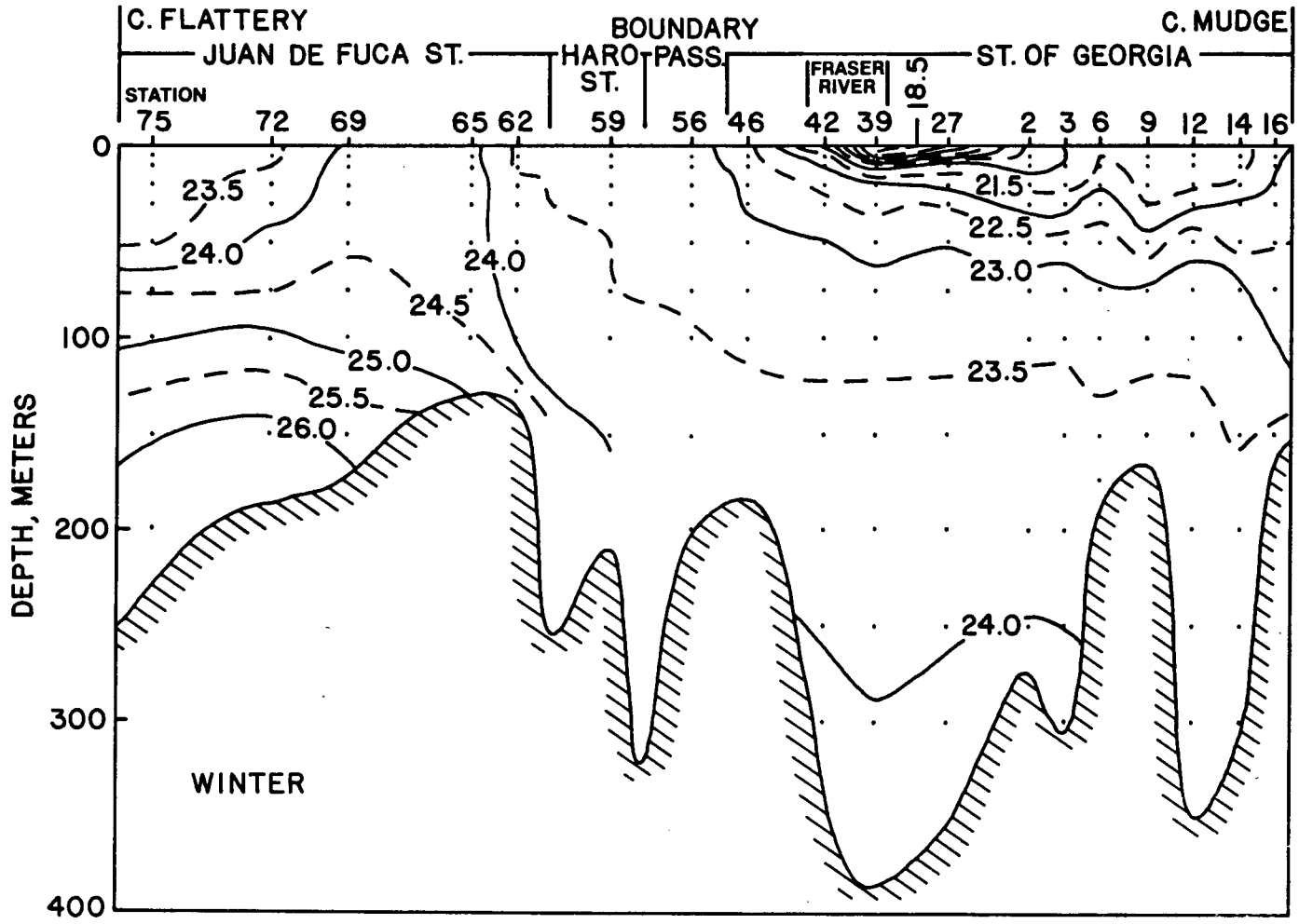

Figure 10.3A Longitudinal section of σ_t for (A) December 1968; (B) July 1969 (from Crean and Ages, 1971).

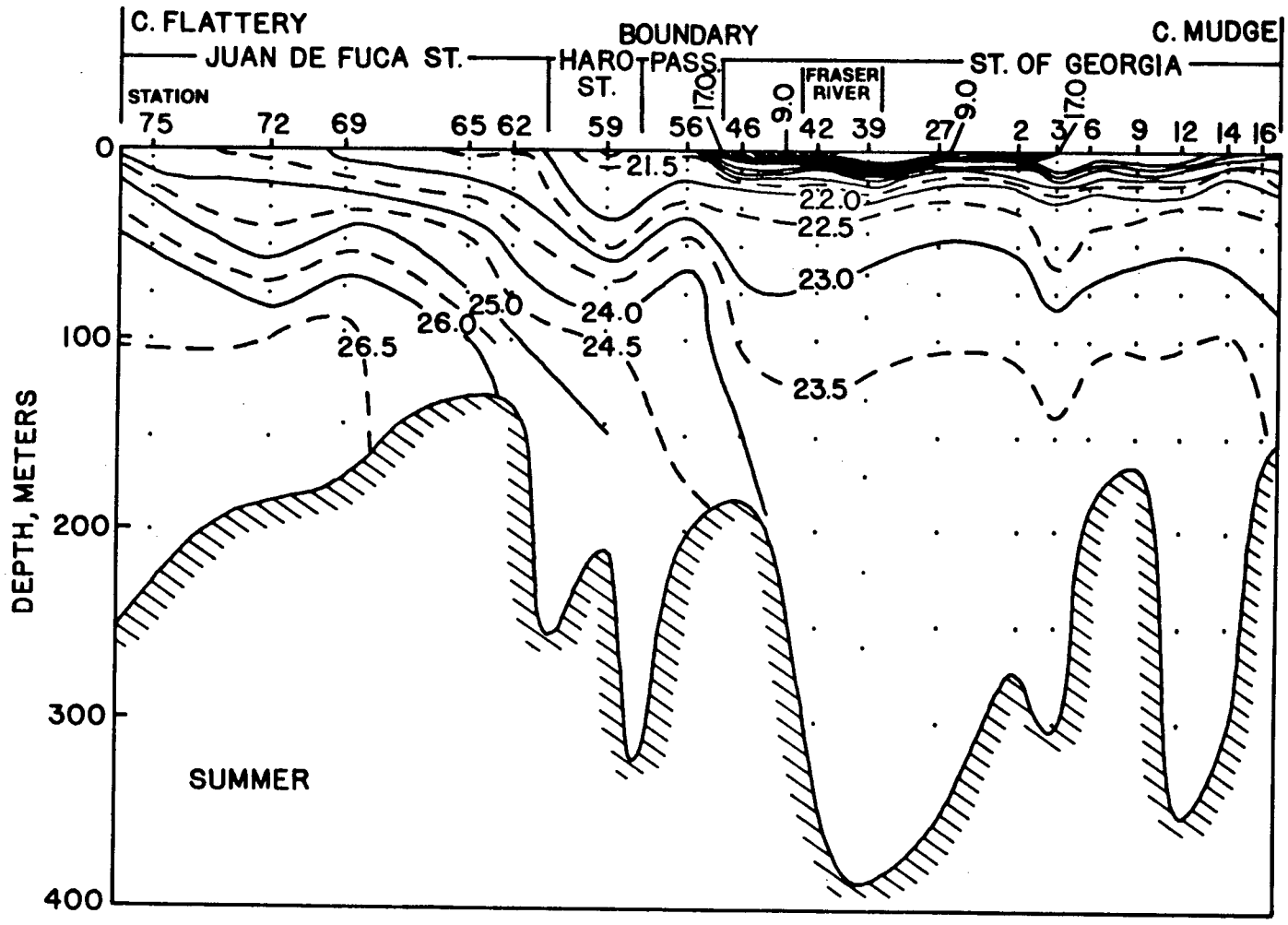
C. FLATTERY
JUAN DE FUCA ST.
BOUNDARY
HARO ST.
PASS
ST. OF GEORGIA
C. MUDGE
FRASER RIVER
STATION
75 72 69 65 62 59 56 46 42 39 27 2 3 6 9 12 14 16
17.0
9.0
9.0
17.0
0
100
200
300
400
DEPTH, METERS
21.5
22.0
22.5
23.0
23.5
24.0
24.5
25.0
26.0
26.5
SUMMER

Figure 10.3B

water from the Fraser River. The Brunt-Väisälä frequency $N = [-g\rho_z/\rho_*]^{1/2}$ generally lies in the range of 3×10^{-3} to 3×10^{-2} rad s^{-1} throughout the water column which is thus well stratified. Here ρ_z is the vertical density gradient, ρ_* is a representative value of the density, and g is the acceleration due to gravity.

The winds in GS are strongly affected by the surrounding mountainous terrain, and they are predominantly up- or down-strait; that is, to the northwest or southeast, respectively (Kendrew and Kerr, 1955). During the winter months of November through March the prevailing wind is up-strait while in the summer months of June to September it is down-strait. In all seasons the strongest winds are from a southerly direction. There is of course a great deal of variation about this average pattern. Although Waldichuck (1957) indicates that a cyclonic gyre exists over the southern strait during the winter, the evidence for this seems weak. We do note, however, that the prevailing wind at Vancouver is usually to the west.

The rotary spectrum of the winds from Sand Heads computed by Chang (1976) is shown in Figure 10.4. A rotary spectrum of a vector process, say $\underline{u}$, is obtained by resolving each frequency component of the discrete Fourier transformed vector $\underline{u}$ into two other components, one of which rotates with a positive frequency (anti-clockwise) and the other with a negative frequency (clockwise). This gives a pair of spectra representing the respective tendency of the process to move in an anti-clockwise or clockwise sense. (The reader is referred to Chang (1976) or Mooers (1973) for a comprehensive discussion of rotary current spectra.) Notice that a plot of the spectrum multiplied by the frequency $(f \circ S)$ against the logarithm of the frequency is variance preserving; that is, the area under the curve is directly proportional to the variance.

In the present case, Figure 10.4 indicates the cyclonic tendency of the wind. The spectra are broadly peaked about 3-5 days but the wind has significant energy to periods as large as 25 days. Approximately 10 percent of the variance is contained in the 10-20-day band and one-third of the variance is in periods exceeding 7 days.

Some results of Chang's analysis of GS currents are presented in Figures 10.5-10.8. The current records examined were collected at stations H06, H16 and H26 as shown in Figures 10.1 and 10.5. Meters were positioned at 3, 50 and 200 m at the western (H06) and central (H16) locations and at 3, 50 and 140 m in the east (H26). Chang did not analyze records from the near surface instruments. Most of the current records were obtained with Aanderaa Model 4 current meters, but several Geodyne Model 850 meters were employed. The currents were sampled either every 10 (Aanderaa) or 15 (Geodyne) minutes. A subsurface buoy mooring was used for the initial year of the experiment, but was replaced thereafter by a surface buoy, taut-rope mooring. Although the threshold level of these meters is 1.5 cm s^{-1}, this presents minimal difficulties in the detection of small, low-frequency currents since stronger tidal currents were superposed on these fluctuations.

The mean currents computed over the 18-month period are shown in Figure 10.6. There are two significant features. The first is the strong, cross-channel flow at the 50-m central location, and the second is the very strong current found at 140 m in the east. The mean speed there is five times greater than that found at the other deep locations, while the root mean square velocity is twice as large. In the east and the west, both shallow and deep currents are closely aligned with the local topography.

Figure 10.7 shows the current spectra obtained by summing the respective positive and negative parts of the rotary spectra computed by

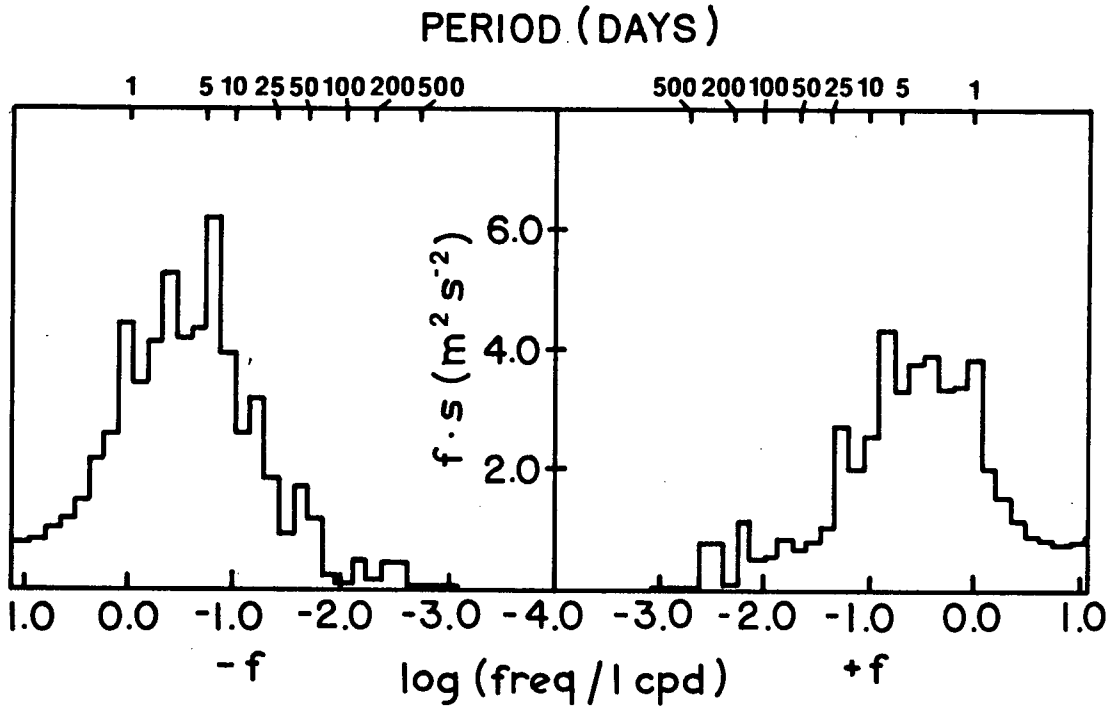

Figure 10.4 Rotary spectrum of the winds at Sand Heads for the 600-day period beginning 3 January 1969 (from Chang, 1976).

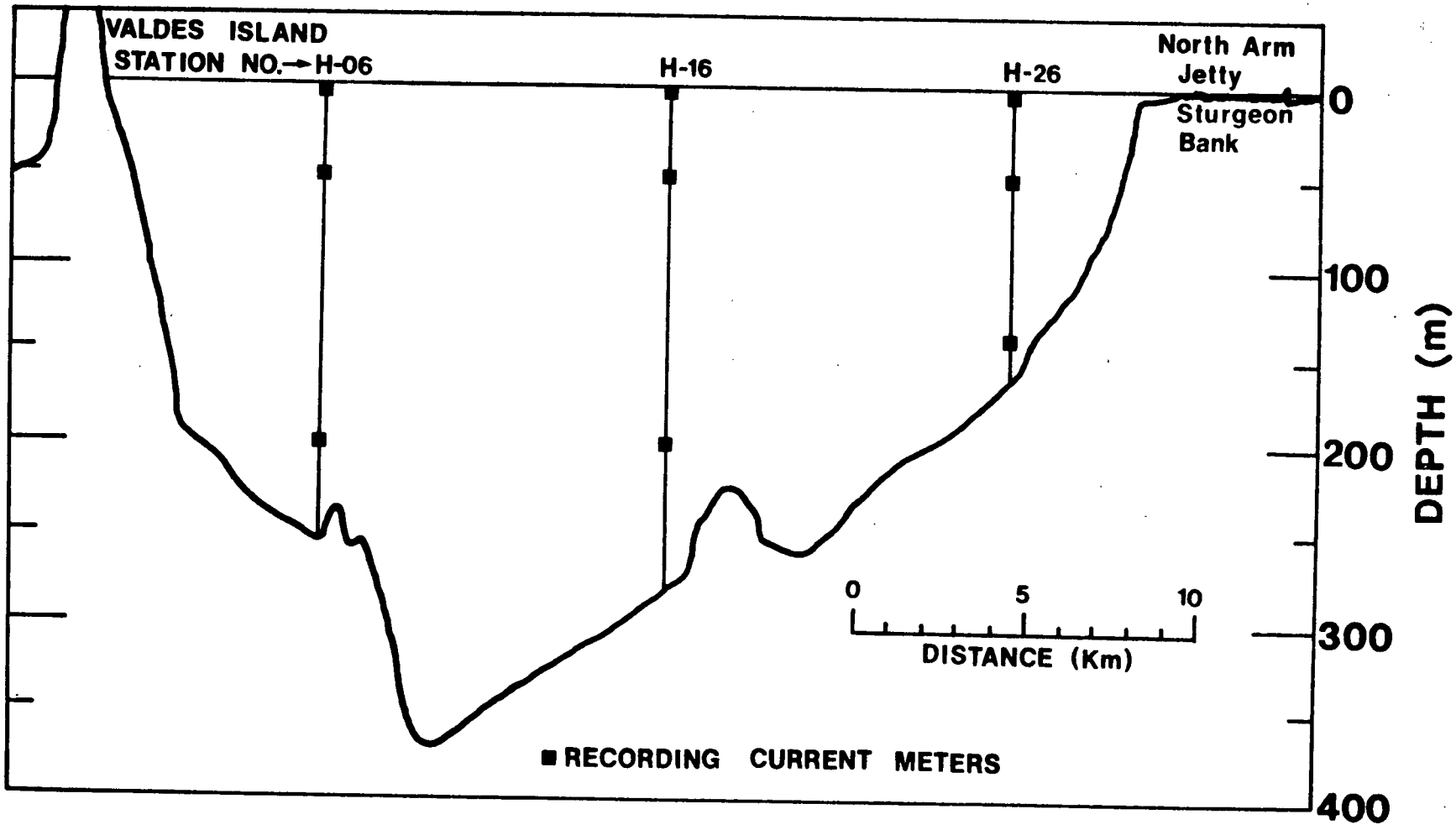

Figure 10.5 Cross section H showing placement of current meters. The moorings are spaced 10 km apart. The deep meters are (from west to east) 50, 80, and 25 m from the bottom (from Tabata et al., 1971).

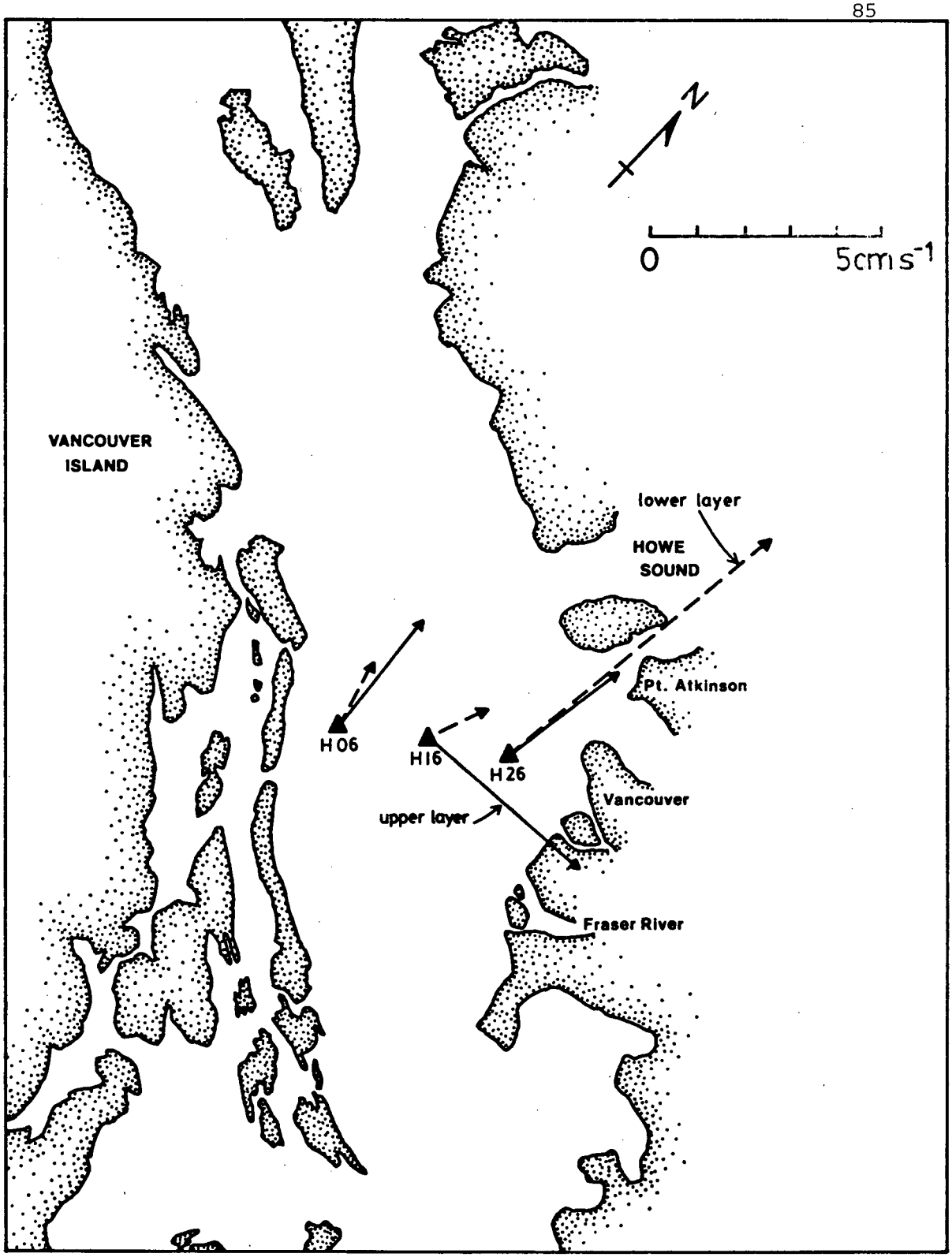

Figure 10.6 Mean currents along line H for the 533-day period beginning 16 April 1969.

Chang. The area under the curve is thus proportional to the total variance of the signal. Examination of this figure reveals the complex nature of the low-frequency currents in GS, but it must be emphasized that most of the fine structure is not statistically significant to 95%. The significant features in Figure 10.7 are: (1) the spectra are broadbanded and appear to peak about 15-25 days, and (2) in contrast to the 140-m signal from H26, the 200-m records contain little energy in comparison with the 50-m records.

Chang (1976) found that coherences between currents at positions separated both horizontally and vertically were generally small at low frequencies as is shown in Figure 10.8. The highest value of the squared coherence between vertically separated currents was observed in the east and was only about 0.3. There the upper- and lower-layer rotary velocities were nearly in phase which may be indicative of a barotropic motion. At the other locations the vertical coherence was very small and the phases were scattered; this result suggests little or no coupling between the upper and lower layers and hence implies mainly baroclinic motions there. In all cases the horizontal coherences were below the 95% noise level.

Chang also analyzed sea level, atmospheric pressure, wind, and water temperature records for the 18-month period. The temperatures were collected by the Aanderaa meters which were equipped to sample currents and temperatures concurrently. In all cases these quantities were essentially uncorrelated with the currents. The highest value of the squared coherence was found between the currents and the wind at the eastern location (about .3 for both 50 and 140 m), which suggests that the surface wind stress may be a possible forcing mechanism. It is not clear from Chang's analysis what other forcing mechanisms are important.

It is apparent, however, that the low-frequency currents must

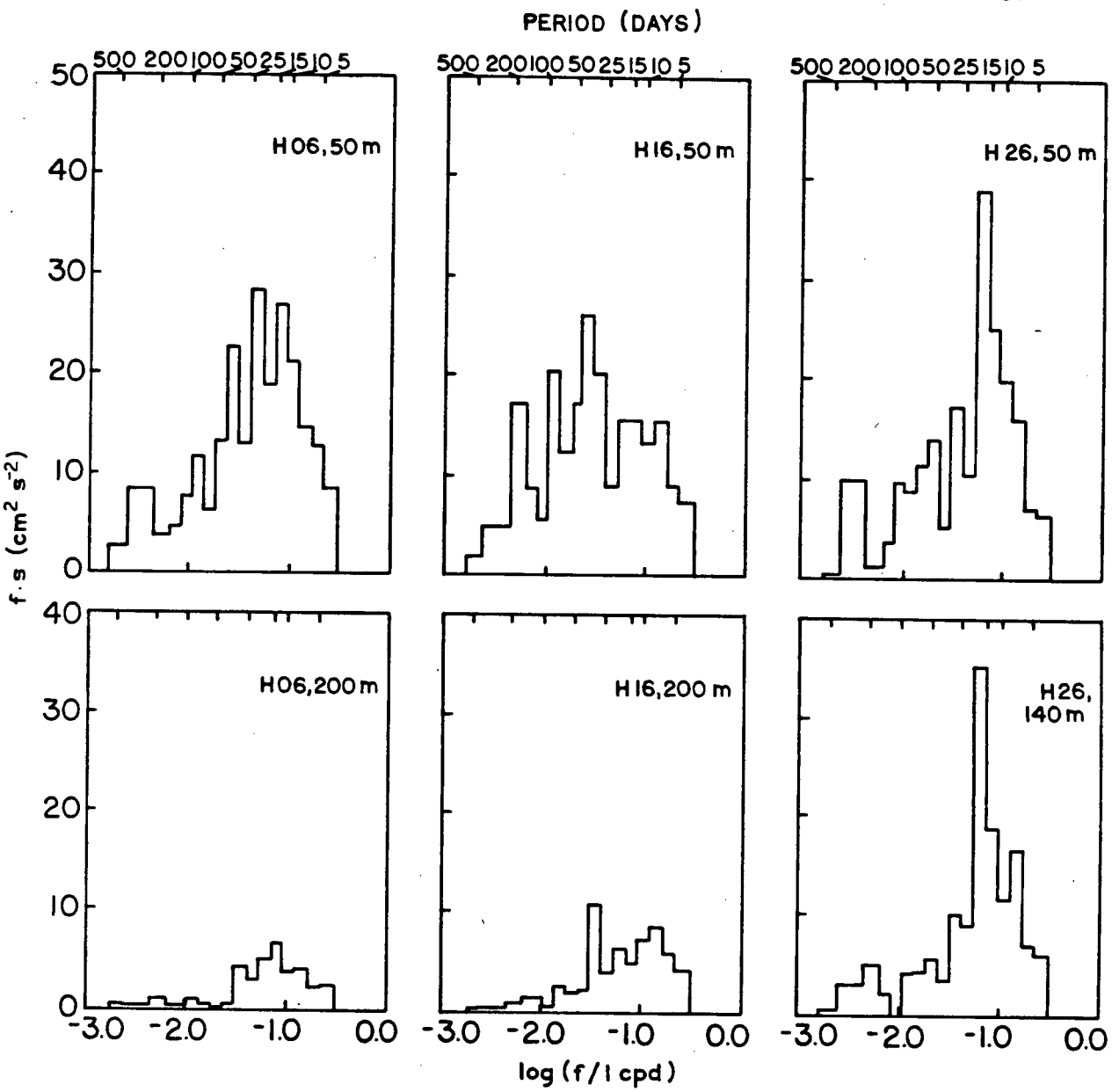

Figure 10.7 Current spectra for line H for the 533-day period beginning 16 April 1969 (adapted from Chang, 1976).

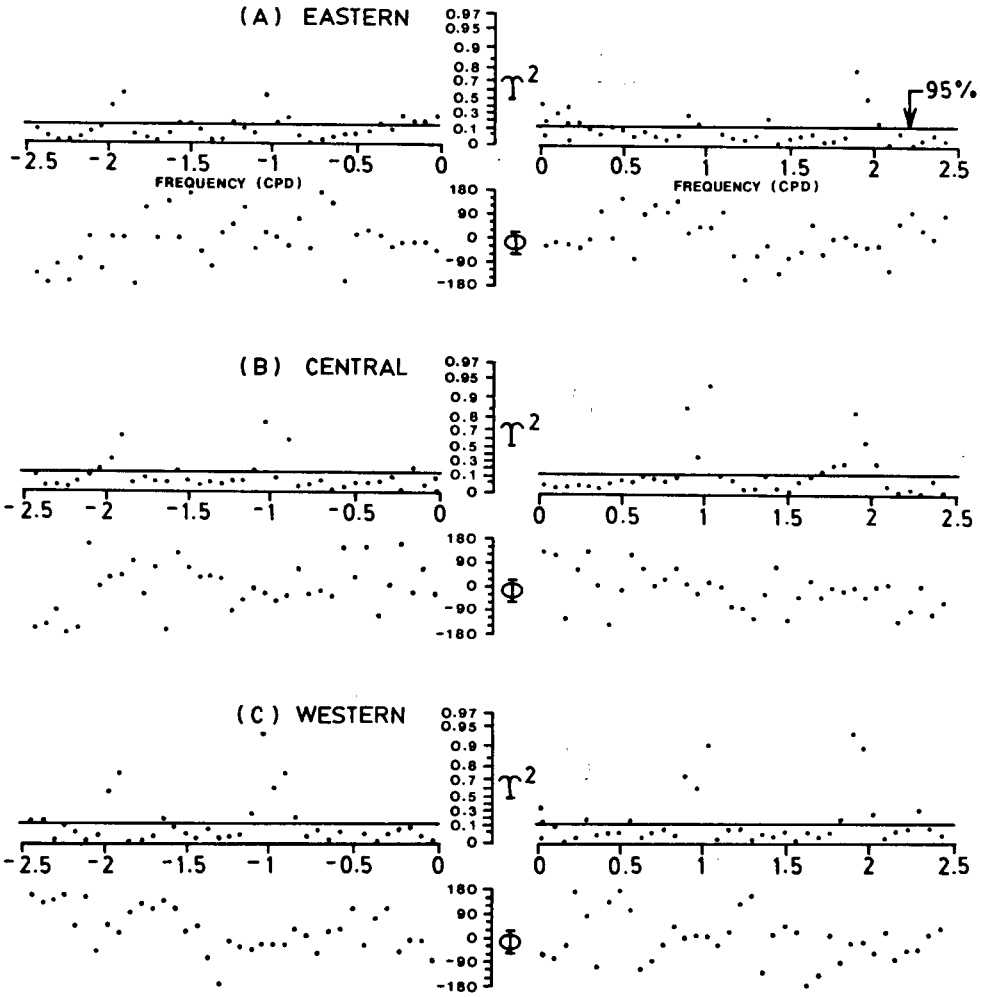

Figure 10.8A Rotary coherence and phase spectra between currents, from (A) vertically separated locations and (B) horizontally separated locations. Notice that the frequency here extends to much higher values than are discussed in the text. The solid line indicates a 95% noise level (from Chang, 1976).

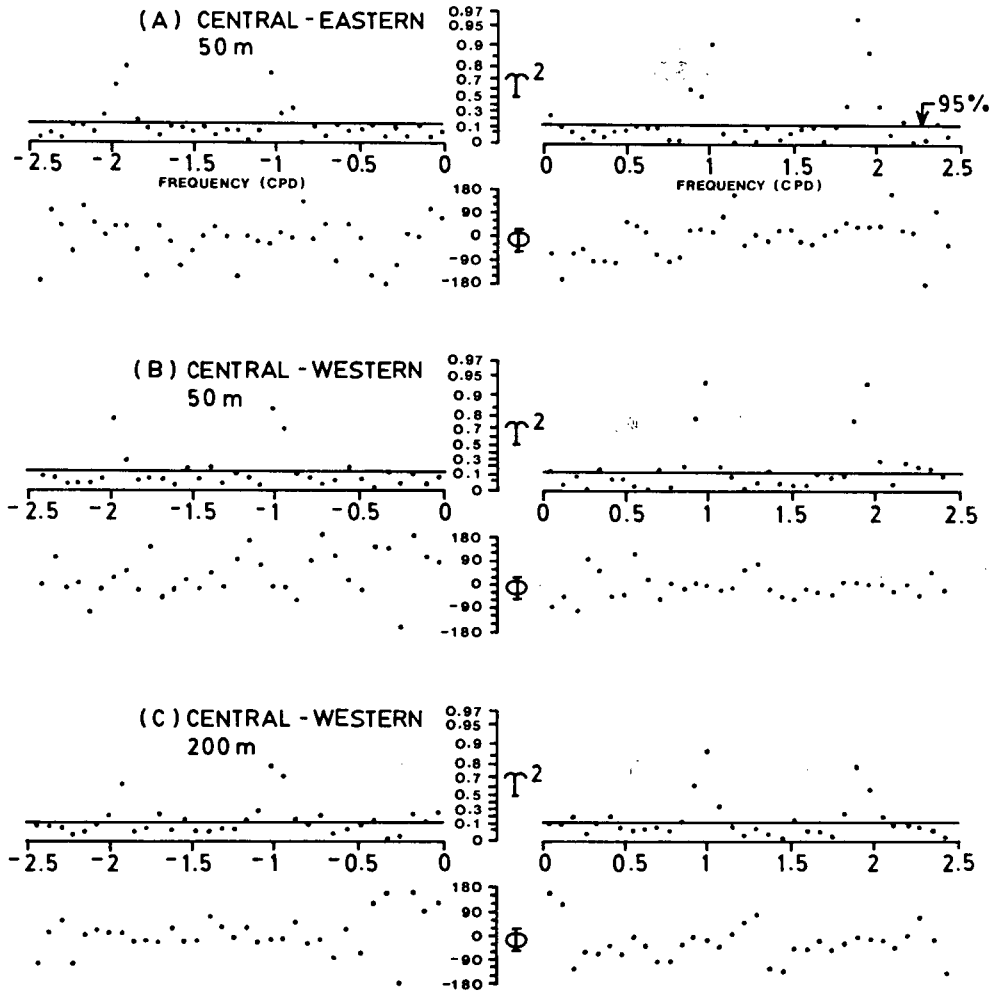
(A) CENTRAL - EASTERN
50 m
(B) CENTRAL - WESTERN
50 m
(C) CENTRAL - WESTERN
200 m
FREQUENCY (CPD)
95%
Υ²
Φ

Figure 10.8B

result from more or less continuous forcing of some kind; otherwise, friction would quickly damp out the motions. Prior to the enumeration of various possible forcing mechanisms, it is useful to consider what character the low-frequency motions might possess. First they could be wavelike. This classification includes both a superposition of plane waves (as in Part I) in which the dependence on the horizontal coordinates is separable and more complex wavetypes (eddies) in which it is inseparable. Waves could be directly forced, for example, by the wind, and move with the phase speed of the atmospheric disturbance, or they could be free and have a characteristic frequency. Moreover, waves could occur intermittently in wave packets or exist almost continuously. Possible subinertial waves include internal Kelvin and topographic planetary waves. Second, the low-frequency currents might be manifestations of transients that could be initiated by a variety of driving mechanisms. Third, they could consist of a superposition of any of these types. Finally, the motions might be describable only in statistical terms.

Any mechanism capable of altering the distribution of momentum, vorticity, or mass in the system might force the low-frequency currents. Such mechanisms include the wind stress and wind stress curl which impart momentum and vorticity, respectively, to the system through the sea surface. In addition, the wind stress may introduce anomalies into the vorticity distribution by forcing water columns across bathymetric contours, thus stretching or compressing vortex lines. Atmospheric pressure differences act in a similar manner at the sea surface. The momentum, vorticity, and mass distributions may be altered internally if the mean flow of the system is inertially unstable. In addition, nonlinear interactions between tidal constituents may result in residual flows and produce tidal stresses

analogous to the usual Reynolds stresses (Heaps, 1978). Similarly, the tides may interact with the topography to generate internal motions. Finally, freshwater influxes or intrusions of saline oceanic water result in density differences which in turn drive currents.

If the magnitude of any of these mechanisms varies in time, the resultant motions should vary in a similar fashion. Thus one might expect the spectrum of currents driven directly by the winds to be peaked about 3 to 5 days as is the wind spectrum. This notion ignores the possible importance of the spatial characteristics of the wind field, however, and it is conceivable that these motions might peak at some other frequency for which the length scales of the winds and currents were comparable. It seems unlikely, however, that the spatial scale of the wind decreases with decreasing frequency. On the other hand, a relatively modest spectral component of the wind might be capable of exciting a free wave at its characteristic frequency.

In the case of tidal forcing, any process dependent upon the strength of the tidal streams should vary with a fortnightly period. This includes the turbulent mixing that occurs in the constricted channels separating Juan de Fuca Strait from GS (Figure 10.1). Thus intrusions of intermediate density water into GS resulting from the mixing of more dense, relatively deep Juan de Fuca water with outflowing, comparatively light GS water could generate currents of fortnightly period. In fact, Herlinveaux (1957, 1969) has noted that semimonthly variations occur in the surface salinity and temperature at various locations in the Juan de Fuca-Strait of Georgia system, and that these variations are most evident near the connecting passages. Webster and Farmer (1976) have substantiated this observation from the analysis of a long timeseries of lighthouse station

data. These findings suggest that the degree of mixing depends on the tidal range and hence varies with a fortnightly period.

It is also possible that Juan de Fuca Strait and GS are dynamically coupled and that influences in one may directly or indirectly force motions in the other. Interestingly, Fissel and Huggett (1976) have shown that low-frequency current fluctuations of about a 15-day period also occur in Juan de Fuca Strait.

Motions could also be driven by one or more of the above-mentioned mechanisms. For example, the Fraser River outflow (Figure 9.1) might interact nonlinearly with the tidal currents resulting in a fortnightly modulation of the basic estuarine flow.

Finally, it is possible that a significant fraction of the observed low-frequency currents in GS can only be classified as geostrophic turbulence. That is, nonlinear interactions between both large- and small-scale motions, irrespective of their source, may be a predominate influence. Rhines (1975) has demonstrated that in a geostrophically turbulent system, small-scale fluctuations tend to evolve into larger-scale, more well-defined, planetary wavelike motions.

Clearly, this discussion of the character of the observed low-frequency currents and possible forcing mechanisms is not exhaustive. Perhaps many or all of the mentioned mechanisms play a significant role in GS dynamics. In Part II of this thesis, the inertial stability of the mean flow and the residual tidal circulation are examined in greater detail. A few comments are also made concerning the possible interaction of the tides, Fraser River outflow, and the winds.

11. Inertial Instability Models

As mentioned in Section 9, at the conclusion of a previous study (Helbig and Mysak, 1976), it was strongly suspected that inertial instability of the mean flow within GS was an agent responsible for a major proportion of the observed low-frequency energy. This belief was based on two facts. First, the phase speed of a low-frequency wave of moderate wavelength would be comparable to mean current speeds as a purely kinematic argument shows. Consider a 14-day wave of length λ. If λ is expressed in kilometres, the phase speed in cm s^{-1} is given by $.08\lambda$; this gives, for example, a value of 8 cm s^{-1} for a 100-km wave, a speed within the range of the currents. Second, based on the findings of Chang (1976), there was no apparent forcing mechanism for the fluctuations.

In particular, it was felt that the instability would be primarily baroclinic, the lateral shear of the currents playing a relatively minor role. This hypothesis was based on two premises. First, vertical shears were generally observed to be larger than horizontal shears (with the exception of the deep eastern station). Second, Helbig and Mysak (1976) showed that for an idealized model of GS, topographic planetary waves exist with frequencies that lie in the observed range for reasonable choices of the wave length. The vertical distribution of horizontal kinetic energy (i.e., that associated with the horizontal motion) for these waves was opposite to that observed. That is, the waves were bottom trapped. It was felt that perturbations of this form, perhaps initiated by the winds, might grow in time by extracting potential energy from the mean flow with a resultant enhancement of upper-layer kinetic energy.

Baroclinic Instability

Therefore, the first step in the analysis of the inertial stability of GS was to extend the model of Helbig and Mysak (1976). A two-layer system confined to a channel with a sloping bottom and with a constant mean velocity in each layer was adopted (Figure 11.1). For parameters characteristic of GS, the results below indicate that instability can occur only for a narrow band of wavelengths. The primary reason for this is the strong stabilizing effect that the narrow channel has on the system, as it limits the effective wavelength of any perturbations. It is interesting that this effect was also largely responsible for the high degree of bottom trapping found by Helbig and Mysak.

This model has been applied by Mysak and Schott (1977) and Mysak (1977) to the Norwegian current and the California undercurrent, respectively, with considerable success. Although the present development of this model was carried out independently, its details are restricted to Appendix D since the model has appeared in the literature.

The dynamics of baroclinic instability derive from the conservation of potential vorticity. The governing equations expressing this were first derived by Pedlosky (1964), and the derivation presented in Appendix D is similar although it differs in some respects. The basic state is specified by the constant currents V_1 and V_2 (see Figure 11.1) which are in geostrophic balance with the mean surface and interfacial displacements. A perturbation with initial velocities small compared with mean currents is applied to the system. If it grows in time the system is said to be unstable. The nondimensional equations governing the perturbed state are

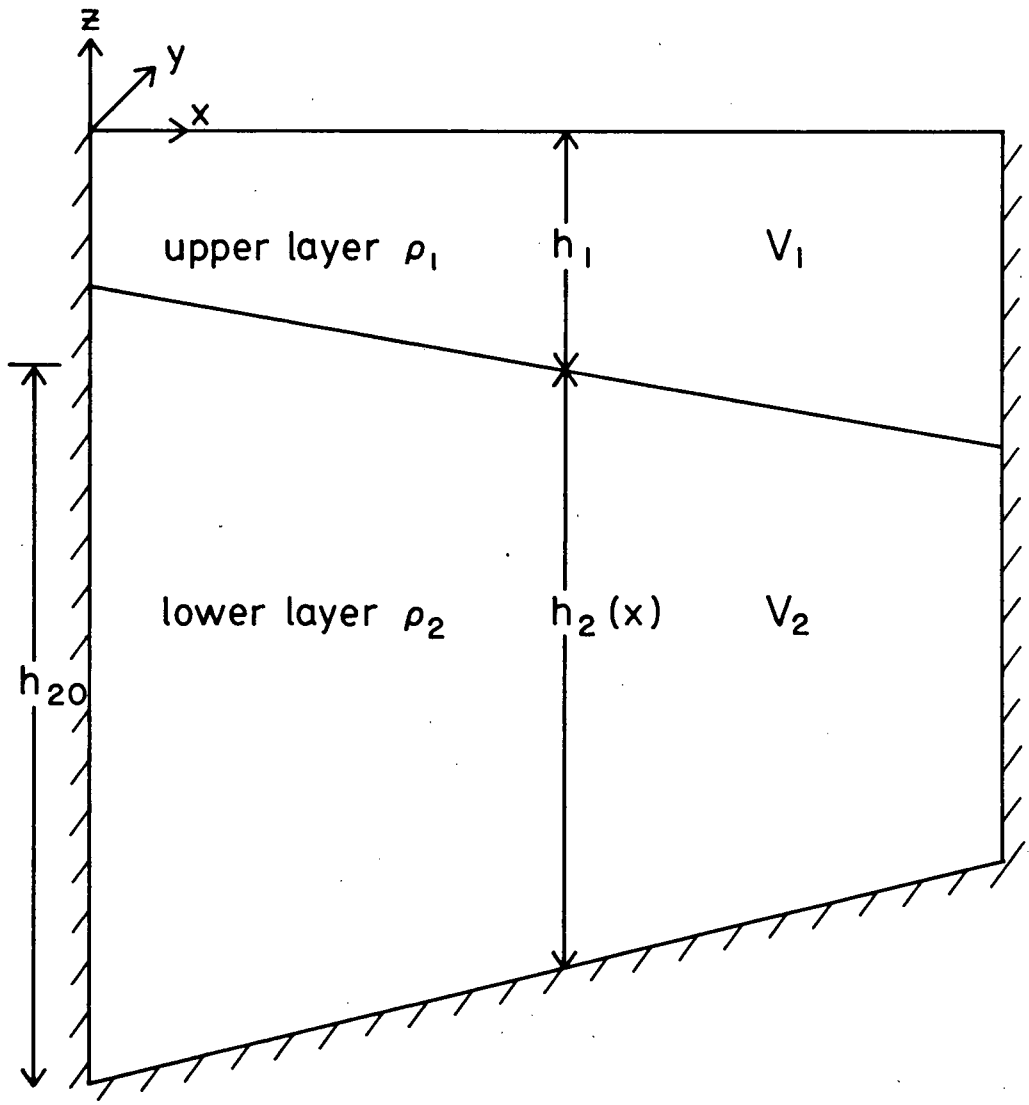

Figure 11.1 The baroclinic instability model. The sloping surface elevation and interfacial displacement are in geostropic balance with the mean currents.

$$[\partial_t + V_1\partial_y][\nabla^2\Phi_1 + F_1(\Phi_2 - \Phi_1)] - \Phi_{1y}[V''_1 - F_1(V_1 - V_2)] = 0 \tag{11.1}$$

$$[\partial_t + V_2\partial_y][\nabla^2\Phi_2 - F_2(\Phi_2 - \Phi_1)] - \Phi_{2y}[V''_2 + F_2(V_1 - V_2) + T] = 0. \tag{11.2}$$

Here Φ_1 and Φ_2 are stream functions for the perturbation velocities,

$$u_i = -\Phi_{iy} \tag{11.3}$$

(11.3)

$$v_i = \Phi_{ix} \tag{11.4}$$

where $i = 1,2$ specifies the layer, and Φ_1 and Φ_2 are defined in terms of the perturbation surface and interfacial displacements ζ_1 and ζ_2, respectively,

$$\Phi_1 = \zeta_1$$

$$\Phi_2 = \zeta_2 + \zeta_1 \,. \tag{11.4}$$

The following scale factors were used in the nondimensionalization: L for the horizontal coordinates (x,y), a typical current U for the velocities (u,v), an advective time L/U, and fUL/g and fUL/g' for ζ_1 and ζ_2, respectively. Also appearing in (11.1) and (11.2) are the layer internal Froude numbers $F_1 = f^2L^2/g'h_1$ and $F_2 = f^2L^2/g'h_{20}$ where $g' = g(\rho_2 - \rho_1)/\rho_2$ is the reduced acceleration due to gravity; T is a

topographic parameter defined by $T = -(L/R_0 h_{20})(dh_2/dx_{dim})$, and $Ro = U/fL$ is the Rossby number for the flow. The negative sign ensures that T is of the same sign as the bottom slope, and the subscript "dim" denotes a dimensional variable.

For wavelike perturbations of the form $\phi_i e^{ik(y-ct)}$, (11.1)-(11.2) reduce to

$$(V_1 - c)[\phi''_1 - k^2\phi_1] - \phi_1[V''_1 - F_1(V_1 - V_2)] + F_1(V_1 - c)(\phi_2 - \phi_1) = 0 \tag{11.5}$$

$$(V_2 - c)[\phi''_2 - k^2\phi_2] - \phi_2[V''_2 + F_2(V_1 - V_2) + T] - F_2(V_2 - c)(\phi_2 - \phi_1) = 0. \tag{11.6}$$

For constant V_1 and V_2, the solution is

$$\left.\begin{aligned} \phi_1 &= A_n \sin n\pi x \\ \phi_2 &= B_n \sin n\pi x \end{aligned}\right\} \quad n = 1,2, \ldots \tag{11.7}$$

where

$$B_n = \left[\frac{K^2 + F_1}{F_1} + \frac{V_1 - V_2}{c - V_1}\right] A_n \tag{11.8}$$

and $K^2 = k^2 + n^2\pi^2$ is the "total" wave number. If the solutions are unstable, A_n and B_n will be complex and the velocities in the upper and

lower layers will be out of phase. The phase speed is given by

$$c = V_1 + \frac{1}{2K^2(K^2 + F_1 + F_2)} \{(K^2 + F_1)(T - SK^2) - F_1SK^2$$

$$\pm ([(K^2 + F_1)(T - SK^2) + F_1SK^2]^2$$

$$+ 4F_1F_2SK^2[T - SK^2])^{1/2}\} \qquad (11.9)$$

where $S = V_1 - V_2$ is the vertical "shear." With no loss of generality, T is restricted to be positive while S may have either sign.

The ratio of the horizontal kinetic energy (HKE) per unit depth in the upper layer to that in the lower layer averaged over the area defined by the channel width and one wavelength in the y-direction is

$$R = \left|\frac{A_n}{B_n}\right|^2 = \frac{F_1^2}{(K^2 + F_1)^2} \frac{(V_1 - c_r)^2 + c_i^2}{[(V_1 - c_r) - F_1S/(K^2 + F_1)]^2 + c_i^2}. \qquad (11.10)$$

By HKE we mean the kinetic energy associated with the horizontal components of motion. An integration of (11.10) over the layer depths gives

$$\overline{R} = (h_1/h_{20})R \qquad (11.11)$$

so that $\overline{R}$ represents the ratio of the total HKE in the upper layer to that in the lower layer.

Two limiting cases are of interest. In the first we set

$V_1 = V_2 = 0$ to obtain

$$c = \frac{T(K^2 + F_1)}{K^2(K^2 + F_1 + F_2)} \tag{11.12}$$

$$R = \frac{F_1^2}{(K^2 + F_1)^2} < 1. \tag{11.13}$$

These results are essentially those obtained by Helbig and Mysak (1976) for bottom intensified, topographic planetary waves in a 2-layer channel. In the second case, we put $T = 0$ to obtain the 2-layer analogue of the classical Eady (1949) solution,

$$c = V_1 - \frac{S}{2(K^2 + F_1 + F_2)} \{(K^2 + 2F_1) \pm (K^4 - 4F_1F_2)^{1/2}\}. \tag{11.14}$$

$$R = h_{20}/h_1 \ . \tag{11.15}$$

From (11.11) we see that $\bar{R} = 1$ and the two layers contain equal amounts of HKE irrespective of their thicknesses.

In the general case, the stable solutions lie between these two extremes. For sufficiently large T, one root of (11.8) corresponds to a shear modified topographic wave while the other represents a topographically modified shear wave. Whether or not these waves are more intense in the upper or lower layer depends upon the choice of parameters. In the present case at wavelengths for which the system is stable, one wave is concentrated in each layer. Unstable waves are found to be more energetic in the upper

layer. On the other hand, for Norwegian current parameters, Mysak and Schott (1977) found unstable waves to be bottom intensified. In a recent study, Wright (1978) has treated this question in much greater detail.

From (11.9) we see that if S is positive a necessary but not sufficient condition for instability is

$$S > T/K^2. \tag{11.16}$$

The bathymetry thus acts to stabilize the flow if the bottom slopes upward to the east and is a destabilizing influence in the opposite case. This agrees with the findings of Blumsack and Gierasch (1972) for a continuously stratified system. However, this notion must be qualified, for the presence of weak topography may render a flow unstable. To see this consider a system with $F_1 = F_2$ and $K^4 = 4F_1F_2$ corresponding to a neutral Eady wave (see 11.14). Then (11.9) becomes

$$c = V_1 + \frac{3T - 8F_1S}{16F_1} \pm \frac{T^{1/2}[9T - 16F_1S]^{1/2}}{16F_1}, \tag{11.17}$$

and if $16F_1S > 9T$ (i.e., $S > 9T/8K^2$), the system is unstable with a growth rate proportional to $T^{1/2}$. DeSzoeke (1975) has studied the interaction of Eady waves with topography.

Numerical results corresponding to the general relation (11.9) are now presented. Figures (11.2) and (11.3) illustrate typical stability boundaries for the system. The former shows the stabilizing effect of a positive bottom slope. As T increases, the region of instability shrinks in size and shifts to smaller wavelengths. There are no unstable waves for

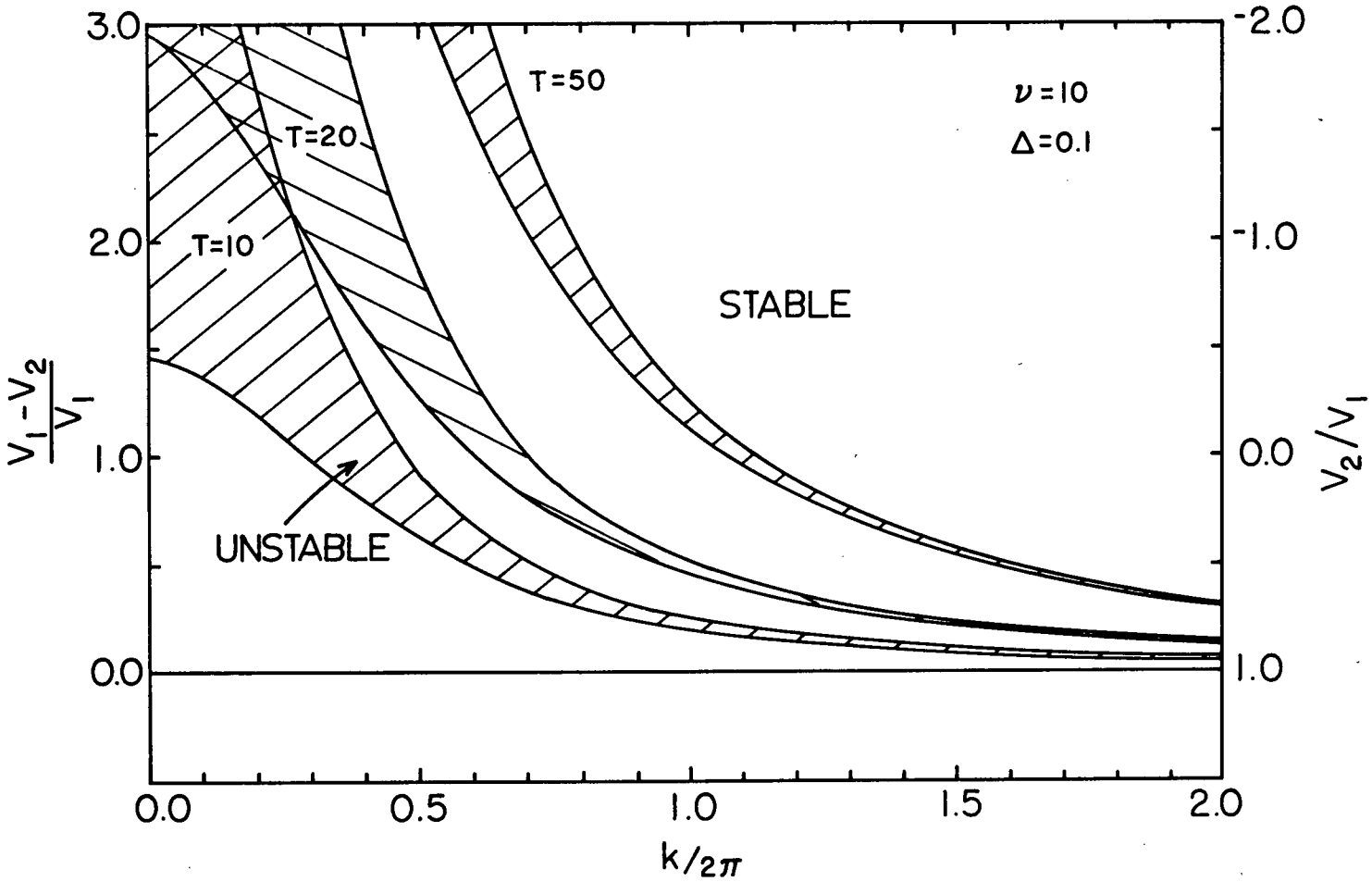

Figure 11.2 Mode 1 stability boundaries for the baroclinic model as a function of the topographic parameter T.

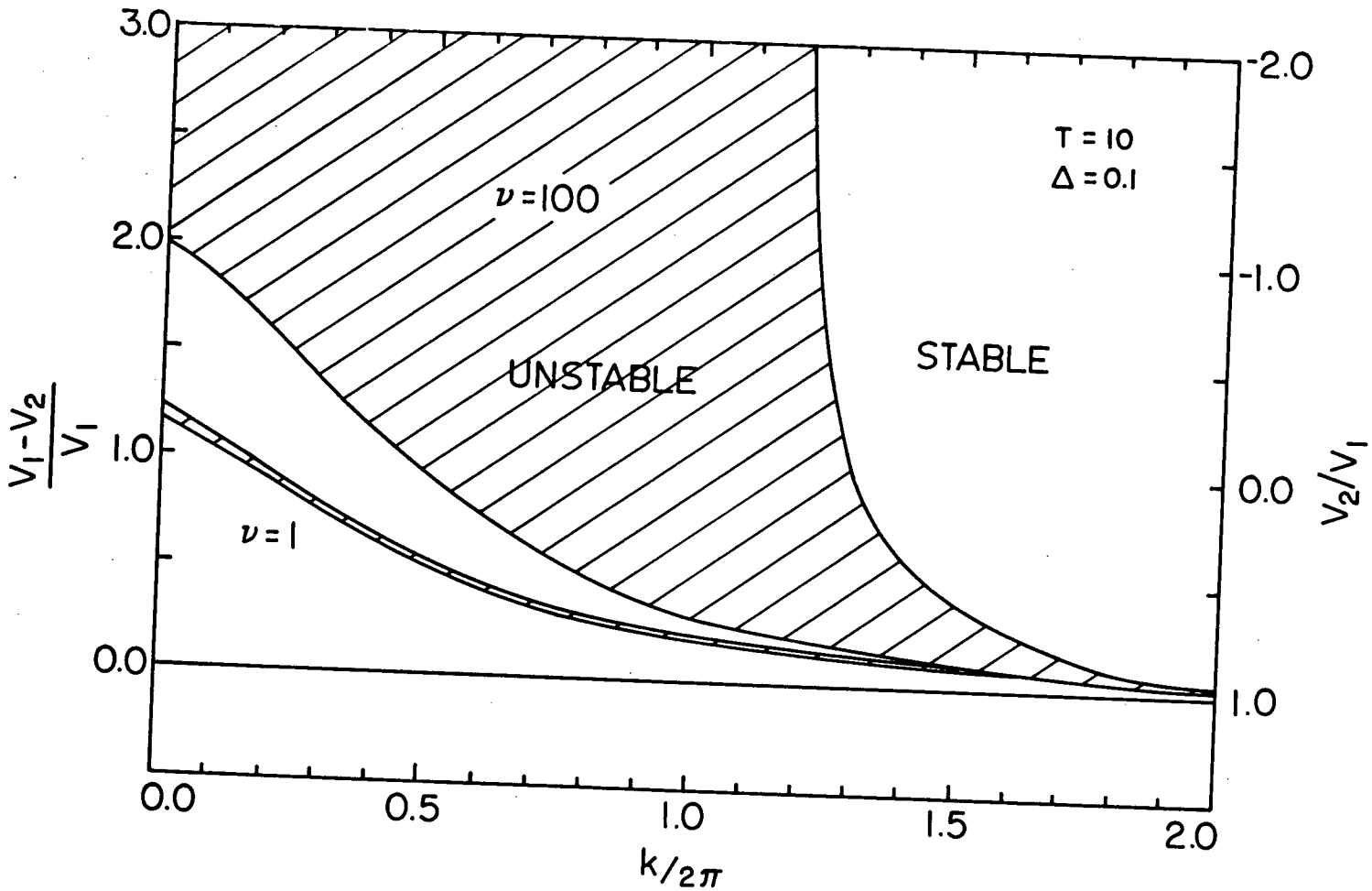

Figure 11.3 Mode 1 stability boundaries for the baroclinic model as a function of internal Froude number $\nu = F_1 + F_2$.

negative S (cf. 11.9). Figure 11.3 illustrates the dependence on the parameter $\nu = F_1 + F_2$ which may be rewritten as the square of the ratio of the channel width L to the internal Rossby radius of deformation r_i,

$$\nu = F_1 + F_2 = \frac{f^2 L^2 (h_1 + h_{20})}{g' h_1 h_{20}} = \left(\frac{L}{r_i}\right)^2 . \tag{11.18}$$

For small ν, i.e., for narrow channels or strong stratification, the region of instability is relatively narrow. As ν increases, corresponding to an increase in the channel width, a decrease in the stratification, or a thinning upper layer, this region spreads out and shifts to higher wavenumbers.

Parameters characteristic of GS are $\nu = 7.5$, $\Delta = h_1/(h_1 + h_{20}) = .14$, and $T = 7.4$ (Helbig and Mysak, 1976). (Note that $F_1 = \Delta\nu$ and $F_2 = (1 - \Delta)\nu$.) For these parameters, the first-mode dispersion curves are shown in Figure 11.4 for the cases $S = 0.5$ ($V_2 = 0.5V_1$) and $S = 1.5$ ($V_2 = -0.5V_1$). In the first case, which is generally representative of GS, the system is unstable only in the wavelength band of 40-46 km. The most unstable wave has an e-folding time of 78 days, a period of 11 days, and is intensified in the upper layer ($R = 1.3$). In the second case, in which the currents are directed in opposite directions, the first mode is unstable for all wavelengths exceeding 93 km. The most unstable wave has a period of 70 days and an e-folding time of 39 days, and is strongest in the upper layer ($R = 2.8$). The higher modes are stable in each case.

Figure 11.5 dramatically illustrates the disparate nature of the two roots of (11.9) for GS parameters. While the phase speed of the shear wave is almost independent of T, that of the topographic wave varies

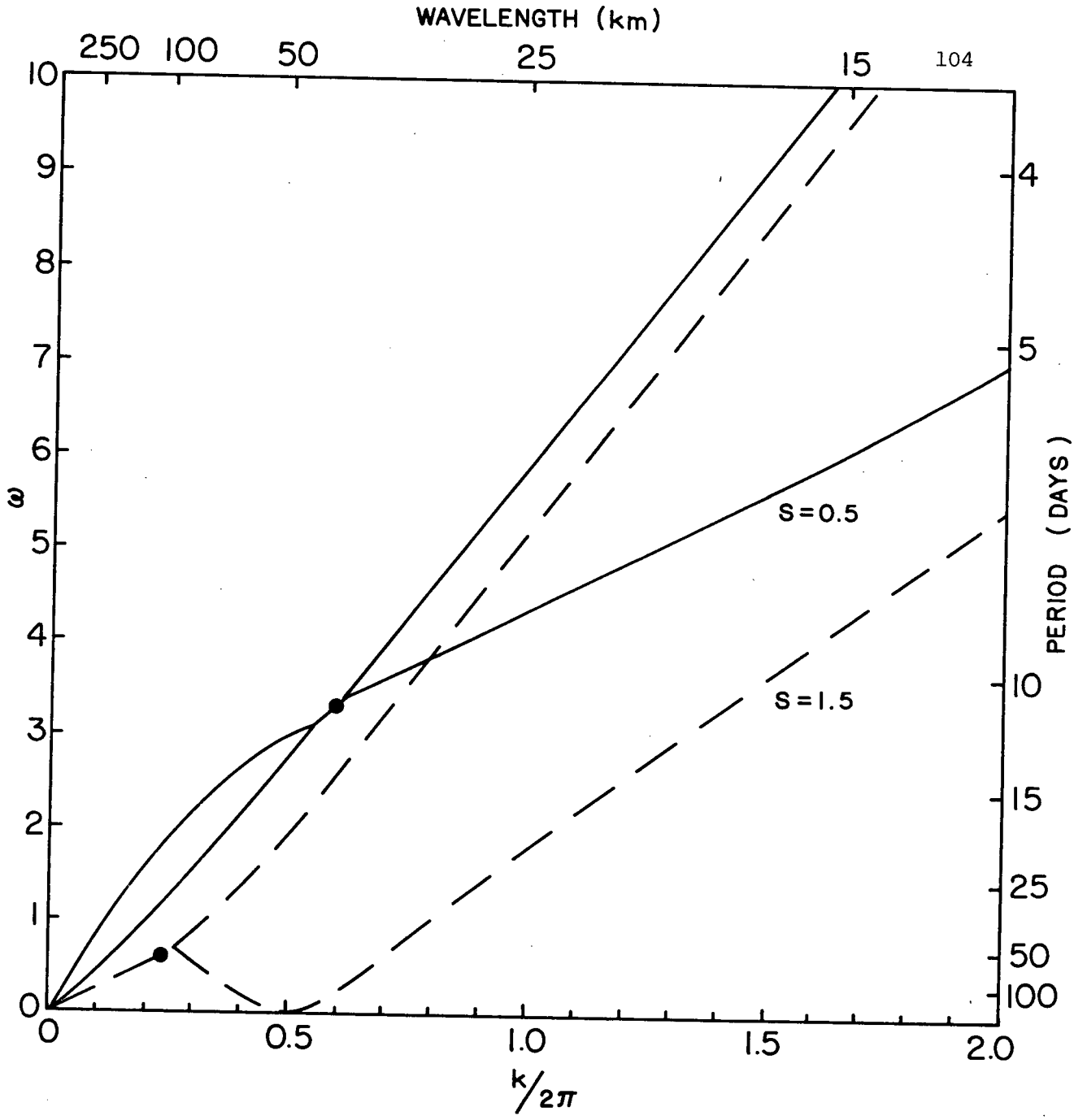

Figure 11.4 Baroclinic model, mode 1, dispersion curves for $S = 0.5$ and $S = 1.5$. The solid circles indicate the most unstable waves. The wavelength and period are calculated using the scale factors of $U = 5$ cm s^{-1} and $L = 25$ km.

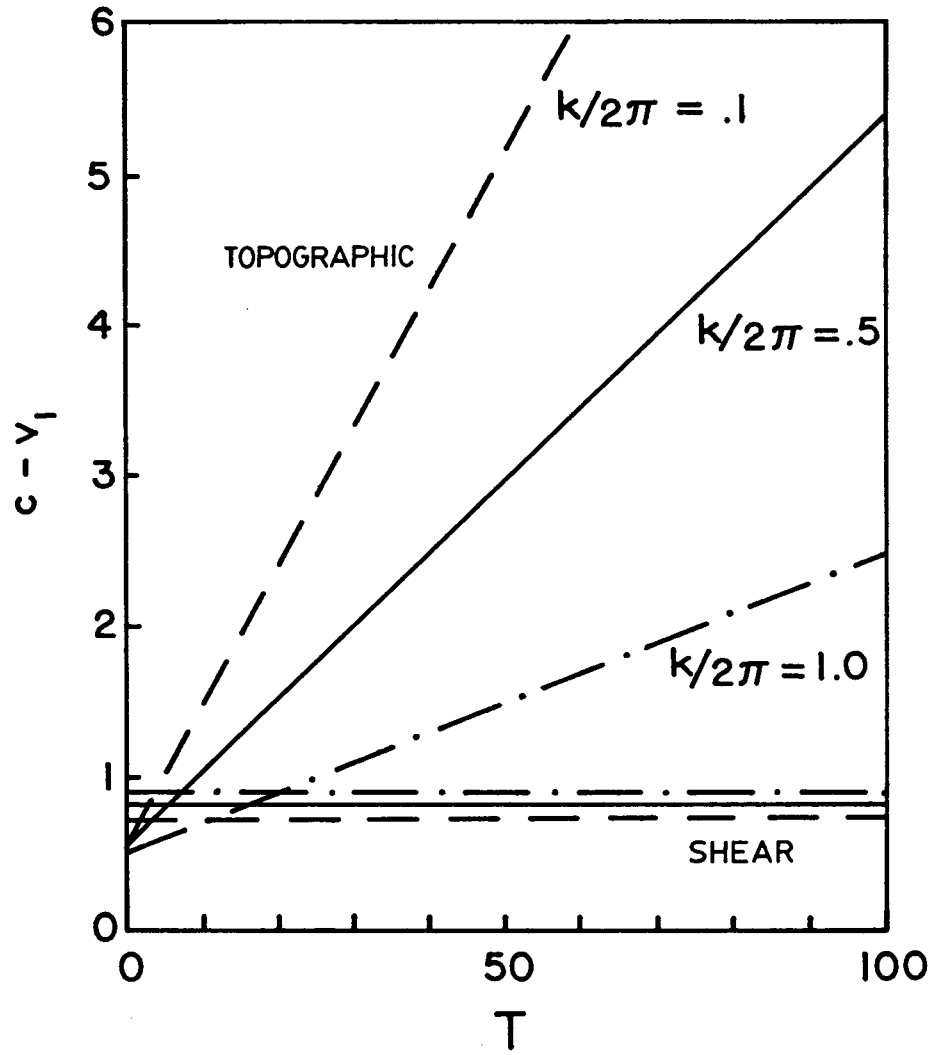

Figure 11.5 The baroclinic model, mode 1, phase speed as a function of topographic parameter for $k/2\pi$ = 0.1, 0.5, and 1.0.

linearly with T.

Barotropic Instability

A simple barotropic model is now considered in order to gain some idea of the importance of horizontal shear. The model is illustrated in Figure 11.6. Although an exponential bottom profile is chosen for simplicity, this choice does not severely limit the conclusions drawn here. Indeed, the sloping topography has little effect on the unstable waves.

The governing equations are abstracted directly from Part I; with $\varepsilon = 0$, (3.8) reduces to

$$(V - c)\left[\left(\frac{\phi'}{h}\right)' - \frac{k^2}{h}\phi\right] - \left(\frac{R_0^{-1} + V'}{h}\right)'\phi = 0. \tag{11.19}$$

We specify

$$V(x) = \begin{cases} V_1 & 0 \le x < d \\ V_2 & d < x \le 1 \end{cases} \tag{11.20}$$

and

$$h(x) = e^{2b(x-1)} \tag{11.21}$$

and thus obtain a constant coefficient differential equation in each region. As before, the boundary conditions are (cf. 3.19)

$$\phi = 0 \quad \text{at} \quad x = 0,1. \tag{11.22}$$

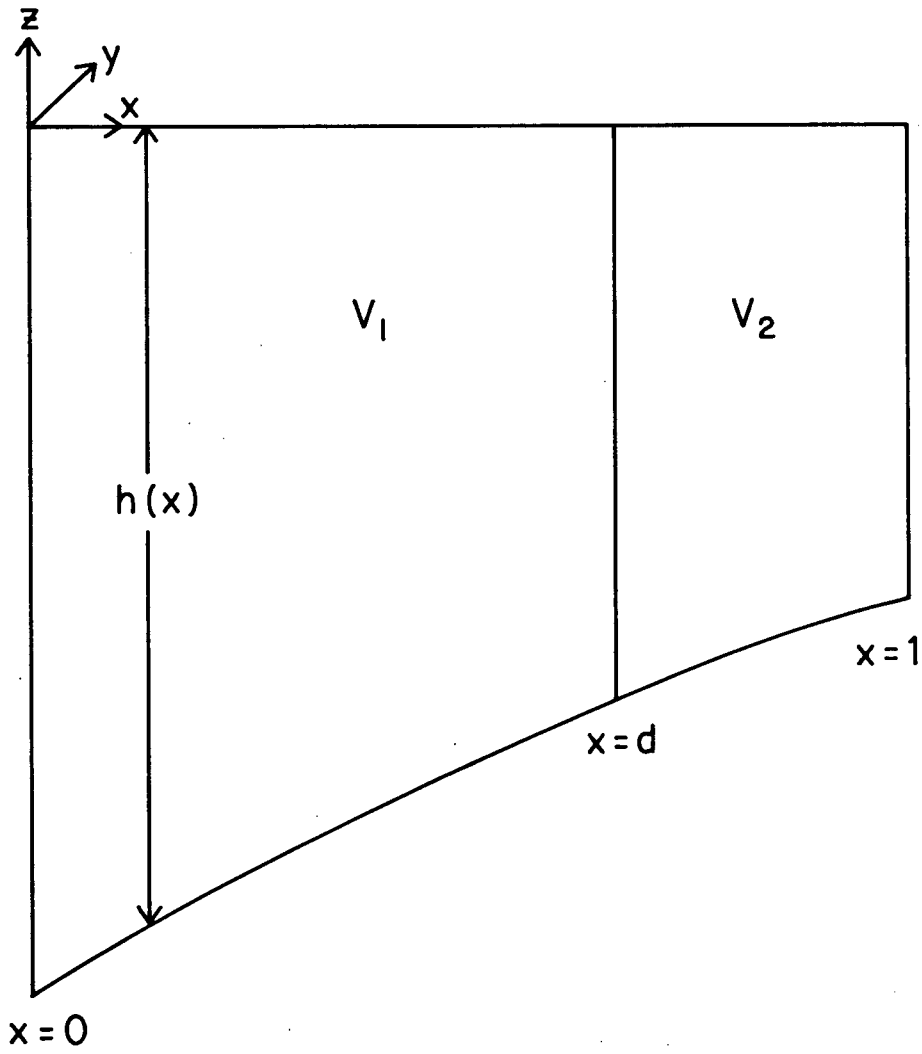

Figure 11.6 The barotropic instability model.

The solution is given by

$$\phi(x) = e^{b(x-1)}\begin{cases} A_1 \sin \lambda_1 x & 0 \leq x < d \\ A_2 \sin \lambda_2 (x - 1) & d < x \leq 1 \end{cases} \tag{11.23}$$

where

$$\lambda_i^2 = \frac{2b}{R_0(V_i - c)} - (k^2 + b^2) \qquad i = 1,2. \tag{11.24}$$

In order that the normal fluxes of mass and momentum be continuous at the material interface centred at $x = d$, $\phi(x)$ must satisfy

$$\left[\frac{\phi}{V - c}\right] = 0 \tag{11.25a}$$

$$[(V - c)\phi' - V'\phi] = 0 \qquad \text{at } x = d. \tag{11.25b}$$

(These relationships are derived in LeBlond and Mysak, 1978; p. 429. However, (11.25b) differs from their (45.9) since they effectively assumed that ϕ is continuous. In the present case it is not, and one must proceed from the integral relationship preceding their (45.9).) Application of these conditions leads to the implicit dispersion relation

$$\frac{(V_1 - c)^2 \lambda_1}{\tan \lambda_1 d} - \frac{(V_2 - c)^2 \lambda_2}{\tan \lambda_2 (d - 1)} - b[(V_1 - c)^2 - (V_2 - c)^2] = 0. \tag{11.26}$$

Several limiting cases are of interest. In the first we put $V_1 = V_2$ to obtain $\tan \lambda_2 d = \tan \lambda_2 (d - 1)$ which has the solution $\lambda_2 = n\pi$ independent of d. This gives

$$c = V_2 - \frac{2b}{R_0(k^2 + b^2 + n^2\pi^2)} \tag{11.27}$$

which is the dispersion relation for a free continental shelf wave in a mean current V_2 (cf. 5.21). In the second case we put $b = 0$ to obtain

$$c = \frac{V_1 + QV_2}{(1 + Q)} \pm \frac{iQ^{1/2}}{1 + Q} |V_1 - V_2| \tag{11.28}$$

where $Q = -\tanh kd/\tanh k(d - 1)$ and is positive. These waves travel at a speed given by a weighted average of the mean currents and grow in time at a rate proportional to the shear. Finally, in the short wave limit of $k \to \infty$, (11.26) reduces to

$$c = \frac{V_1 + V_2}{2} \pm i \frac{(V_1 - V_2)}{2} . \tag{11.29}$$

Equations (11.28) and (11.29) represent a pair of shear waves, one of which is unstable and another which decays in time.

As these special cases suggest, there are at most three solutions to (11.26). For nonzero b and S, where $S = V_2 - V_1$, there exist a pair of complex roots for all k, corresponding to amplified and damped modified shear waves. Provided that both λ_1 and λ_2 are real, a third, real root exists and represents a shear modified CSW. This restriction may be expressed as

$$c > V_{1,2} - \frac{2b}{R_0(k^2 + b^2)} \quad . \tag{11.30}$$

The region in k, S space in which CSW's exist is shown in Figure 11.7. Along the line $V_1 = V_2$ only a CSW is found.

To determine a value of S appropriate to GS, the mean currents along line H were depth averaged as

$$u_{BT} = \frac{[h_1 u_1 + h_2(x) u_2]}{[h_1 + h_2(x)]} \; ; \tag{11.31}$$

h_1 was chosen as 50 m and h_2 was determined for each mooring. The results are shown in Figure 11.8. A reasonable choice is $V_2 = 1.0$, $V_1 = 0.5$ (with a scale velocity of 5 cm s^{-1}), d = 0.66, and b = - 0.3. The dispersion relation for these values is shown in Figure 11.9. It is seen that a CSW exists for wavelengths greater than 55 km. An unstable shear wave of 15-day period has an e-folding time of about 8 days, a phase speed of about 4 cm s^{-1} and a wavelength of 44 km. It is possible therefore that a shear instability of this type might play some role in GS dynamics. However, in the next section it is shown that the motions in the 15-day band are predominantly nonwavelike in the sense of the waves studied here. This implies shear instability is of limited importance in GS.

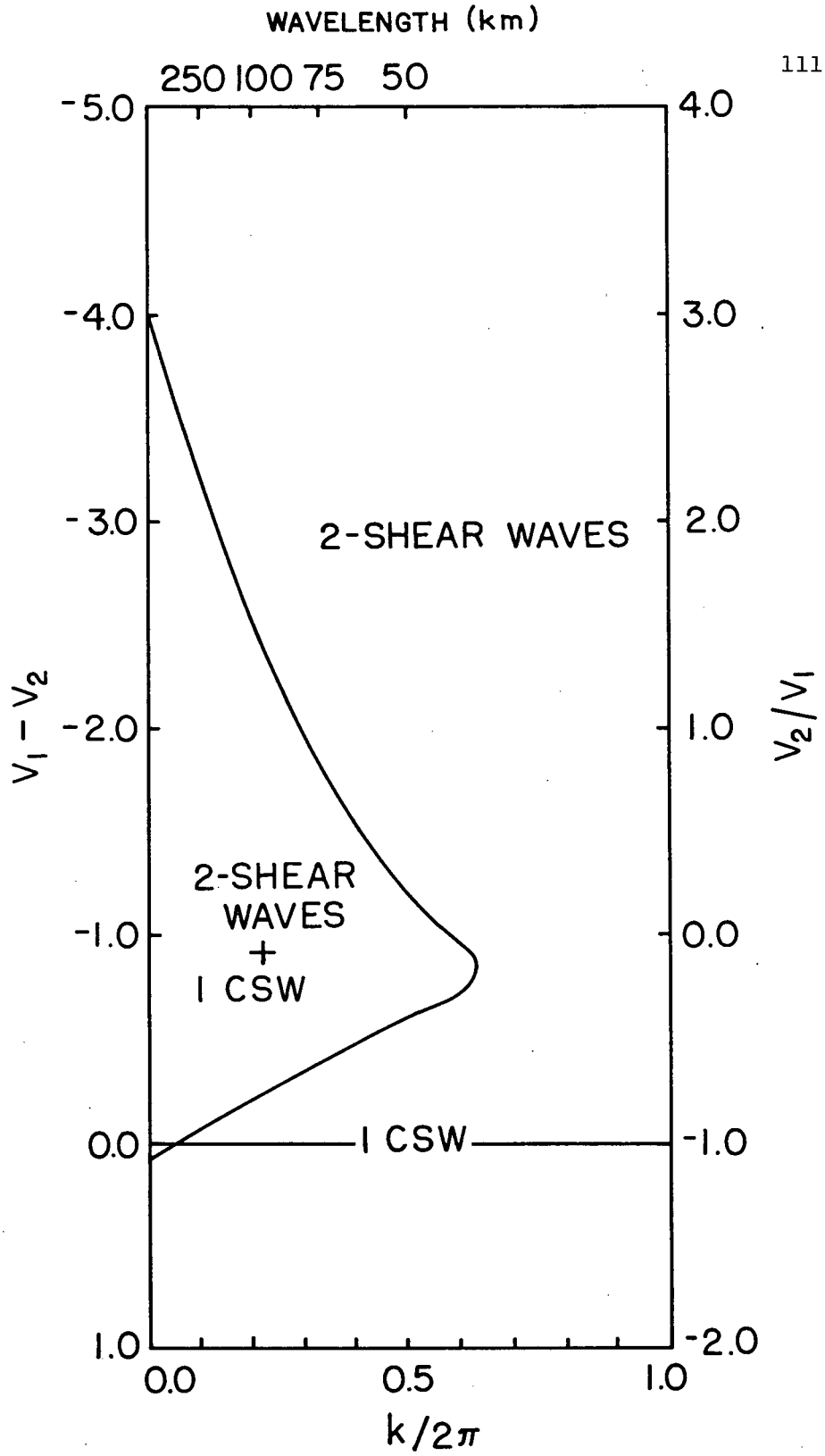

Figure 11.7 The region in (k,S) space in which continental shelf waves exist.

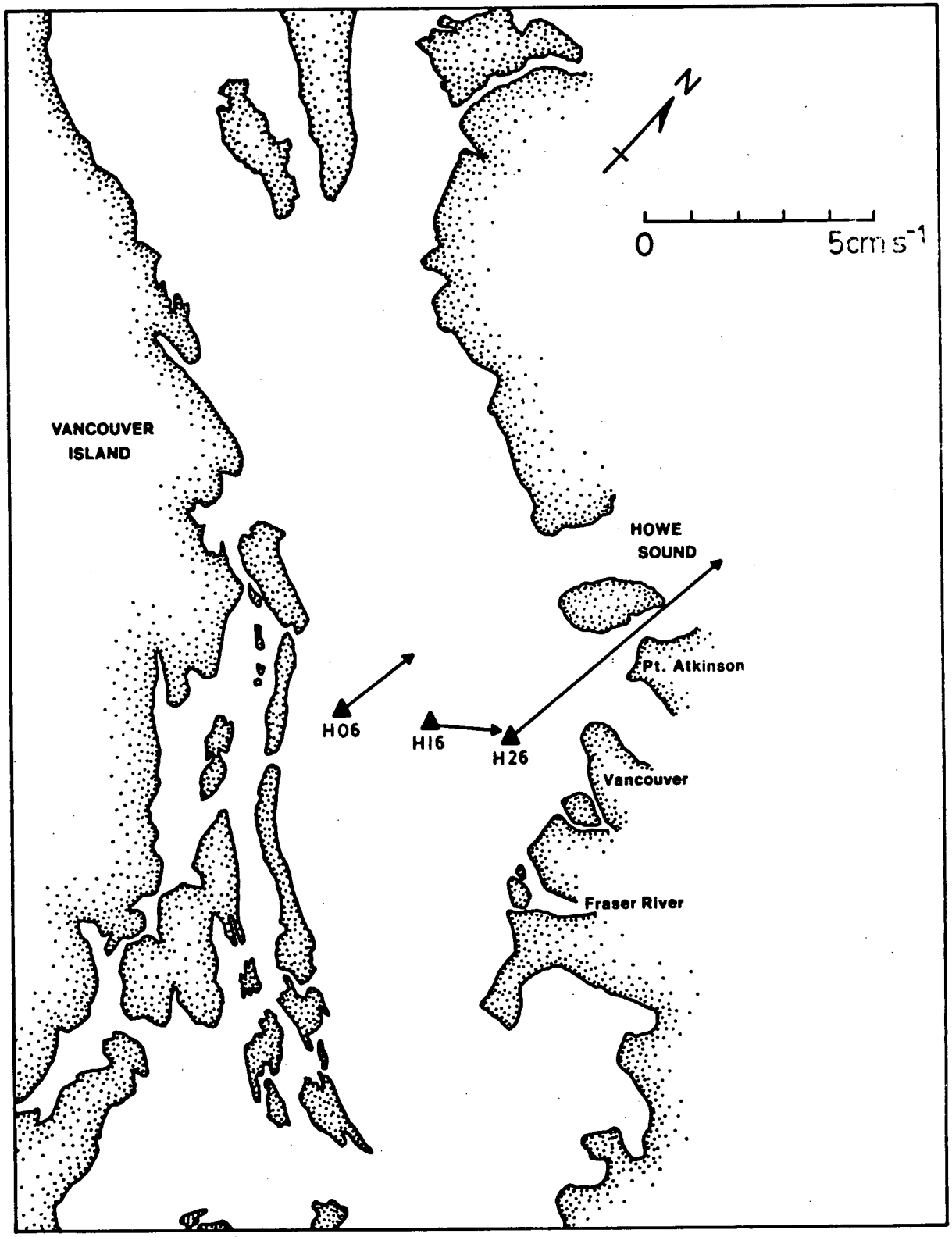

Figure 11.8 Computed barotropic mean currents along line H for the 18-month period beginning April 1969.

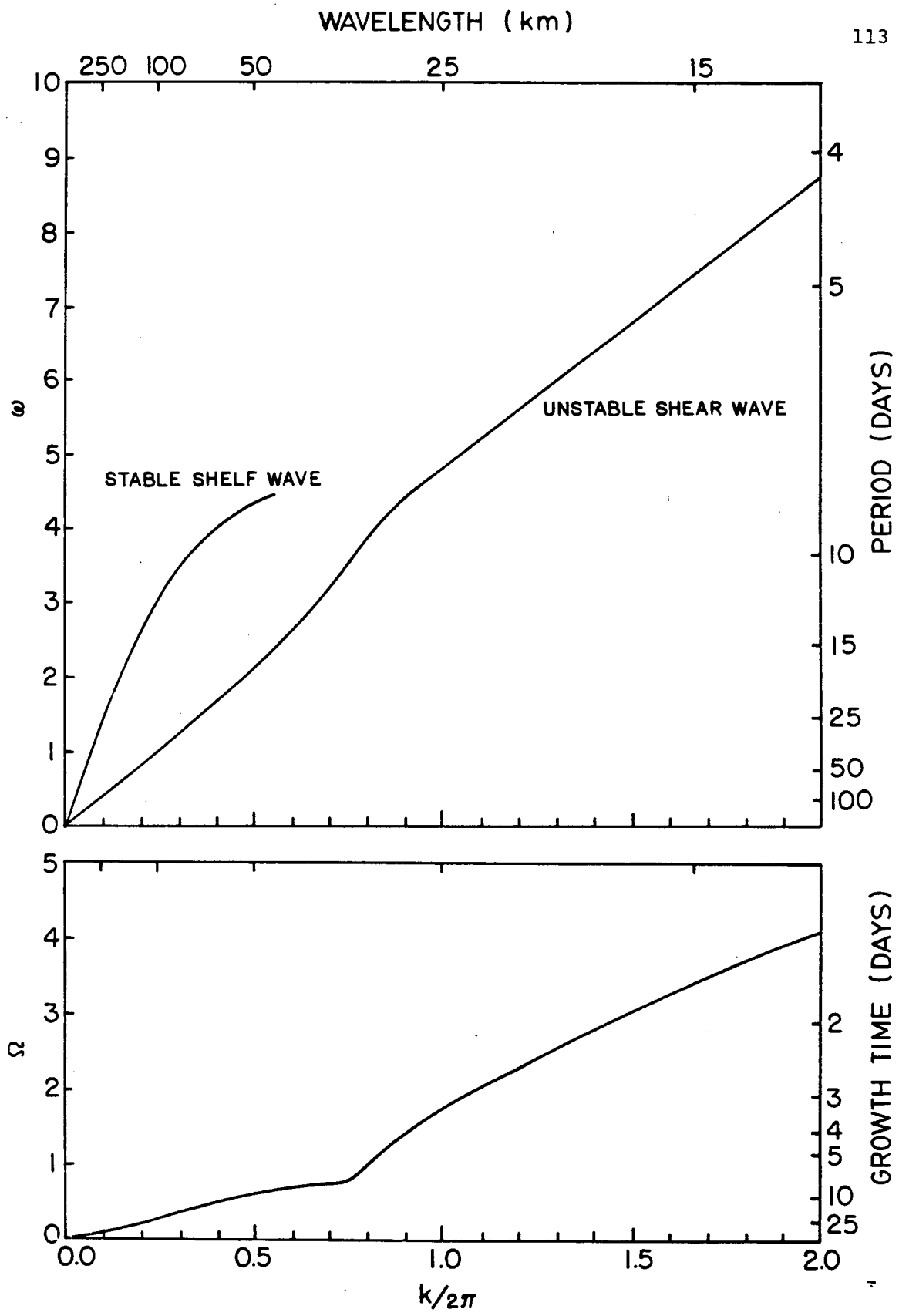

Figure 11.9 Barotropic model dispersion curves for $S = 0.5$. The growth time is defined as the e-folding time, ω is the frequency, and Ω is defined as $k \cdot \mathrm{Im}\, c$. The wavelength and period are computed using the scale factors of $u = 5$ cm s^{-1} and $L = 25$ km.

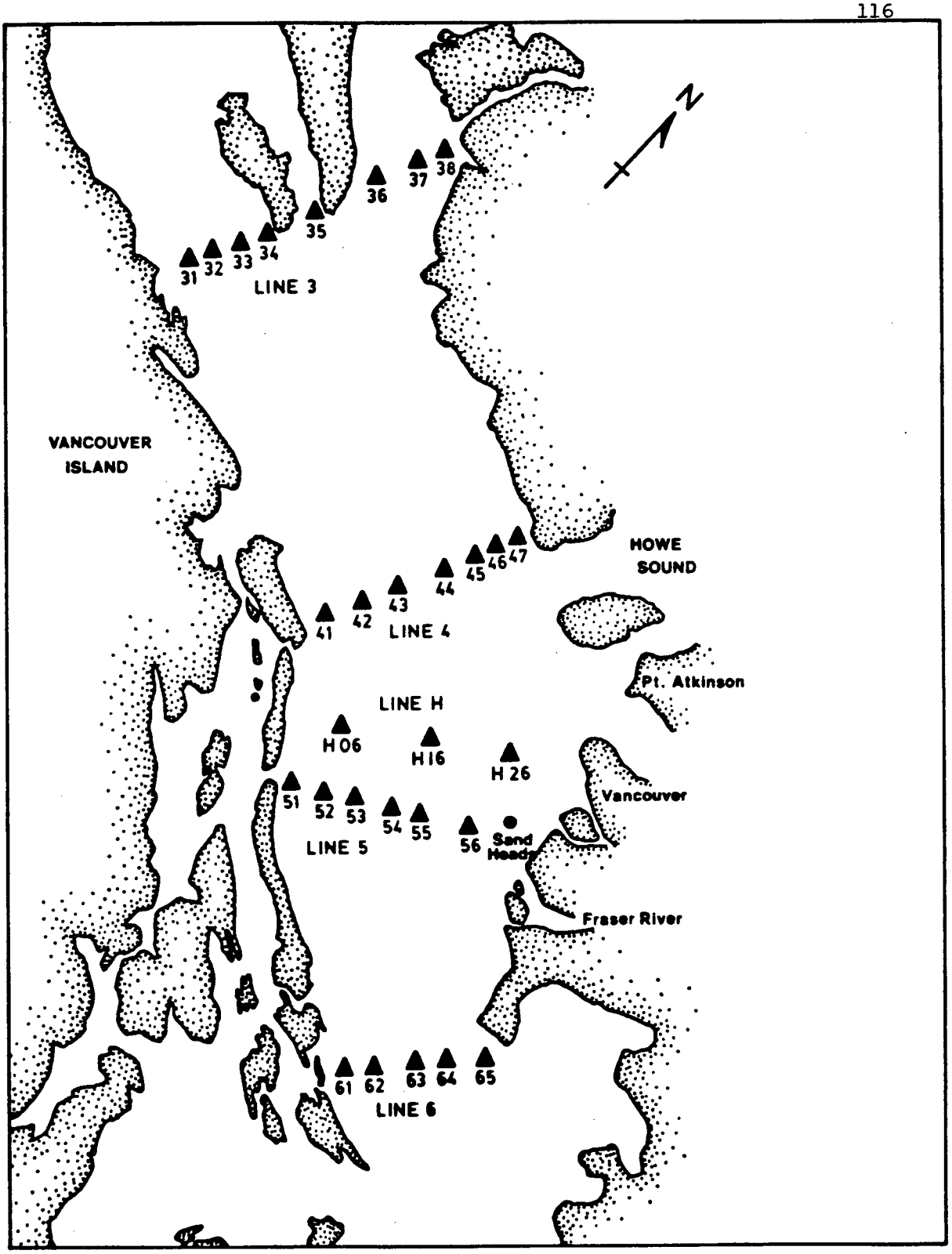

Figure 12.1 Plan view of the Strait of Georgia showing current meter locations. These lines should not be confused with those of Fig. 10.1. Winds were recorded at Sand Heads.

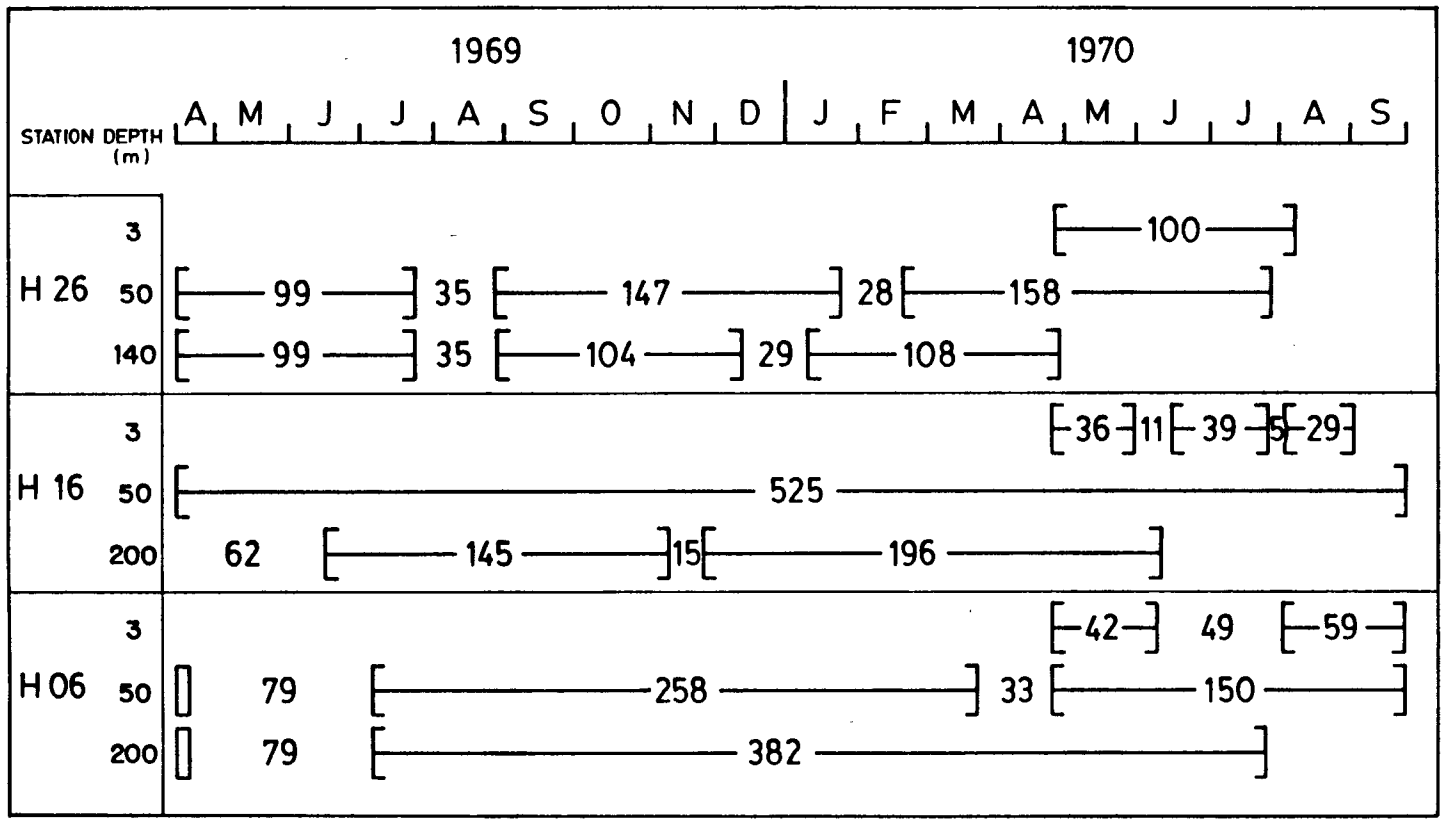

Figure 12.2A Periods of existent current meter records.

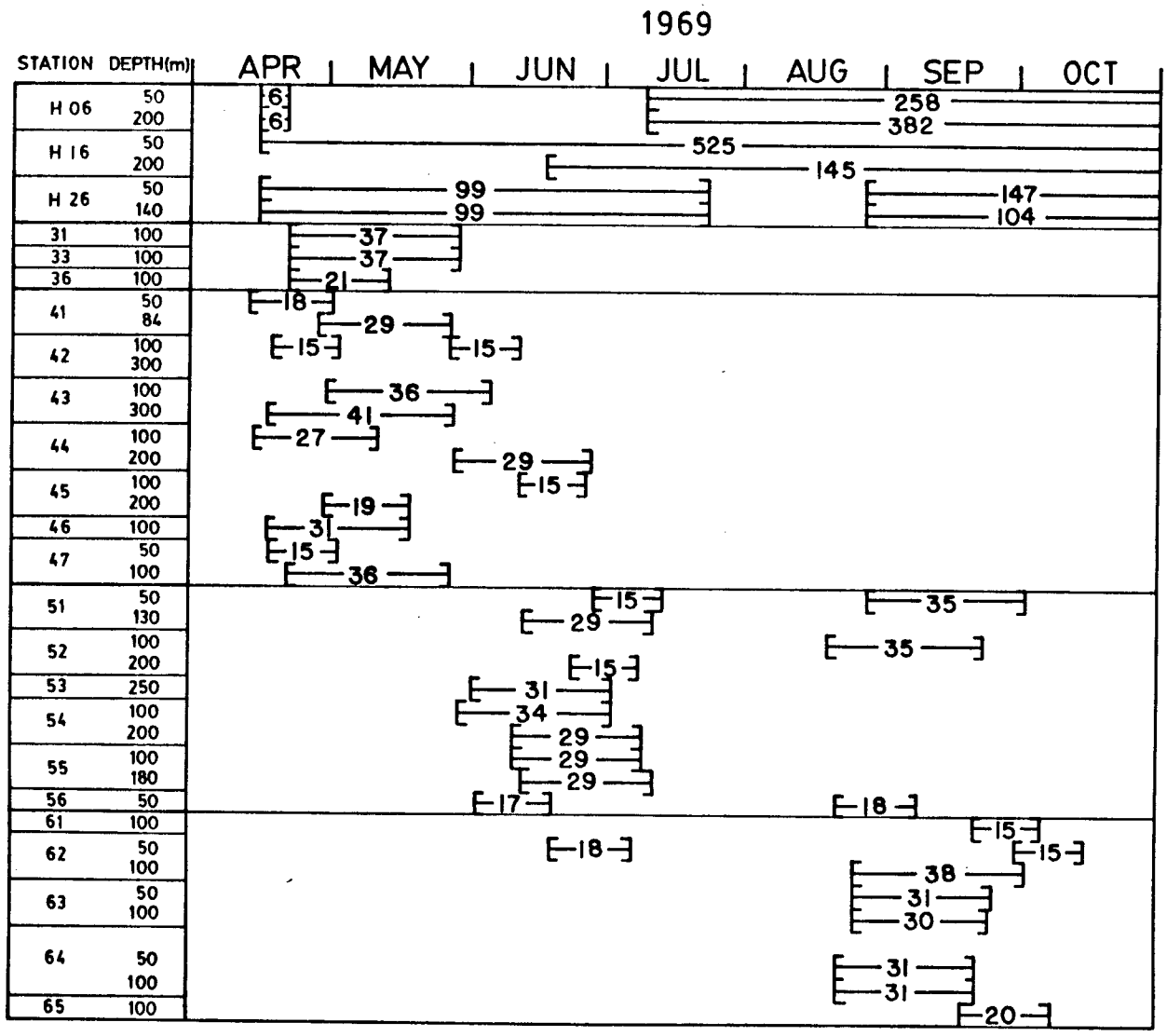
1969
STATION
DEPTH(m)
APR
MAY
JUN
JUL
AUG
SEP
OCT
H 06
50
200
H 16
50
200
H 26
50
140
31
100
33
100
36
100
41
50
84
42
100
300
43
100
300
44
100
200
45
100
200
46
100
47
50
100
51
50
130
52
100
200
53
250
54
100
200
55
100
180
56
50
61
100
62
50
100
63
50
100
64
50
100
65
100
6
6
258
382
525
145
99
99
147
104
37
37
21
18
29
15
15
36
41
27
29
15
19
3
15
36
15
29
35
35
15
31
34
29
29
29
17
18
15
18
15
38
31
30
31
31
20

Figure 12.2B

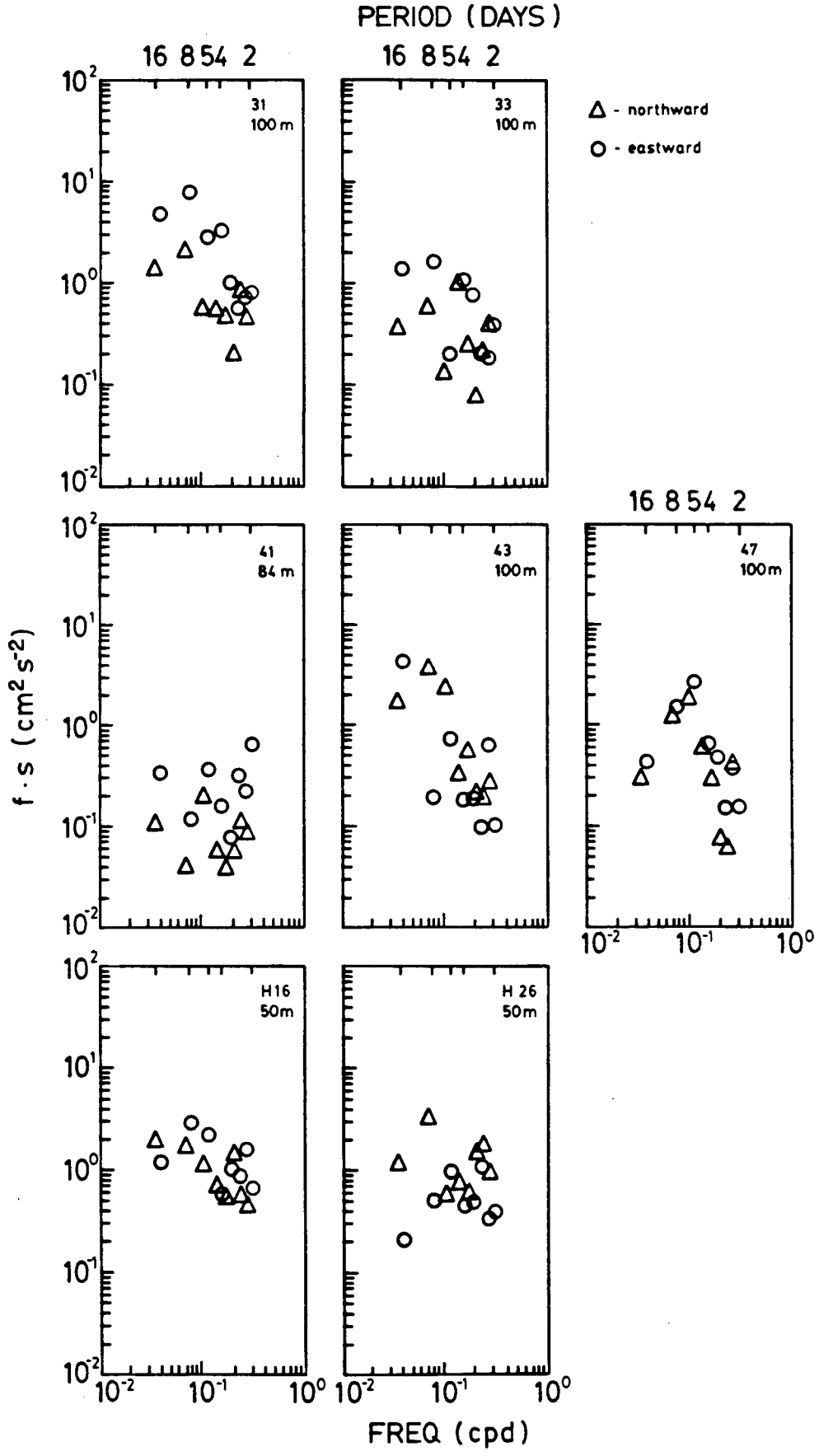

Figure 12.3A Current spectra for the 26-day period beginning (A) 2 May 1969 and (B) 29 August 1969.

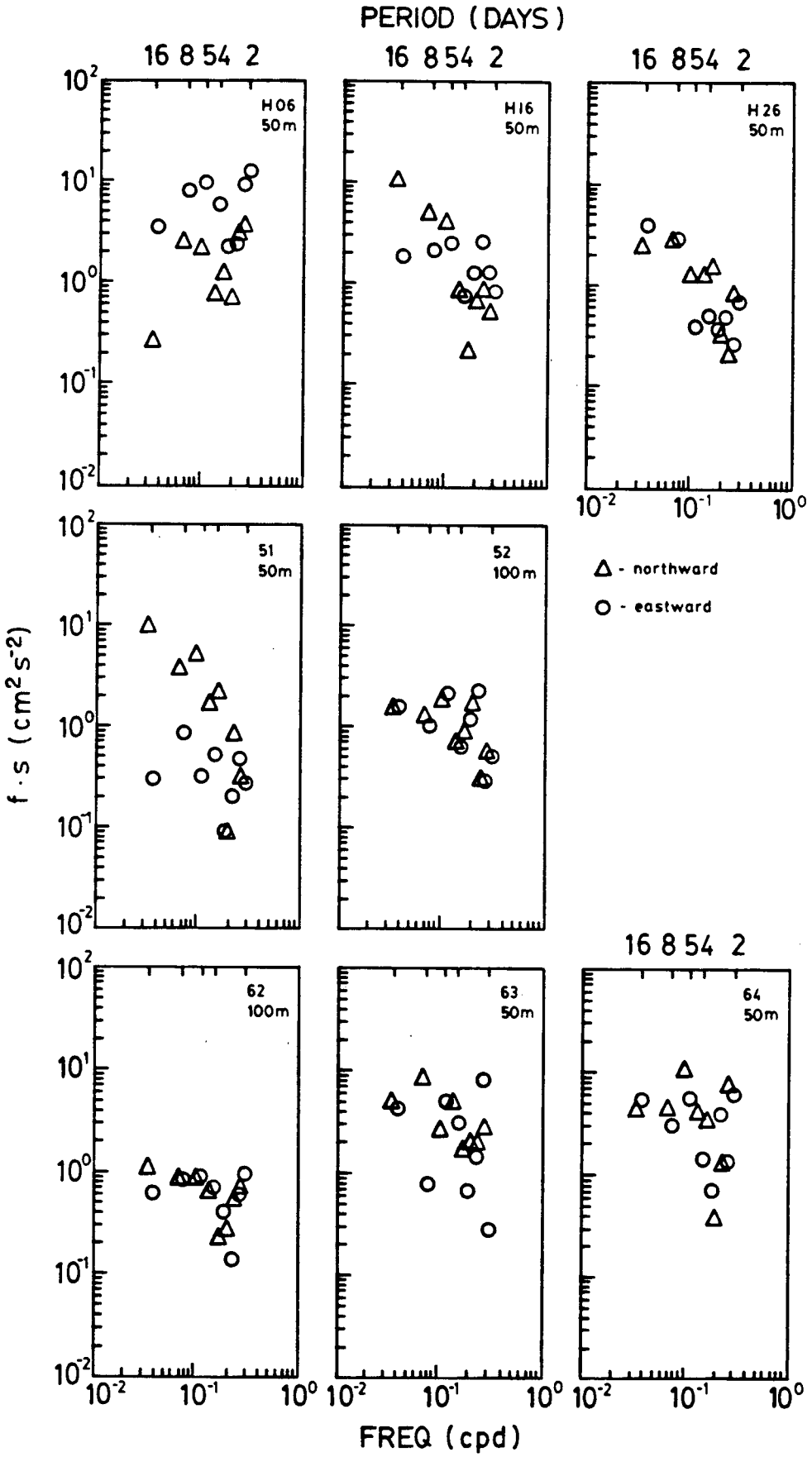
PERIOD (DAYS)
16 8 54 2
H06
50m
16 8 54 2
H16
50m
16 8 54 2
H26
50m
51
50m
52
100m
△ - northward
○ - eastward
62
100m
63
50m
16 8 54 2
64
50m
f·s (cm²s⁻²)
FREQ (cpd)

Figure 12.3B

course, none of the peaks are statistically significant to 95 percent but these spectra do indicate the existence of low-frequency energy at locations north of line H. The comparatively quiet spectrum from Station 41 may be due to the fact that the meter lies in the "shadow" of a topographic high just to its south.

Spectra computed from lines 5, 6 and H records for the 26-day period beginning 29 August 1969 are shown in Figure 12.3b. These time series were treated as above, and the spectra all indicate low-frequency energy. The record from Station 64, 50 m is of dubious quality and thus is of limited value for comparison with H26, 50 m.

Mean currents were calculated directly from the time series, and current ellipses (see, for example, Stone, 1963) were constructed from the average of the lowest two spectral bands. The ellipses are illustrated in Figure 12.4 by their major and minor axes, although in several cases, the latter is too short to be visible. Due to the statistical limitations of the data, no indication is given of either the direction of rotation of the oscillating current vector around the ellipse or of the relative phases between ellipses. Of course, the ellipse parameters are subject to contamination by trends during the period of analysis since these affect the lowest-frequency spectral estimates, and thus the ellipses calculated here must be viewed with caution. Of particular interest in Figure 12.4A is the cross-channel oscillating flow suggested at H16, 50 m and Station 43, 100 m. The pattern of mean currents illustrated in Figure 12.4B is extremely interesting since it indicates a closed, clockwise, mean circulation in the lower strait. While this may not be true for longer periods, it lends support to Waldichuck's (1957) conjecture that a gyre exists. It is, however, of the opposite sense to that indicated by Waldichuck. During this

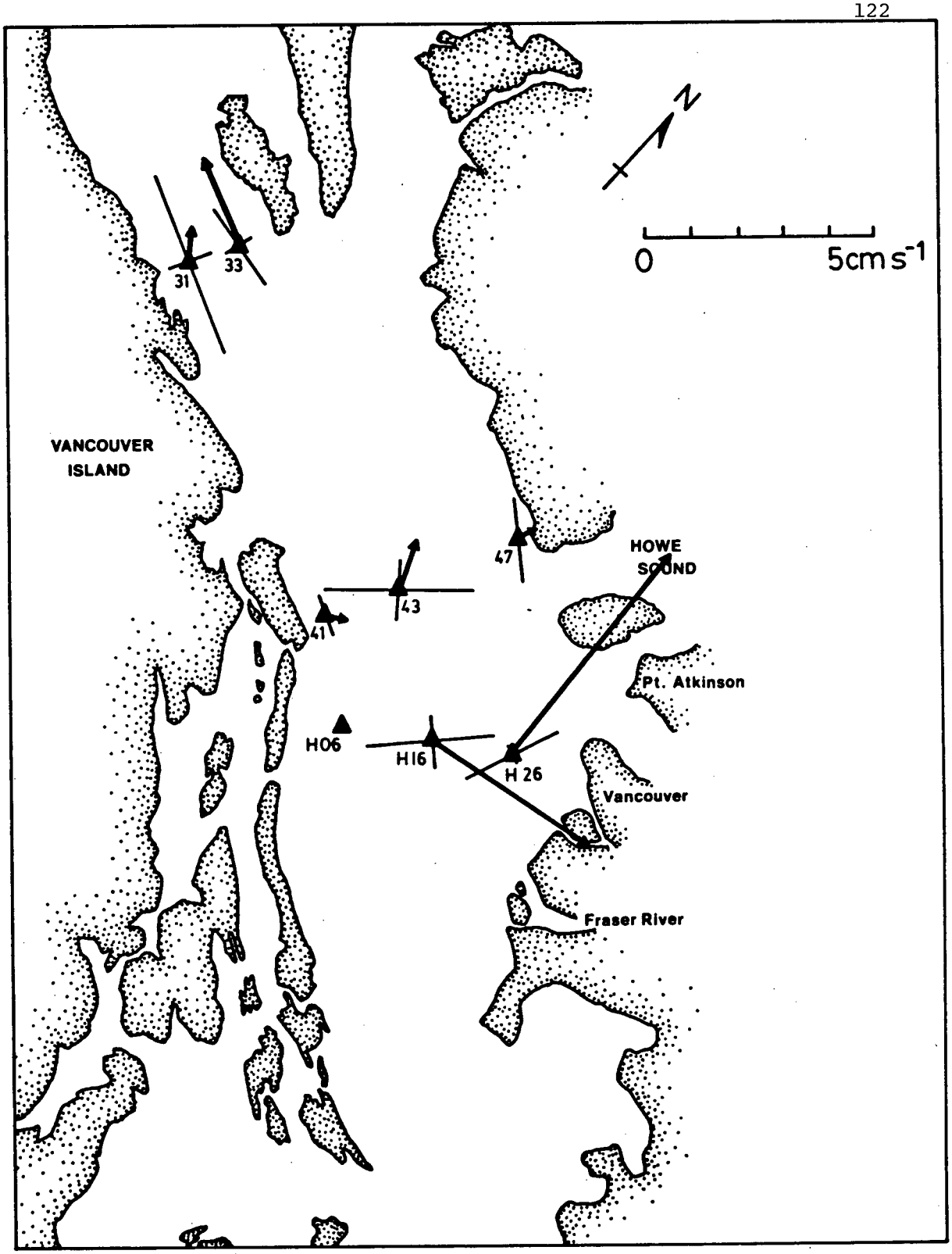

Figure 12.4A Mean currents and the 6-32-day band current ellipses for the 26-day period beginning (A) 2 May 1969 and (B) 29 August 1969. The ellipses are indicated by their major and minor axes.

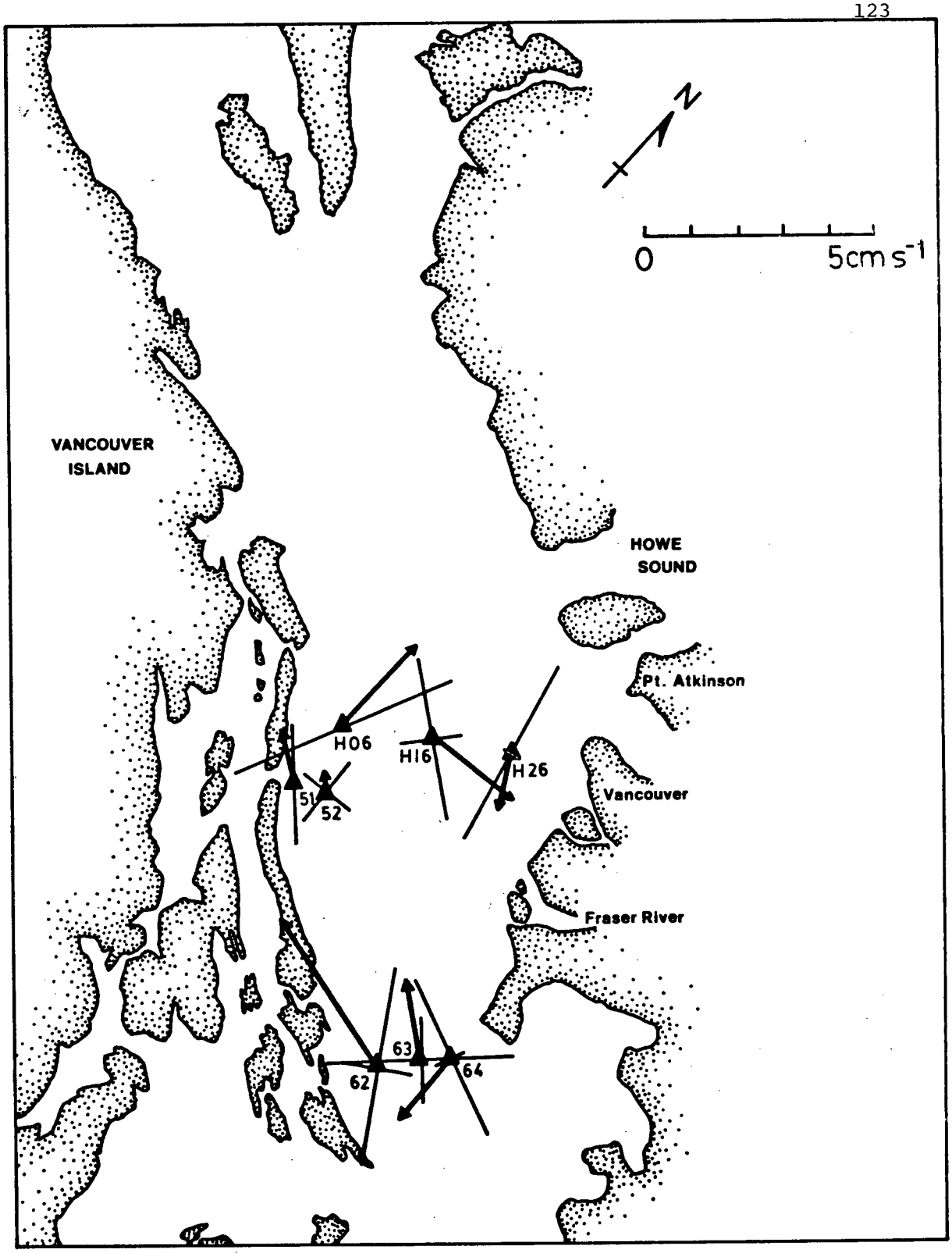
N
0
5cm s⁻¹
VANCOUVER
ISLAND
HOWE
SOUND
Pt. Atkinson
H06
H16
H26
51
52
Vancouver
Fraser River
63
62
64

Figure 12.4B

period, the flow at H26, 50 m is southward whereas the 18-month mean flow is northward (Figure 10.6). This implies that the gyre may not be a permanent feature. A closed circulation is not indicated for the central strait during May 1969 (Figure 12.4A). The strong axial current present at H26, 50 m is not observed at Station 47, 100 m.

Wind-Driven Motions

The dynamics of low-frequency, large-scale motions are due in large part to the conservation of potential vorticity, and it is the wind stress curl that enters the vorticity equation as a forcing function. In addition, if the system under consideration possesses significant bottom topography, the wind stress itself may induce vorticity by forcing water columns across bathymetric contours thus squeezing or stretching vortex lines. Indeed, in a barotropic system the vorticity input by this mechanism may far exceed that due to the wind stress curl (Gill and Schumann, 1974).

Chang (1976) calculated cross-spectra between the winds and currents along line H and found the coherence to be generally small at low frequencies. However, the use of rotary spectra does not reveal relationships between the various rectangular components of the currents and the winds. Moreover, the fact that the current spectra are peaked at about 14 days (at least for the eastern and western stations), that the motion may be barotropic at H26, and that the period of a free CSW for GS parameters is about 14 days for a variety of bottom profiles (see, e.g., LeBlond and Mysak, 1977; or Csanady, 1976) suggests very strongly that the wind stress might force modified CSW's. It is therefore sensible to examine the relationship between the wind stress and the currents by computing components spectra. Sufficient data do not exist to adequately determine the wind

stress curl, which at any rate is a difficult task due to the effect the complex orography of the British Columbia coast has upon the winds. That is, measurements taken at land-based stations are not necessarily representative of conditions at sea. One could attempt to evaluate the wind stress curl from atmospheric surface-pressure maps, but it is a tedious exercise and is not pursued here. We note as before, however, that the ensuing analysis implies that the low-frequency currents are not simple wavelike motions of the type studied in this thesis. In this respect, therefore, it is unlikely the wind stress curl plays a significant role.

Figure 12.5 shows the spectrum of the wind stress at Sand Heads for the 500-day period beginning 4 April 1969. Sand Heads is located in shallow water at the mouth of the Fraser River (see Figure 12.1) adjacent to a relatively flat region. Thus winds measured there should be comparatively free of local topographic influences. The wind stresses were computed using a quadratic law with a value of 1.5×10^{-3} for the drag coefficient. Its exact value is unimportant in this discussion since it enters only as a scale factor.

Figure 12.5A shows the true northward and eastward components of the wind stress. Both are peaked at about 3 days, but significant variance is present to periods up to at least 20 days. The mean axis of GS is directed approximately 50° west of north, and the spectra rotated by 50° are shown in Figure 12.5B. Since significantly higher coherences were found in test runs using the rotated wind stress time series, they were employed in the following analysis. On the other hand, in the vicinity of line H, the topography runs nearly north-south. Therefore the currents were not rotated. All subsequent figures refer to the rotated wind stress and nonrotated currents.

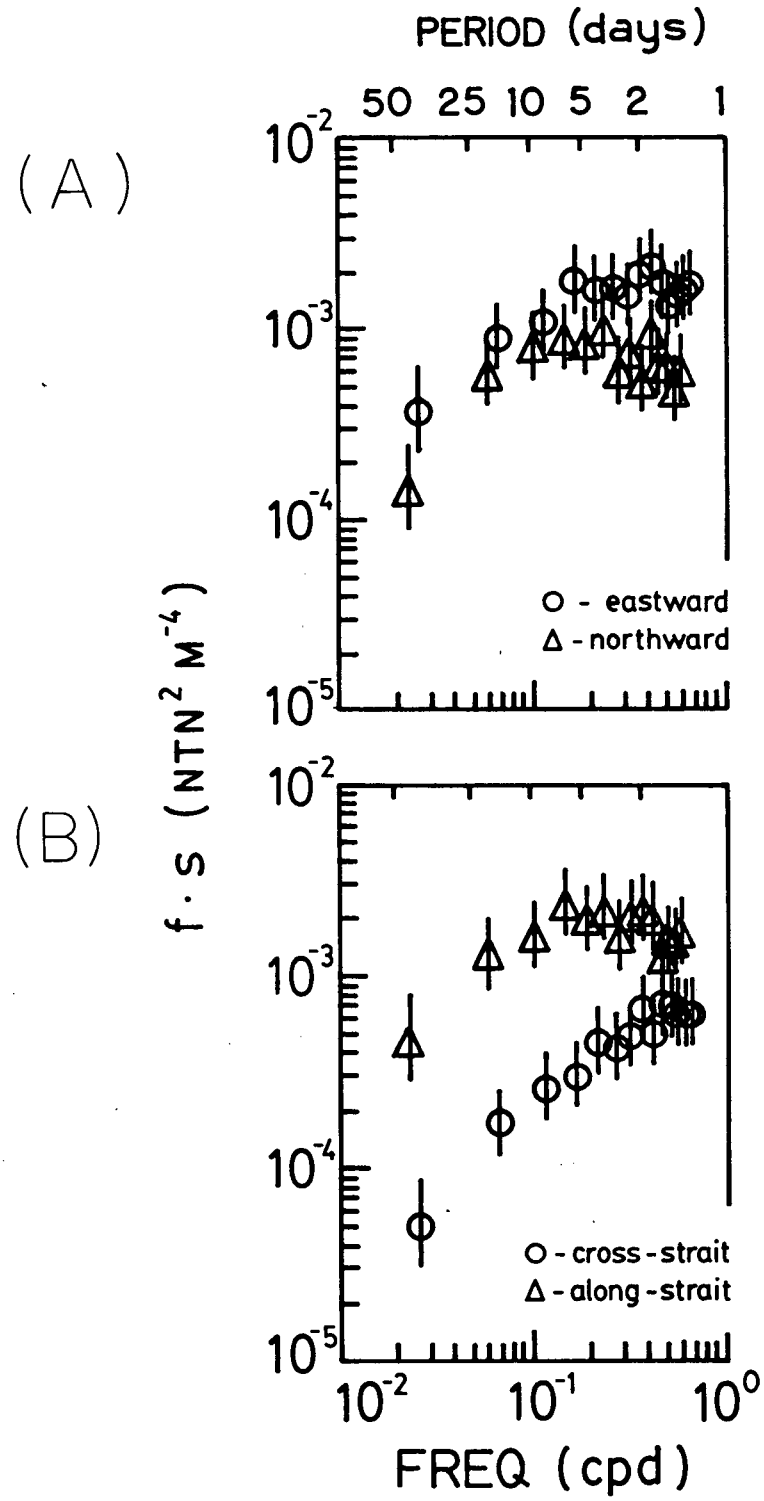

Figure 12.5 Spectrum of the wind stress at Sand Heads for the 500-day period beginning 4 April 1969: (A) the north and east wind stress components; (B) the wind stress components rotated anti-clockwise by 50°.

The 209-day period beginning 29 August 1969 was selected for analysis, as records existed at all stations along line H (Figure 12.2). Large gaps in the time series were deleted from good as well as bad records and the time series were linearly interpolated across short gaps of the order of a day or two. The resulting record was 136 days in length.

Current spectra computed from these time series are shown in Figure 12.6; the spectrum of the wind stress is essentially that shown in Figure 12.5. Two exemplary plots of coherence and phase between the currents and the along-strait wind stress are shown in Figure 12.7. They illustrate the generally low coherence observed which decreases with increasing frequency and the tendency for the currents to be either in phase or 180° out of phase with the along-strait component of the wind stress.

A more detailed presentation of the coherence and phase relationships is shown in Figure 12.8 for the 34- and 13-day bands. Statistically significant coherences are found in many cases, although in some, due respect must be paid to the amount of energy in the given signal. Thus, for example, the meaning of high value of $\gamma^2 = .6$ in the 34-day band calculated for H06, 200 m, is unclear due to the corresponding low value of the spectrum there (Figure 12.6). The most striking feature, however, is the consistency with which the phase estimates cluster about either 0° or 180°. This tendency together with the fact that phase determination may be good even though the corresponding coherences are insignificant (Schott and Düing, 1976) instills some degree of confidence in the calculated phases. More specifically, phases between currents and the along-strait wind stress tend to be close to 180°, while those between the currents and the cross-channel wind stress lie near 0°. The along-strait wind stress is, of course, considerably more energetic than the cross-channel component.

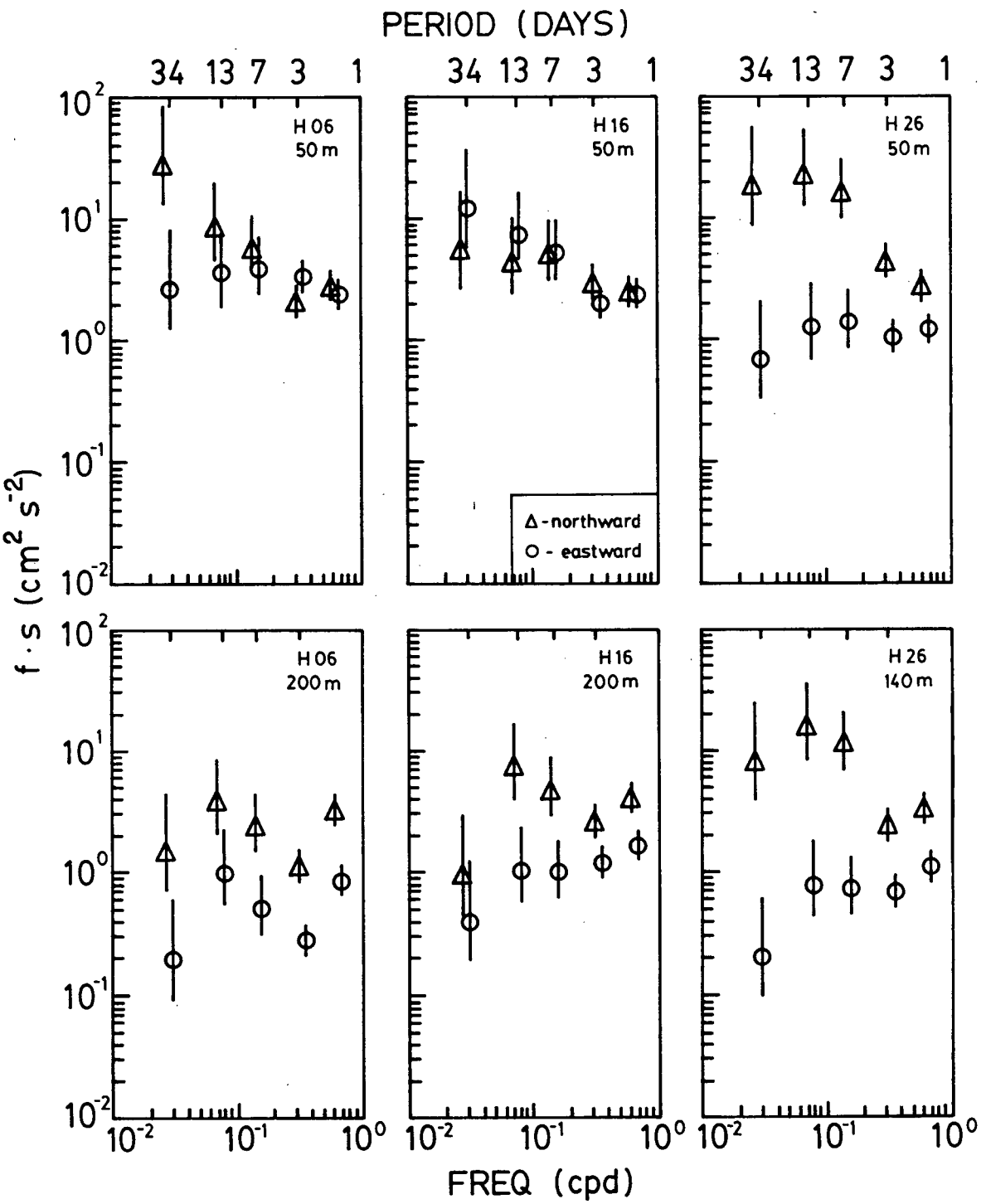

Figure 12.6 Line H current spectra for the 136-day analysis period. The vertical bars indicate 95% confidence limits.

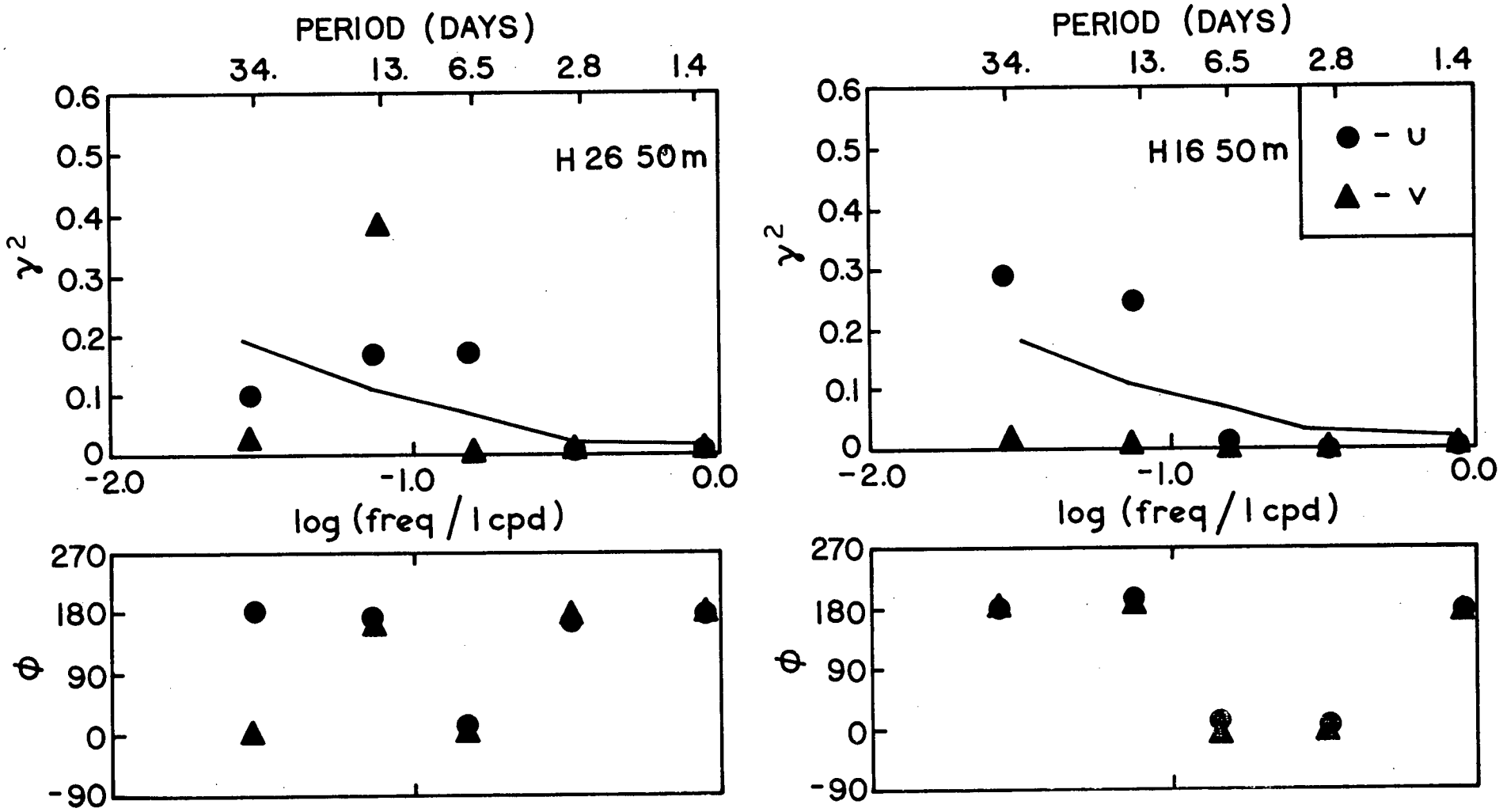

Figure 12.7 Coherence and phase between the wind stress and currents at H26, 50 m and H16, 50 m. A positive phase indicates the current leads the wind. Here u and v refer to the eastward and northward velocity components. The solid line indicates the 95% noise level.

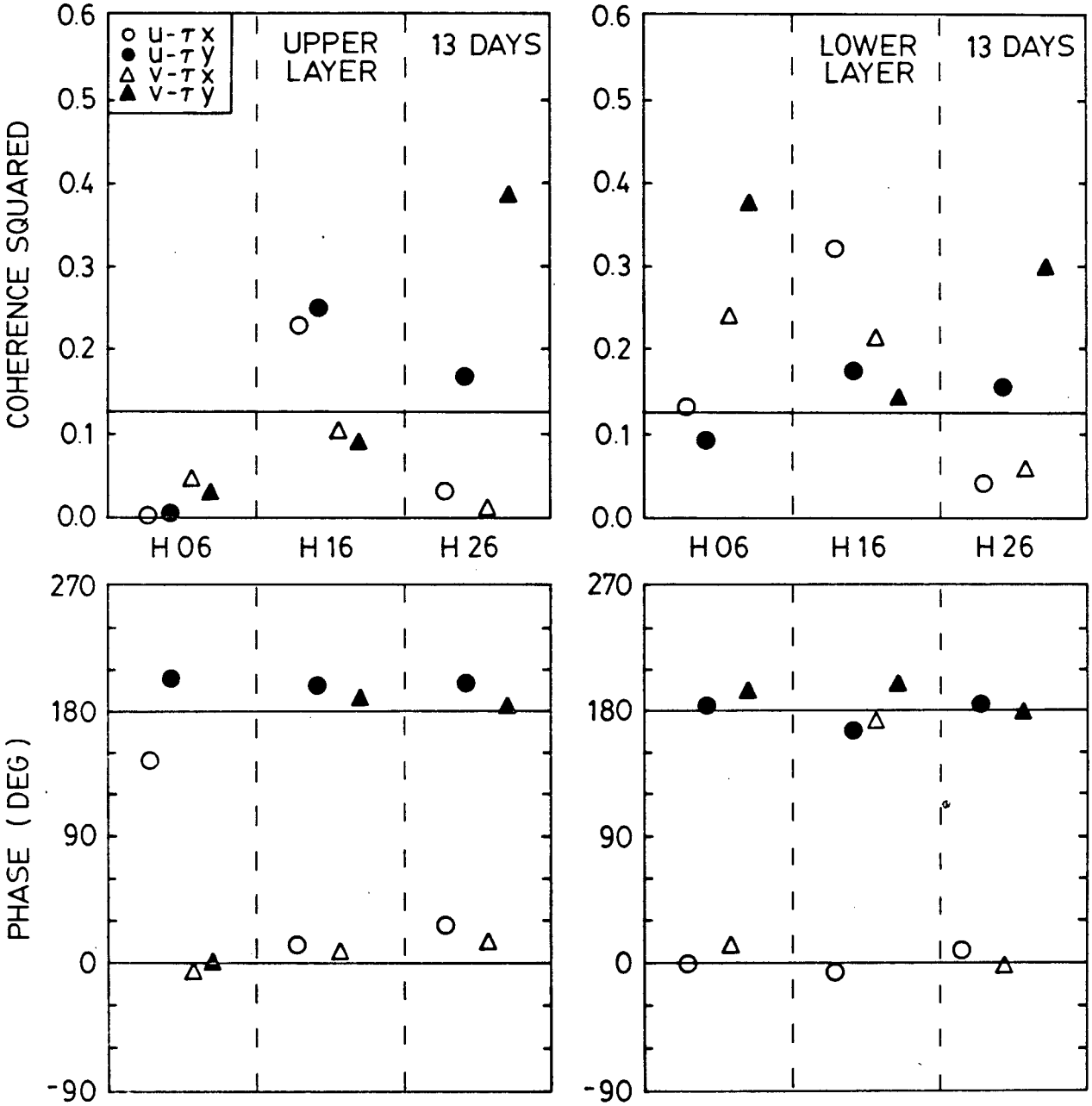

Figure 12.8A Coherence and phase between line H currents and the wind stress for: (A) the 13-day band, and (B) the 34-day band. The solid lines in the coherence plots indicate the 95% noise levels. A positive phase indicates the current leads the wind.

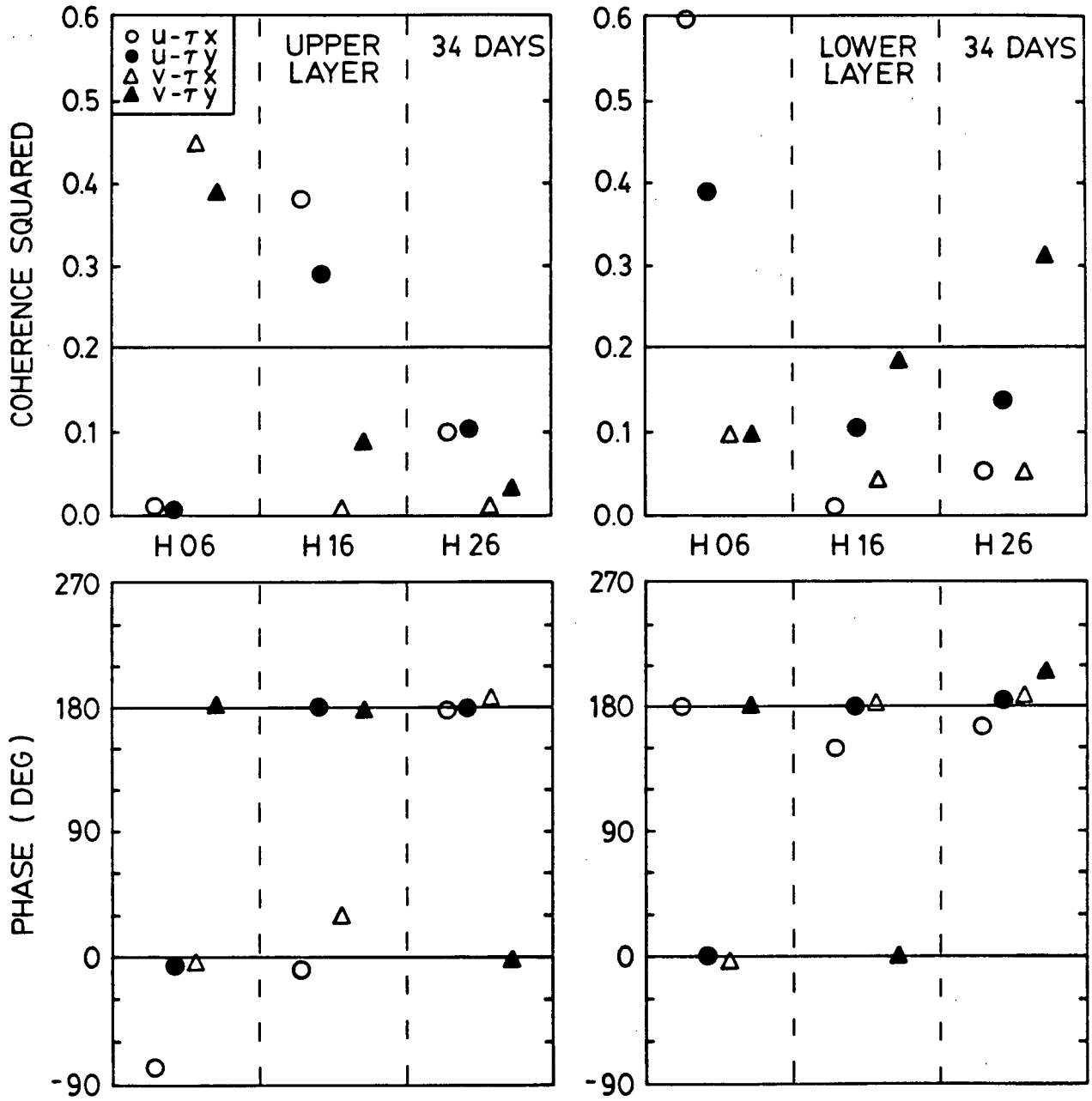
COHERENCE SQUARED
PHASE (DEG)
u-τx
u-τy
v-τx
v-τy
UPPER LAYER
LOWER LAYER
34 DAYS
H06
H16
H26
0.6
0.5
0.4
0.3
0.2
0.1
0.0
270
180
90
0
-90

Figure 12.8B

These phase results should not be interpreted to mean, for example, that the currents flow down-channel when the winds blow up-channel. They imply simply that the currents are in opposition to the given spectral component of the along-strait wind. The relationship in the time domain between the currents and winds will be examined shortly.

Table III lists the coherences and phases calculated between velocity components for the 13- and 34-day bands. If a motion is composed of the types of waves studied here, then the phase difference between u and v should be somewhere near 90°. Deviations from this value may be caused by friction (see, e.g., Csanady, 1978) or by instability (see Section 4). With the exception of the value of $\phi = 117°$ for H26, 140 m at 34 days, examination of Table III shows that if a significant coherence is found, the corresponding phase is either near 0° or 180°, that is, the motion is linearly polarized. This implies, with the noted exception, that the motion is not wavelike. This is true, in particular, for the observed 13-day current oscillations at H26 for which the previous evidence strongly suggested the contrary. On the other hand, the results for 34 days for H26, 140 m, do suggest a wavelike character and it is enticing to speculate that this might be a bottom-enhanced wave of the type described by Helbig and Mysak (1976). There is no direct evidence, of course, to support this speculation, and the motion is just as likely to be barotropic. We note, however, that CSW's of 34-day period should have wavelengths in excess of the length of GS (see, e.g., Figure 11.5).

The mean currents and current ellipses for the 13- and 34-day bands are shown in Figures 12.9 and 12.10. While the mean flow is similar to that calculated for the full 18 months (Figure 10.6), the deep currents in both the east and west are considerably stronger. Indeed, at H06 the

Table III. Calculated coherence squared and phase between velocity components for the 136-day period of analysis. A positive phase indicates that v leads u.

		13 days		34 days	
Station	Depth	γ^2	ϕ (deg)	γ^2	ϕ (deg)
H06	50	.36	- 4	.08	52
	200	.24	- 11	.10	- 178
H16	50	.01	3	.05	39
	200	.29	179	.69	179
H26	50	.37	5	.18	177
	140	.51	2	.48	117

upper- and lower-layer mean flows are nearly the same. The current ellipses bear a striking resemblance to the respective mean velocities. Although trends during the period of analysis may contaminate the 34-day band (which is averaged over the second to sixth frequencies), they should exert minor influence on the 13-day band (which is averaged over frequencies 7-14). These results thus may imply a dynamical relationship between the mean and fluctuating flows, a point which is discussed further in the next section. It is evident from the figures that the channel boundaries exert a strong topographic influence on the near-shore currents.

Approximate barotropic and baroclinic time series were formed by depth averaging the 136-day records. Indeed, the period of analysis and the treatment of the data records were selected for this purpose. The velocity time series were combined as

$$\underline{u}_{BT} = (h_1\underline{u}_1 + h_2\underline{u}_2)/(h_1 + h_2)$$

and

$$\underline{u}_{BC} = h_2(\underline{u}_1 - \underline{u}_2)/(h_1 + h_2)$$

to give barotropic ($\underline{u}_{BT}$) and upper-layer baroclinic ($\underline{u}_{BC}$) records, respectively. The upper-layer depth h_1 was chosen as 50 m since this corresponds to a reasonable fit of a two-layer model to the observed density distribution (Helbig and Mysak, 1976). The lower-layer depth h_2 was then simply obtained from the total depth at each mooring. The vertical velocity profile is, in reality, much more complex. If a greater number of meters had been used at each station, the method of empirical orthogonal functions could have been employed to resolve the vertical structure (see, e.g., Mooers and Brooks, 1978). No other choices of h_1

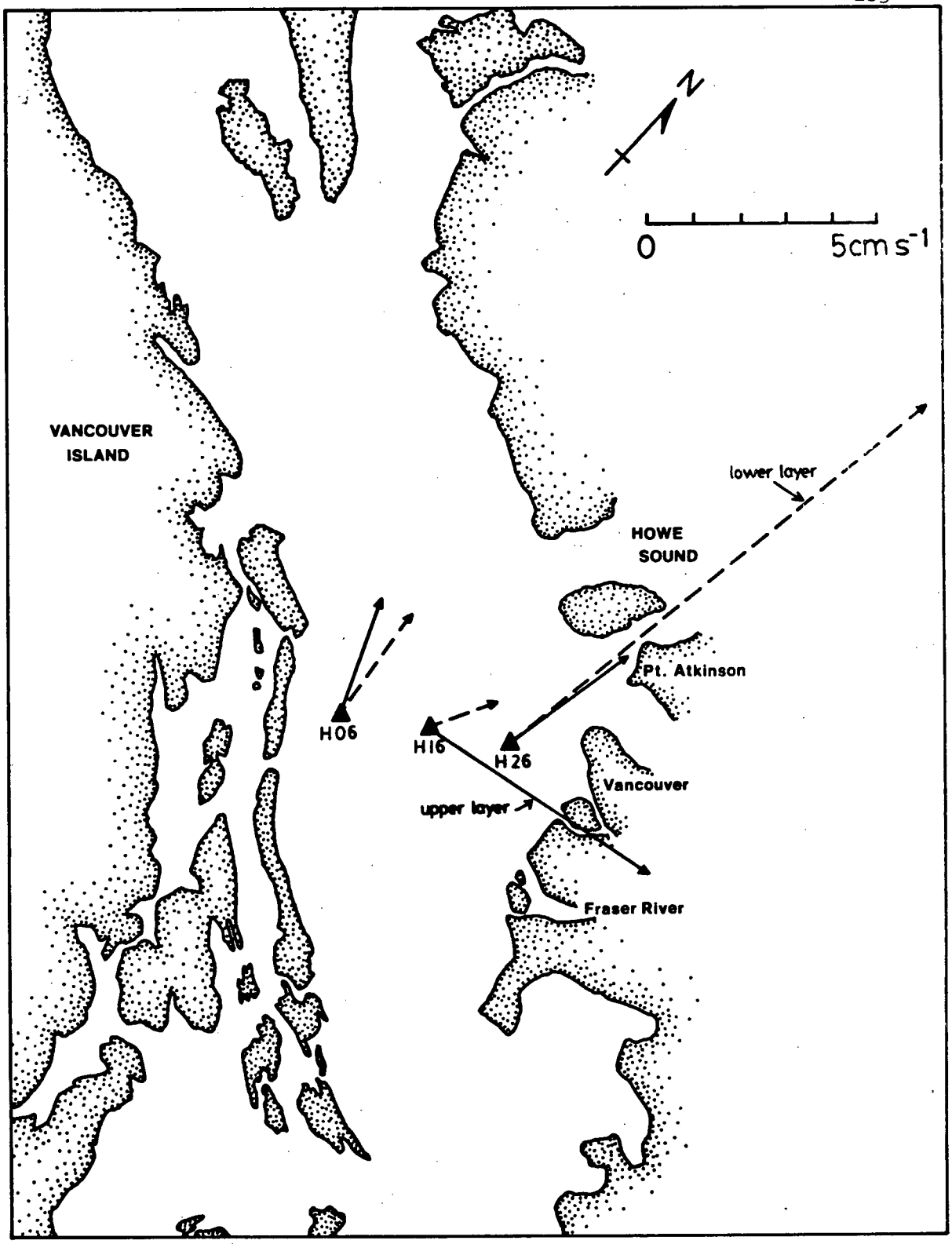

Figure 12.9 Mean currents along line H for the 136-day analysis period.

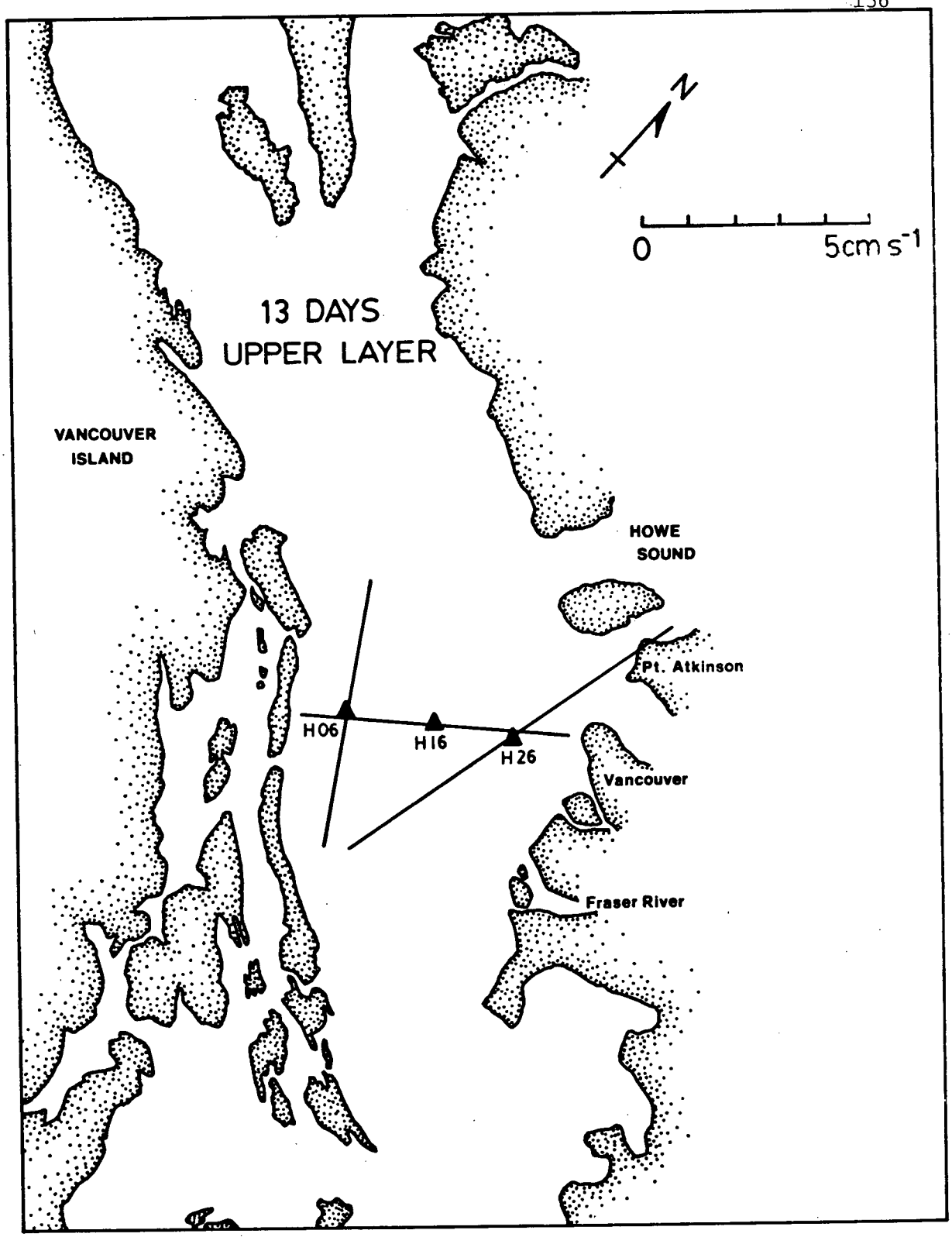

Figure 12.10A Line H current ellipses for the 13-day band: (A) upper layer, (B) lower layer; and the 34-day band: (C) upper layer, (D) lower layer.

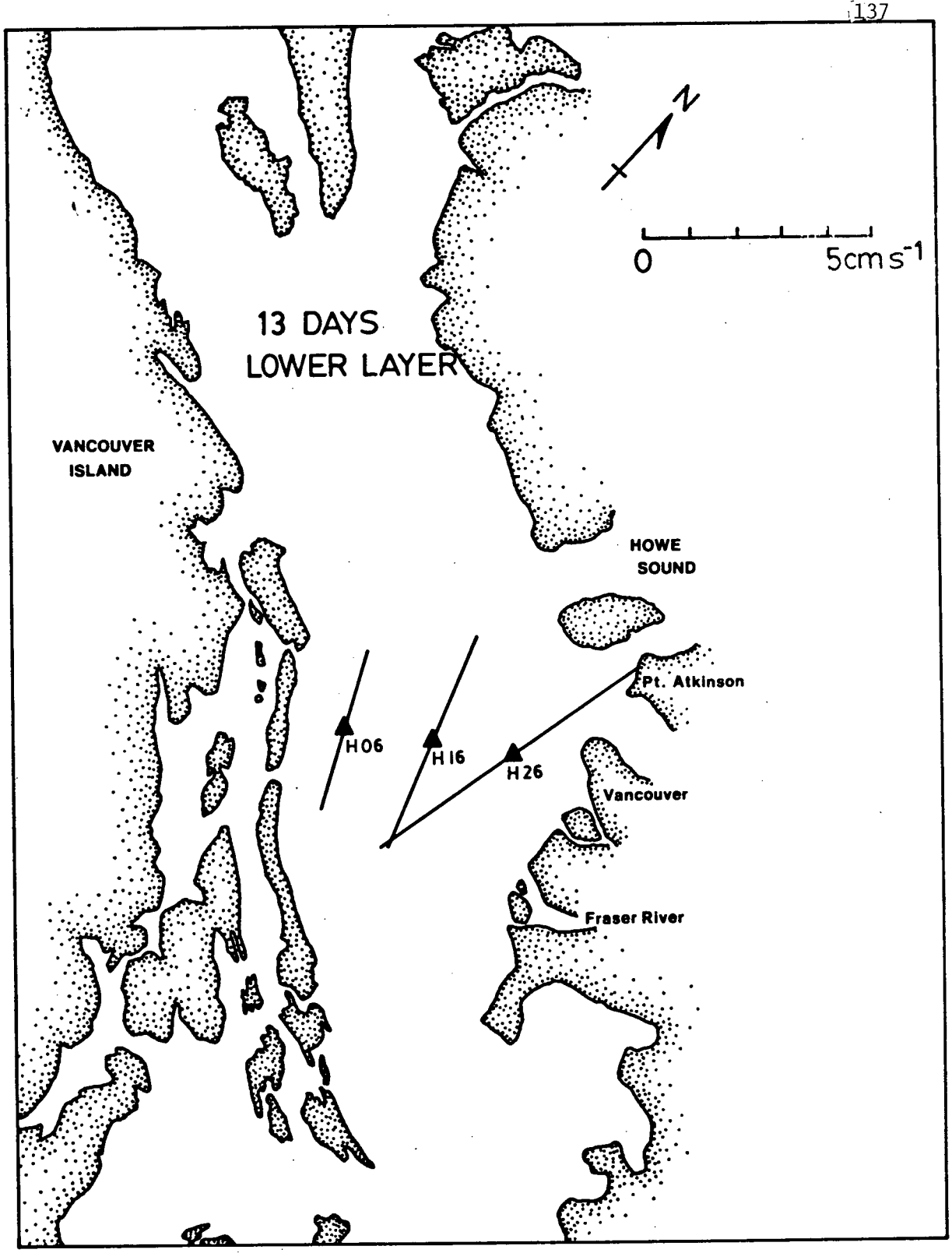

Figure 12.10B

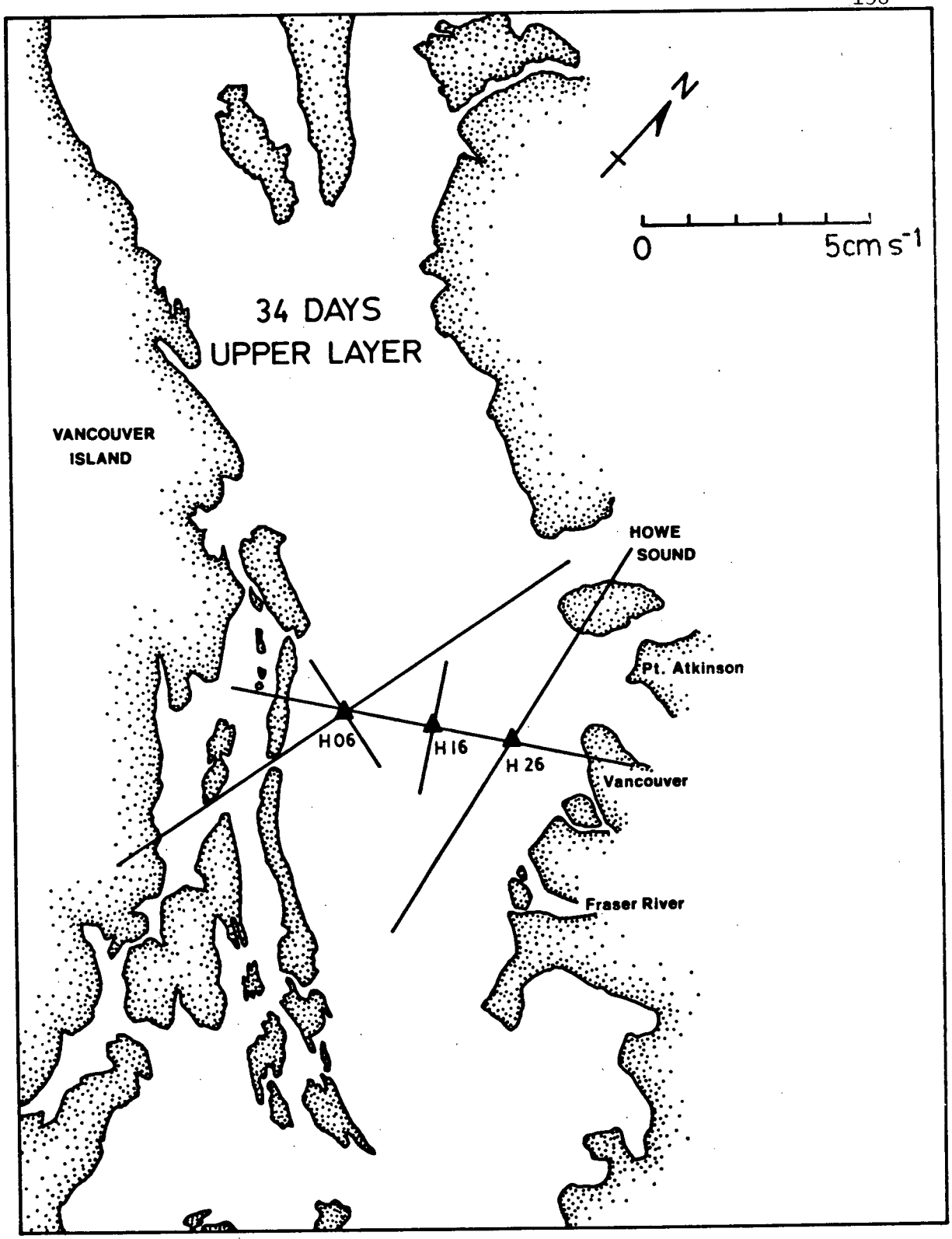

Figure 12.10C

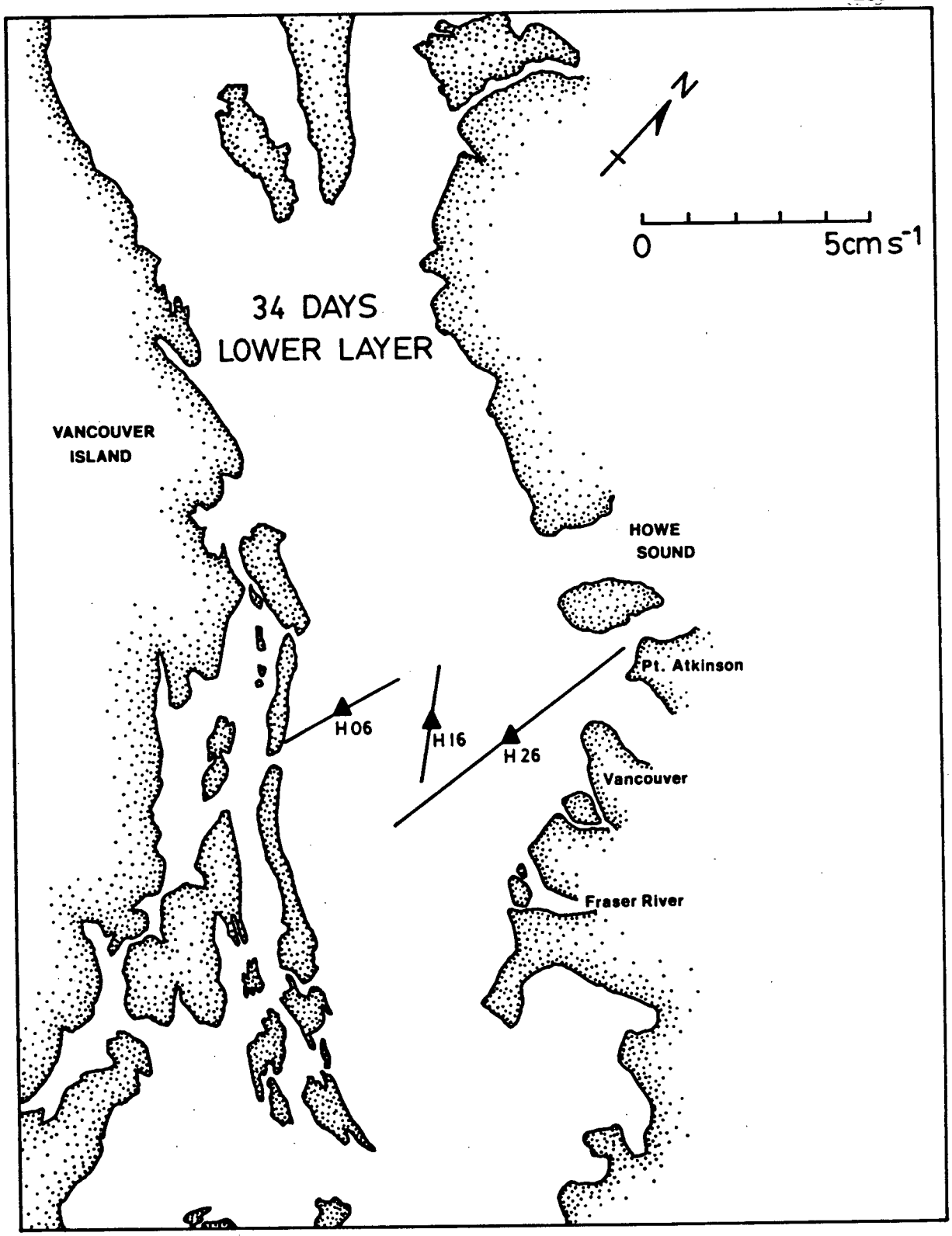

Figure 12.10D

were tried.

Each time series was spectrally analysed, but the barotropic and baroclinic spectra were almost indistinguishable from the lower- and upper-layer spectra, respectively. The results were inconclusive with regard to correlation between the wind and currents. In some cases higher values of γ^2 were found but in others the correlation was diminished. It is difficult to determine, therefore, if the separation was successful.

The barotropic and baroclinic mean currents for the 136-day period are shown in Figure 12.11. While the barotropic means are similar to the lower-layer means of Figure 12.9, the baroclinic means are less suggestive of a gyrelike circulation than are the upper-layer means.

One current meter, that at H16, 50 m, operated almost continuously over the 18-month period. Consequently, the 500-day time series of currents and winds beginning 17 April 1969 was analysed for comparison with spectra computed from shorter record lengths. The current spectrum is very similar to that shown in Figure 12.6. In general, the calculated coherences between the currents and winds are decreased from those shown in Figure 12.8 for both the 34- and 13-day bands. Interestingly, in the former band, the coherence between the velocity components increased from 0.05 to 0.23. The computed phase differences were similar, and in particular both the u and v components were nearly 180° out of phase with the wind stress.

In order to obtain an appreciation in the time domain of how the water column responds to the wind, the two-month period of March-April 1970 was selected for more intensive study. This period was chosen for two reasons. First, records were available for all meters for most of the period. Second, during this time several significant storms occurred, some with northwest and some with southeast winds. The time series of winds and

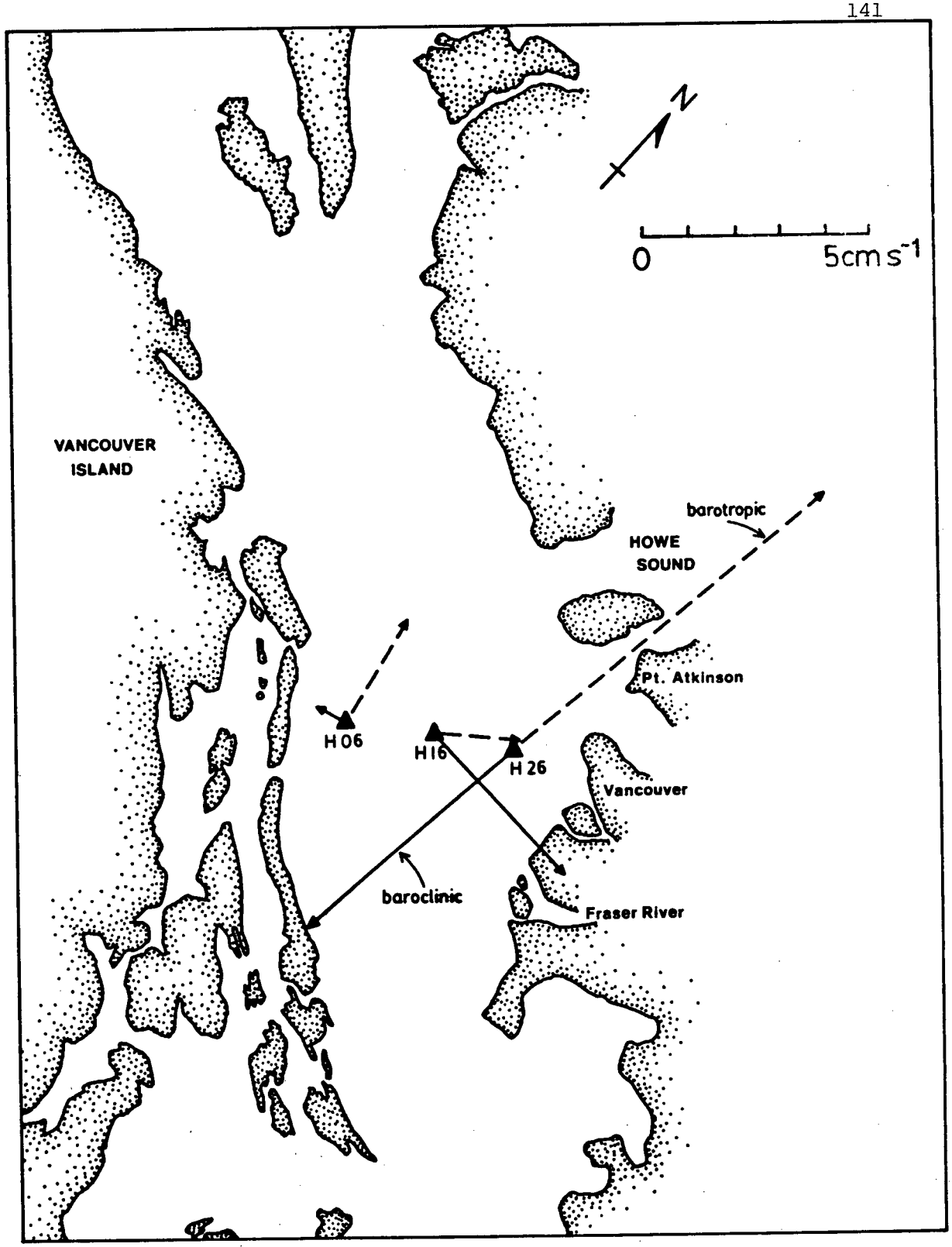

Figure 12.11 Computed barotropic and upper layer baroclinic mean currents for the 136-day analysis period.

currents were filtered with an $A_{24}{}^2 A_{25}/(24^2 \cdot 25)$ filter (Godin, 1972) in order to remove diurnal and semidiurnal oscillations. This is a low-pass filter and produces a record with a twelve-hour time step. The results are shown in Figure 12.12. Notice that the wind has been advanced five days with respect to the currents. As before, the wind stress was rotated to bring it into alignment with channel geometry.

Seven wind events are identified in Figure 12.12; peak values of the wind stress occur for E_3 (down-strait) and E_6 (up-strait). For the 50-metre record at H26, the signature of the wind on the currents is clear, and the currents lag the wind by about five days. Similarly, the response at the 140-m station is apparent for the first month. For the second month, however, some ambiguity exists in the assignment of $E_3 - E_7$. If the choice indicated is correct, then a down-strait wind does not necessarily produce a down-channel current (compare events E_3, E_4, and E_7). This is opposite to the response observed at 50 m. It is not possible to definitively correlate currents and winds at the central 50-m station, but the correlation at 200 m is clear-cut, again with a 5-day lag. It is also not possible to make the assignment at H06, 50 m for the one-month record that exists. As was the case for the deep eastern meter, correlation of winds and currents at H06, 200 m, is ambiguous in the second month. Unlike the eastern station, however, the chosen assignment indicates direct response to the wind with a 9-day lag. In the first month the lag is about 7 days.

In an attempt to determine if the response to the winds observed at 50 m is representative of the entire upper water column, progressive vector diagrams of the currents at 3 m and 50 m [Tabata and Stickland, 1972a; 1972b; 1972c; Tabata et al., 1971] were compared with one another and the wind for the period beginning April 1970 (Figure 12.2).

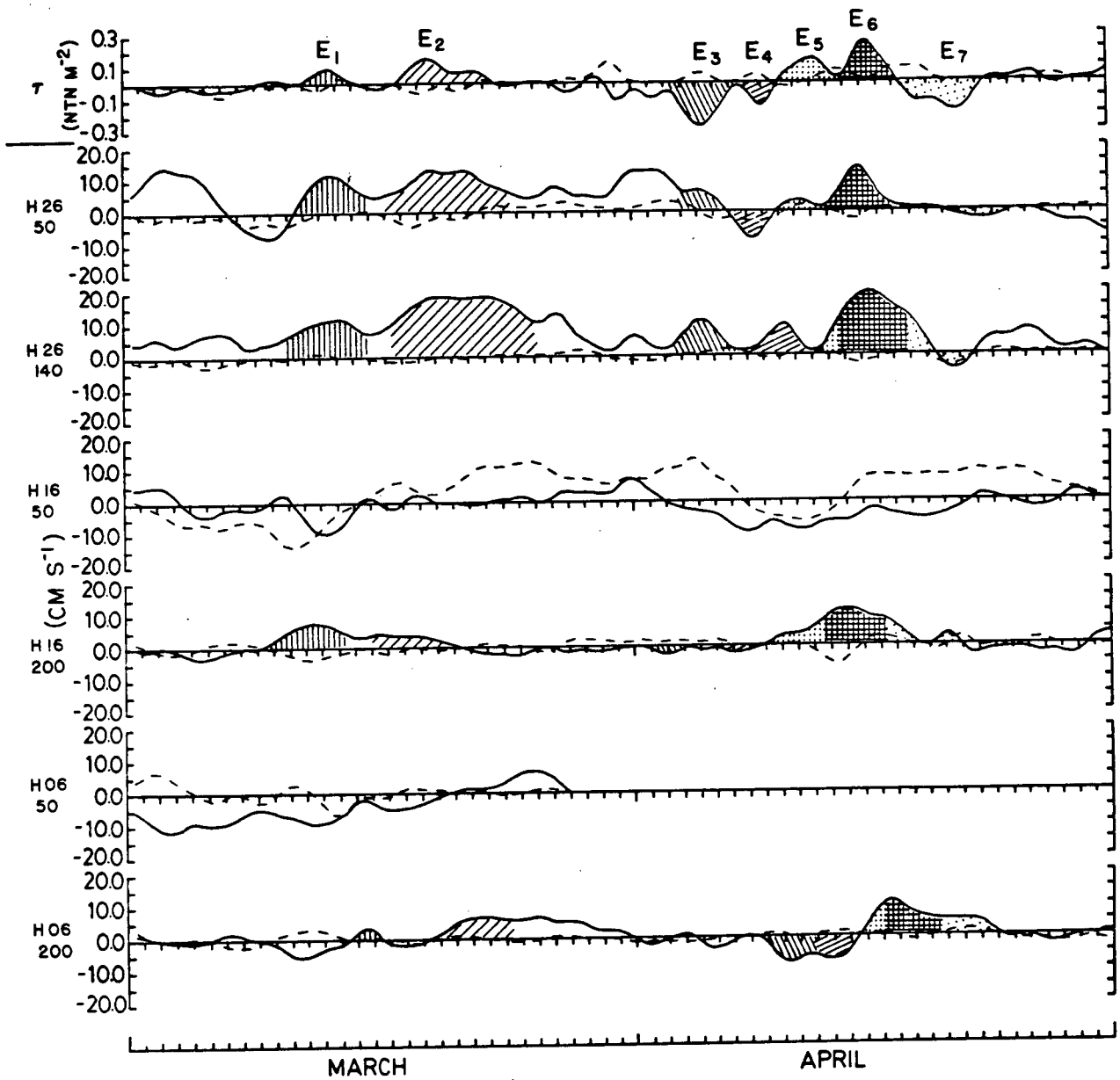

Figure 12.12 Low-pass filtered time series of wind stress at Sand Heads and currents along line H. A solid line represents either the along-strait (northwestward) component of wind stress or the northward component of current. A dashed line represents either the cross-channel wind stress (northwestward) or eastward current component. The wind stress time series is advanced by 5 days.

At all stations there were times during which the currents at both levels were obviously correlated and in phase with each other and the wind. But there were also times during which the currents were out of phase with each other or the wind. Similarly, the horizontal relationships between the 3-m currents were unclear. However, the currents at H06 and H16 were, at times, highly correlated and in phase. Therefore, by comparison with the 3-m currents, it is difficult to state if the measurements at 50 m are representative of the entire upper layer.

In summary, examination of the data has indicated several interesting features. First, the low-frequency fluctuations are not isolated to the vicinity of line H or the southern strait. Second, as suggested by the spectra and response to the wind, Station H26 may lie in an oceanographic domain distinct from the other two stations. Third, the oscillating currents bear a resemblance to the mean flow which may indicate that the two are dynamically linked. If this supposition is valid, then three alternatives are possible: (1) the fluctuations are due to the mean currents (inertial instability), (2) the mean flow is a byproduct of the oscillations (transients, arrested waves; see, e.g., Csanady, 1978), or (3) they are both caused by some other agency of the type outlined in Section 10. The first possibility may be ruled out on the basis of results of Section 11 and the fact that the components of the observed oscillating currents tend to be in phase. The last alternative is explored briefly in the next section. Finally, the wind obviously plays some role in GS dynamics but its role is not clear.

13. Nonlinear Tidal Interactions

In an earlier study, Helbig and Mysak (1976) discounted the possibility that the tides were responsible for the low-frequency motions in GS. However, they were referring to the fortnightly M_f tide and did not consider the possibility of nonlinear interactions between tidal constituents. In a system like GS with large variations in bottom topography and channel geometry, it is likely that such interactions produce significant fortnightly variations in the tide. These interactions occur between tidal constituents through frictional or advective terms, and the resultant oscillations are known as shallow-water constituents. The harmonic constants for diurnal, semidiurnal, and higher-frequency tidal constituents are listed in Table IV and were obtained from the analysis of a 38-day record of tidal heights observed at Point Atkinson (see, e.g., Figure 12.1). From the frequencies given in Table IV, one may show that interactions between the M_2 and K_2, M_2 and S_2, O_1 and K_1, and O_1 and P_1 constituents all produce shallow-water constituents of fortnightly period. For example, the $M_2 - S_2$ interaction gives the MS_f constituent with a 14.76-day period, while the $O_1 - K_1$ interaction results in a 13.66-day oscillation.

In this section two types of tidal interactions are considered. The first I term direct, nonlinear interaction and is that just outlined. The second or indirect, nonlinear interaction consists of the interaction of the tide with another agency. In particular, I speculate upon the interaction of the tide with the Fraser River outflow.

To determine the significance of the first mechanism, results generated from the Department of the Environment numerical tidal model of

Table IV. Results of the harmonic analysis of tidal elevations at Point Atkinson for the 38-day period beginning 6 April 1976. The P_1 and S_1 constituents are inferred from K_1, NU_2 is inferred from N_2, T_2 and K_2 are inferred from S_2. (Dr. J. A. Stronach, private communication.)

Constituent No.	Name	Frequency (cpd)	Amplitude (cm)	Greenwich phase (deg)
1	ZO	0.0	30.2087	0.0
2	2Q1	0.85695237	0.1155	96.73
3	Q1	0.89324397	0.6998	326.92
4	O1	0.92953563	3.9706	215.33
5	NO1	0.96644622	0.4666	276.69
6	P1	0.99726212	2.8014	347.70
7	S1	1.00000000	0.3242	154.08
8	K1	1.00273705	7.9255	95.47
9	J1	1.03902912	0.4867	359.38
10	OO1	1.07594013	0.1736	221.21
11	MNS2	1.82825470	0.1048	322.62
12	MU2	1.86454678	0.3987	317.05
13	N2	1.89598083	2.0722	249.94
14	NU2	1.90083885	0.3795	228.27
15	M2	1.93227291	9.3629	148.55
16	L2	1.96856499	0.2994	262.76
17	T2	1.99726295	0.1426	24.32
18	S2	1.99999905	2.2687	298.19
19	K2	2.00547504	0.4967	220.37
20	2SM2	2.06772518	0.0464	1.47
21	MO3	2.86180973	0.0132	137.41
22	M3	2.89841080	0.0187	247.17
23	MK3	2.93500996	0.0152	87.29
24	SK3	3.00273800	0.0095	203.48
25	MN4	3.82825470	0.0106	276.20
26	M4	3.86454678	0.0353	139.86
27	SN4	3.89598179	0.0083	281.85
28	MS4	3.93227291	0.0283	341.27
29	S4	4.00000000	0.0093	291.57
30	2MN6	5.76052761	0.0569	146.10
31	M6	5.79681969	0.0709	33.69
32	MSN6	5.82825565	0.0220	266.26
33	2MS6	5.86454582	0.0826	198.62
34	2SM6	5.93227386	0.0209	334.93
35	3MN8	7.69280148	0.0086	51.41
36	M8	7.72909451	0.0177	97.38
37	3MS8	7.79681969	0.0077	327.90
38	M12	11.59364128	0.0087	99.16

the Juan de Fuca-Strait of Georgia system (Crean, 1976; 1978) were examined. This is a two-dimensional, vertically integrated model utilizing an explicit, forward-stepping, finite difference scheme; adjoining inlets and northern passages to the open ocean are simulated as one-dimensional channels. In the latest version, a 2-km mesh size is employed. The system is driven by specifying tidal elevations along the open boundaries; these elevations are obtained from a 61 harmonic constituent tide.

A 13-day time series of velocities and elevations with a time step of 15 minutes has been generated from this model. To determine the residual currents, the velocity time series was first smoothed to one hour with an $A_4^2 A_5/(4^2 \cdot 5)$ filter (Godin, 1972) and then low-passed filtered to 12 hours with the $A_{24}^2 A_{25}/(24^2 \cdot 25)$ filter previously described which effectively eliminates oscillations with frequencies exceeding 0.8 cpd. By residual, we refer to the remaining low-frequency components. Three days of data were lost in the application of the two filters leaving a 10-day time series. The residual flow along line H is indicated in Figure 13.1 for 3 separate days; the average flow over the 10-day period is shown in Figure 13.2. The currents calculated for the grids encompassing stations H26, H16 and H06 are illustrated in Figure 13.3. The tidal elevation and range based on the predicted tides for Point Atkinson are also shown in Figure 13.3 for the period of the analysis.

It is evident that a coherent pattern of residual circulation exists, and that it is dependent upon the tidal range. It is also clear that the strongest residual flows occur near the eastern boundary. Unfortunately, the time series is insufficiently long to fully resolve a fortnightly variation, and it is possible that the very strong flows occurring at the beginning of the analysis period may be transients associated

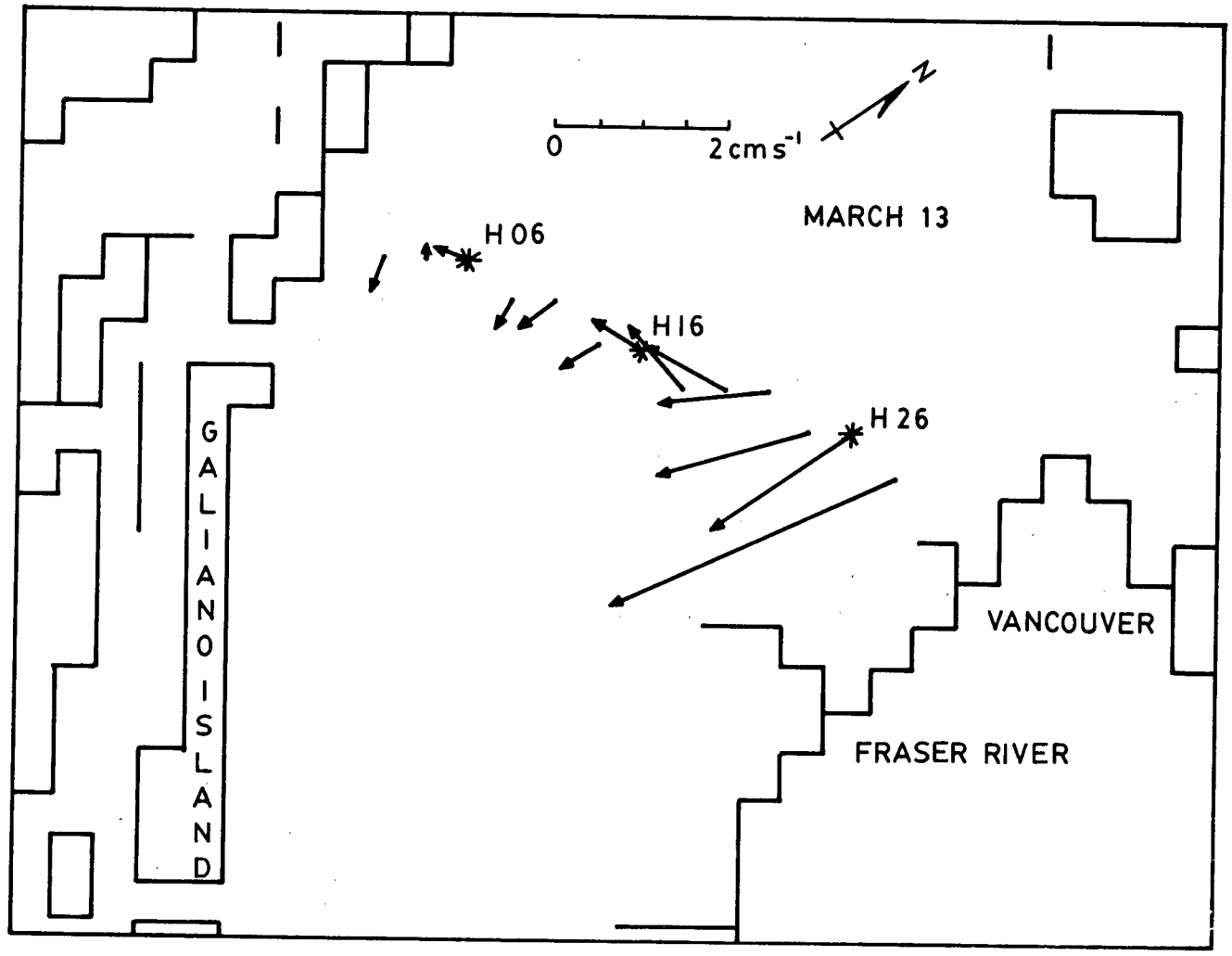

Figure 13.1A Daily, barotropic, residual tidal flow along line H.

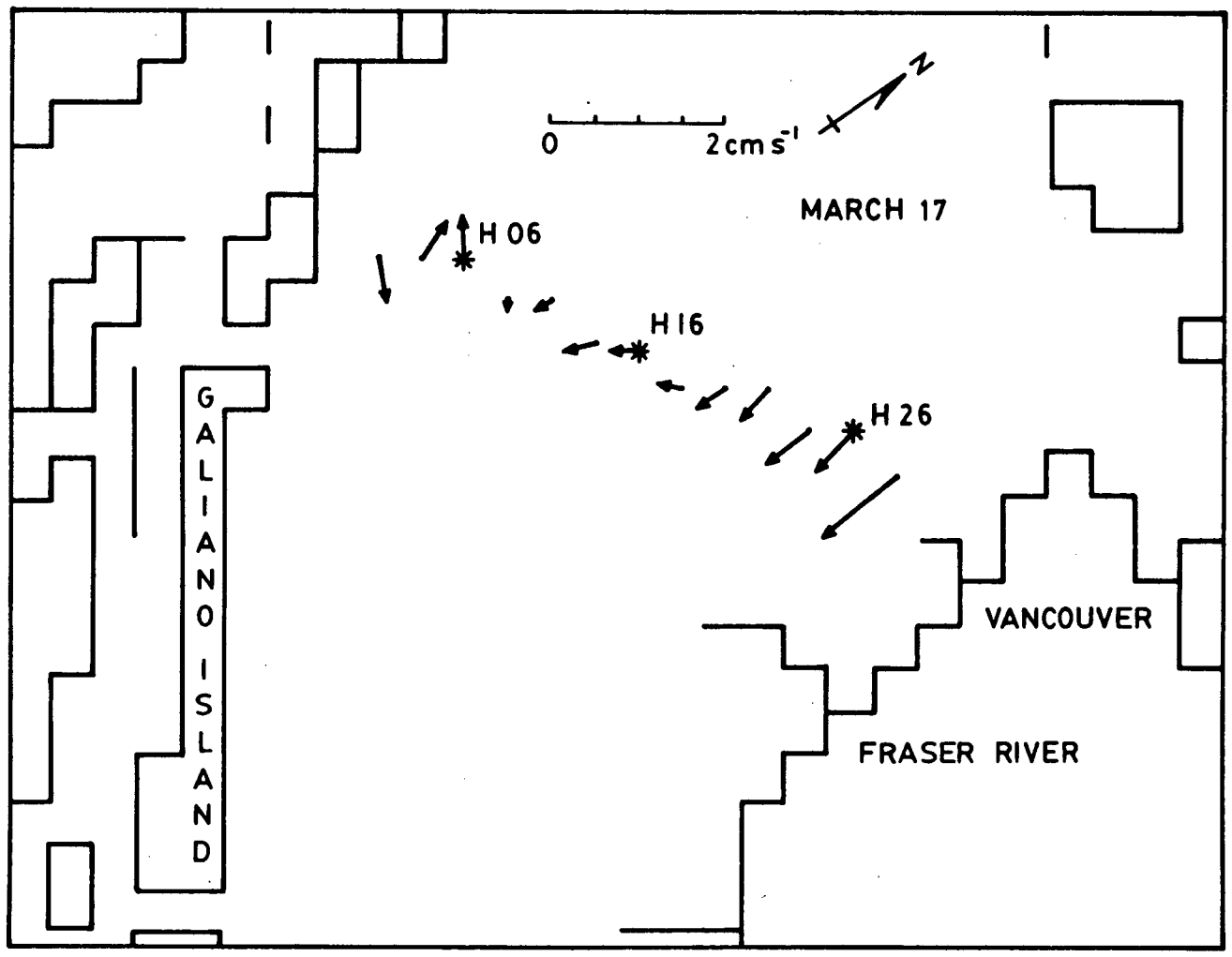
0
2cm s⁻¹
N
MARCH 17
H 06
H 16
H 26
GALIANO ISLAND
VANCOUVER
FRASER RIVER

Figure 13.1B

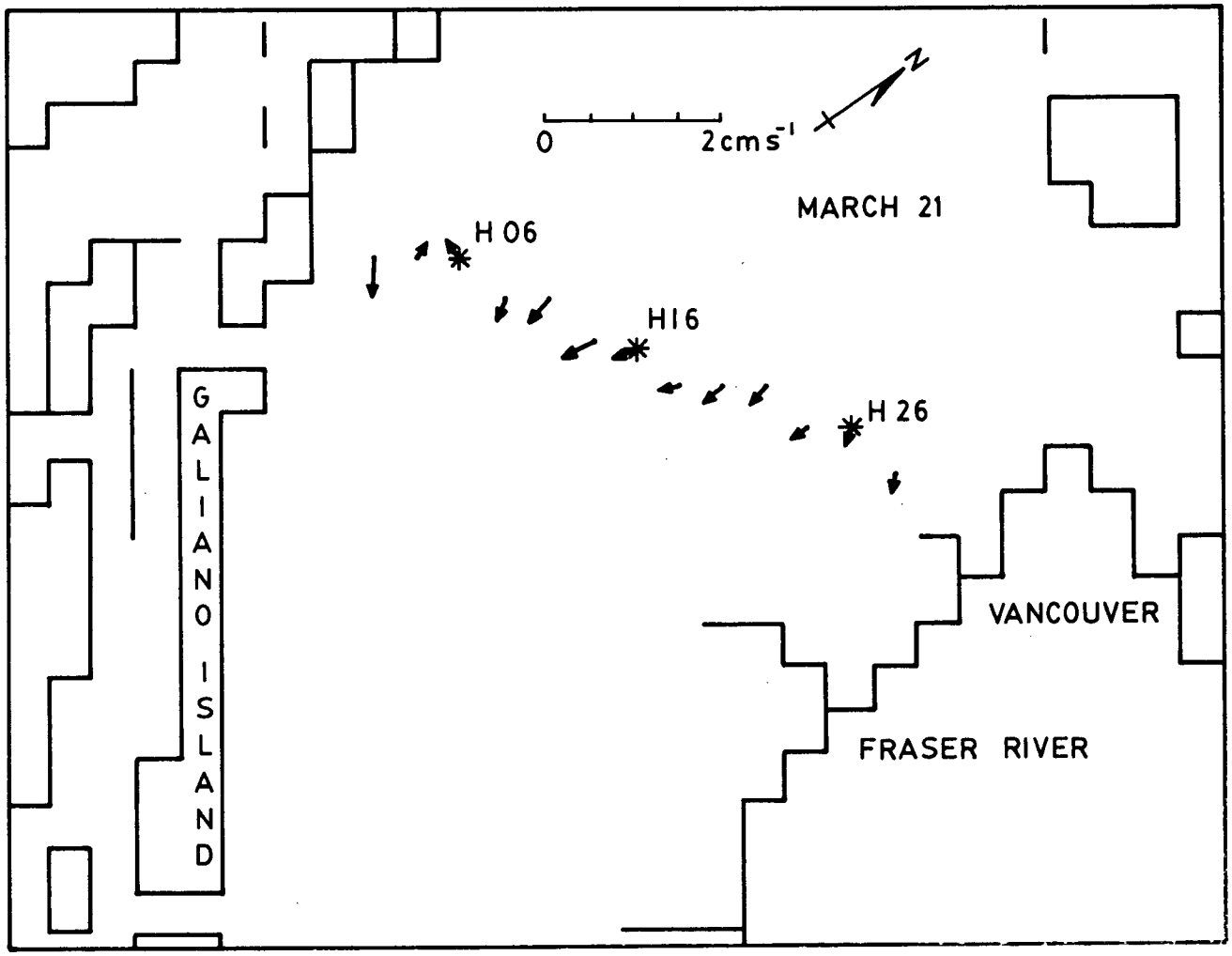
0
2cms⁻¹
N
MARCH 21
H 06
H16
H 26
GALIANO ISLAND
VANCOUVER
FRASER RIVER

Figure 13.1C

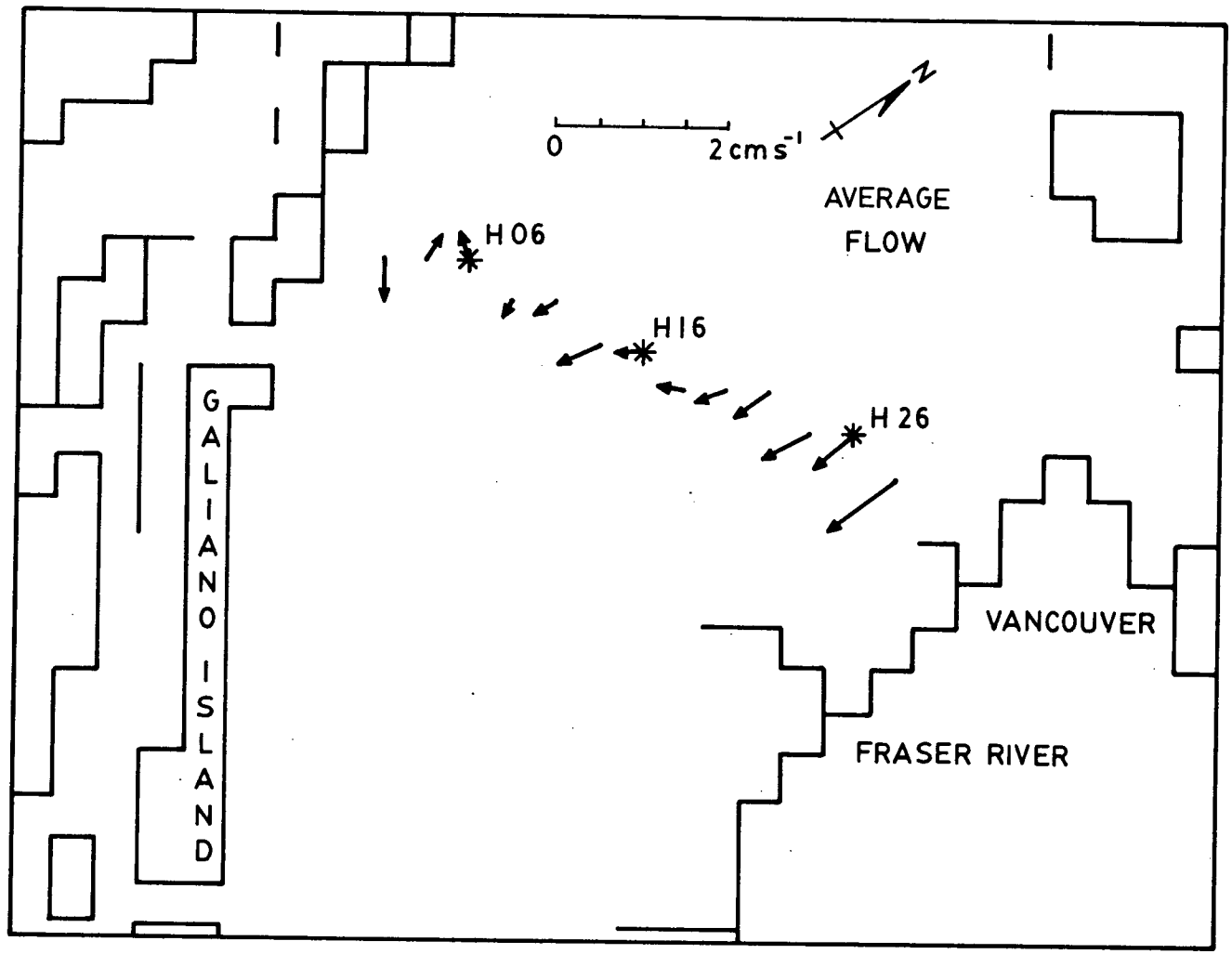

Figure 13.2 The residual barotropic, tidal flow averaged over 10 days.

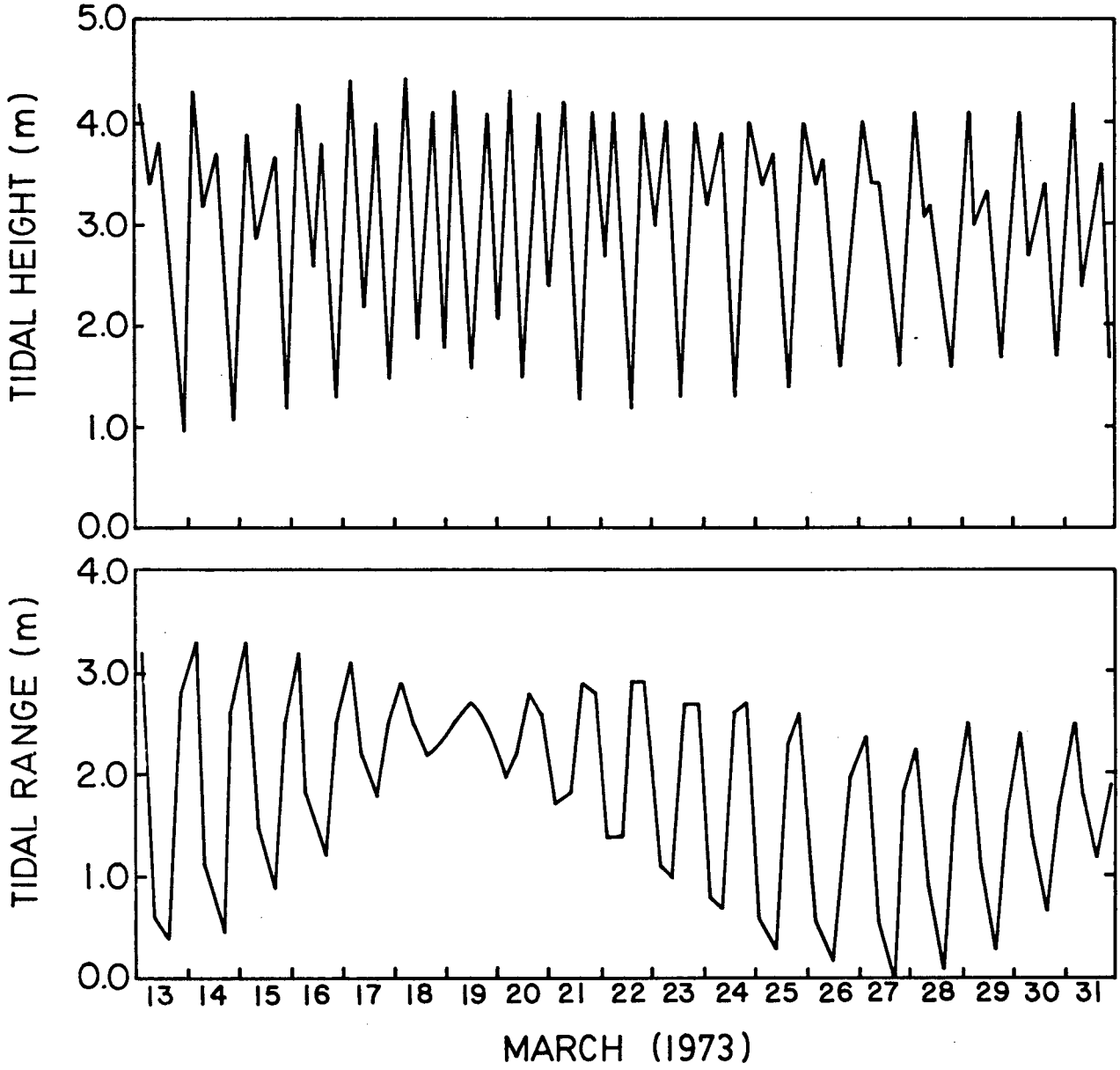

Figure 13.3A Time series of predicted (A) tidal height and tidal range at Pt. Atkinson and calculated (B) residual current magnitude and direction along line H.

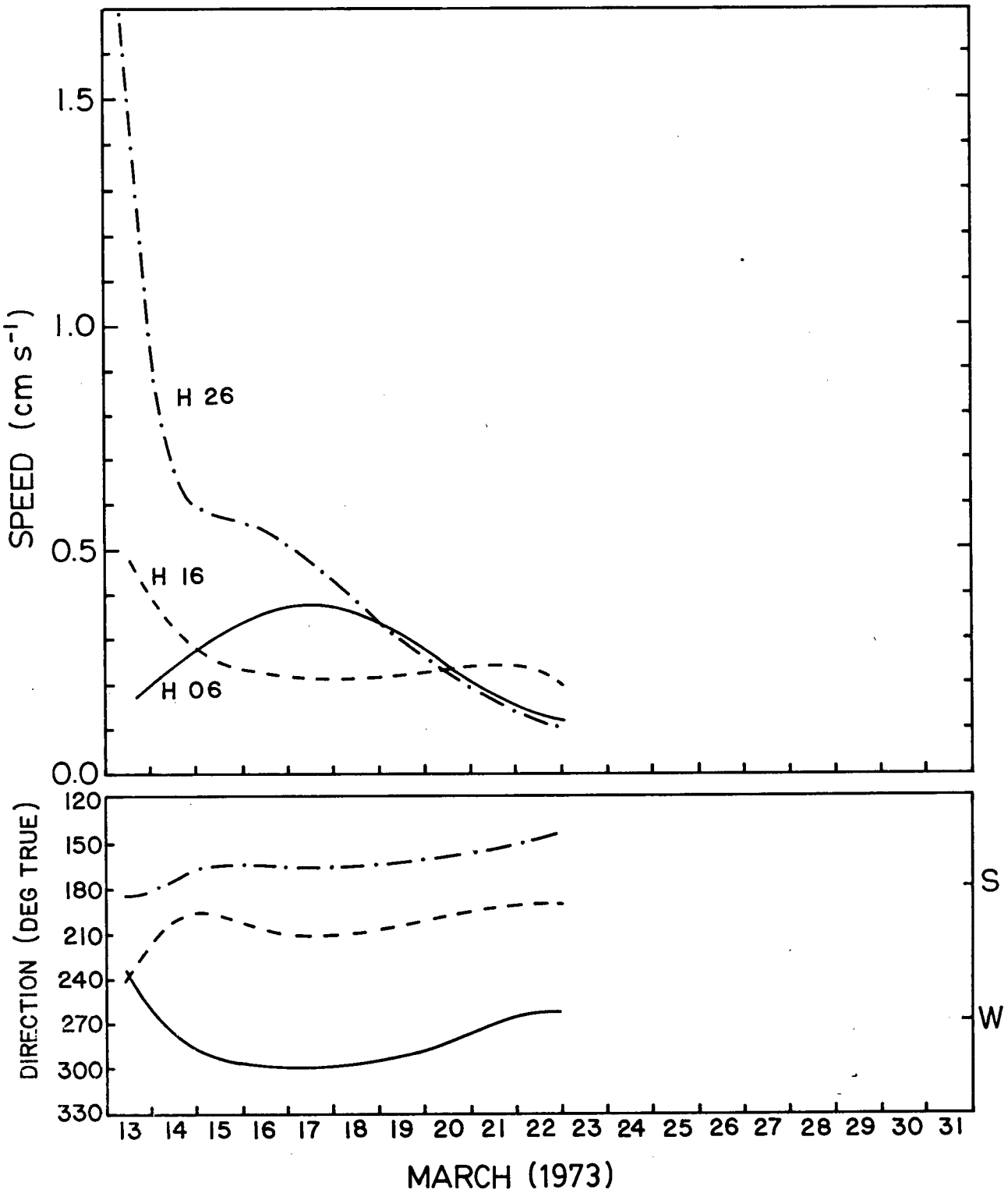
SPEED (cm s⁻¹)
1.5
1.0
0.5
0.0
H 26
H 16
H 06
DIRECTION (DEG TRUE)
120
150
180
210
240
270
300
330
S
W
13 14 15 16 17 18 19 20 21 22 23 24 25 26 27 28 29 30 31
MARCH (1973)

Figure 13.3B

with starting the model from an initial state of rest. However, the model was run for two (tidal) days prior to the 13-day period in order to avoid this problem. At any rate, it is clear that the residual motions are of insufficient strength and improper direction to serve as an explanation of the observed low-frequency motion along line H.

On the other hand, nonlinear tidal interactions may be important in other ways, for example, in the generation of internal tides or in interaction with the Fraser River. While the residual flow does not resolve the present problem, it clearly merits further investigation. In particular, it is likely to be significant in the southern tidal passes (Crean, 1978; Figures 12 and 13).

Finally, I speculate on the possibility that the tide interacts nonlinearly with the Fraser River outflow to produce, in part, the observed low-frequency currents. An examination of the Fraser River discharge at some distance upstream from the mouth indicates no consistent fortnightly or monthly variations (Figure 13.4); the discharge is dominated by the large annual peak that occurs in late spring and is due to the melting of the snowpack. However, near the river mouth the tide modulates the river flow, indeed the region comprises a salt-wedge-type estuary. If the magnitude of this interaction varies with tidal range, then it is possible that motions that are driven by the pressure gradient due to Fraser River water lying above GS water may vary with a fortnightly period. The hypothesis as expressed is obviously crude and ignores effects due to density differences, for example, but it is offered as a speculative possibility that could be examined in the future. However, there is some evidence for it. Figure 13.5 shows the low-frequency river speed at the mouth obtained by low-pass filtering current records. Unfortunately, it is superimposed on an increasing

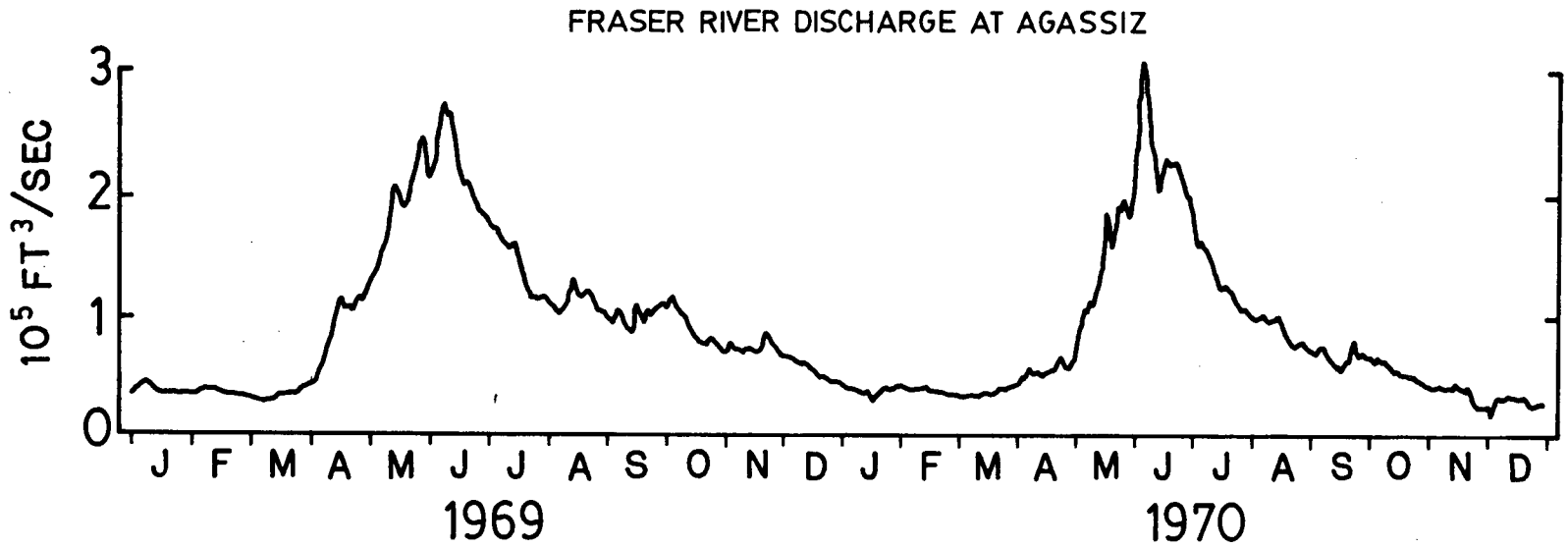

Figure 13.4 The Fraser River discharge approximately 60 miles upstream at Agassiz, British Columbia (from Chang, 1976).

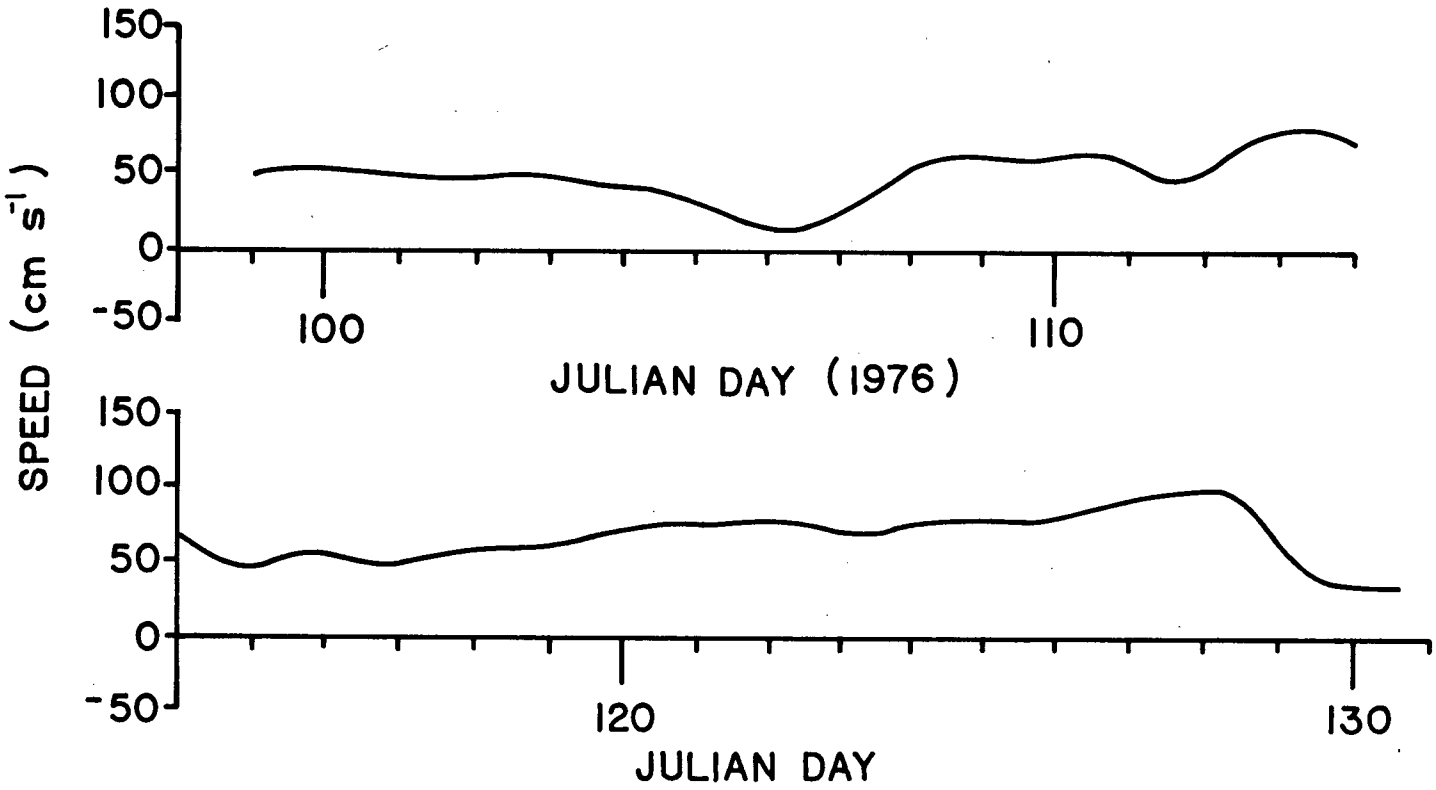

Figure 13.5 Low-pass filtered time series of river speed at the Fraser River mouth (Stronach, 1977)

discharge due to the onset of freshet. Nevertheless, a significant variation in the speed is evident in the first 12 days of the record. In addition, the analysis of Chang (1976; Figures 40 and 42) suggests that the mean current direction at H26 turns to the south in periods of high-river runoff.

This speculation has the advantage of predicting that the most significant flow should occur along the eastern boundary since the pressure head due to the river should be localized there. In a period of high runoff this mechanism might be offset. Moreover, the theory allows for interaction with the winds which would serve to modify the outflow. It is clear, however, that this hypothesis must be part of a more encompassing theory of the modulation of the estuarine flow in the Juan de Fuca-Strait of Georgia system. Other effects such as the influence of the strength of tidal mixing in the southern tidal passes must be examined. Moreover, friction has yet to be considered. It is hoped, however, that the present work will stimulate numerical modelers to work on this system and to examine not only short-period effects but also longer period ones.

14. Summary of Part II

From the analysis of current and wind data taken in the Strait of Georgia and from the consideration of simple inertial instability models, the following conclusions may be drawn from Part II.

1. The observed fluctuations are not due to simple wavelike motions. That is, they are not composed of free, forced, or unstable plane waves of the type considered in this thesis. This conclusion is based on the finding that the components of the fluctuating currents tend to be in phase.

2. The oscillations may bear some dynamical relationship to the mean currents. This notion is based on the general resemblance of the mean and fluctuating currents.

3. As evidenced from the spectra and the response to the wind, the eastern station may respond to forcing differently than the central and western stations.

4. The wind plays some role in determining the low-frequency currents. This is suggested by the facts that (a) statistically significant although small coherences are calculated between the currents and winds, (b) that the corresponding phases consistently lie near 0° or 180°, and (c) in the time domain, the response of the water column to a wind event is often evident.

5. Baroclinic instability of the mean flow is an unlikely mechanism in GS due to the narrow region of instability in parameter space.

6. A barotropic instability model indicates that shear instability might be of some significance but (1) militates against this

possibility.

7. The barotropic, residual tidal circulation is of insufficient magnitude and the wrong direction to account for the observations.

BIBLIOGRAPHY

Allen, J. S., 1975: Coastal trapped waves in a stratefied ocean. J. Phys. Oceanogr., 3, 300-325.

Blumsack, S. L., and P. J. Gierasch, 1972: Mars: The effects of topography on baroclinic instability. J. Atmos. Sci., 29, 1081-1089.

Brooks, D. A., and C.N.K. Mooers, 1977a: Free, stable continental shelf waves in a sheared, barotropic boundary current. J. Phys. Oceanogr., 7, 380-388.

_____, 1977b: Wind-forced continental shelf waves in the Florida Current. J. Geophys. Res., 82, 2569-2576.

Brooks, I. H., and P. P. Niiler, 1977: Energetics of the Florida Current. J. Mar. Res., 35, 163-191.

Buchwald, V. T., and J. K. Adams, 1968: The propagation of continental shelf waves. Proc. Roy. Soc. London, A 305, 235-250.

Buckley, J. R., 1977: The currents, winds and tides of northern Howe Sound. Ph.D. thesis, University of British Columbia, 228 pp.

Chang, P.Y.K., 1976: Subsurface currents in the Strait of Georgia, west of Sturgeon Bank. M.Sc. thesis, University of British Columbia, 183 pp.

Chang, P., S. Pond, and S. Tabata, 1976: Subsurface currents in the Strait of Georgia, west of Sturgeon Bank. Journal of the Fisheries Research Board of Canada, 33, 2218-2241.

Crean, P. B., and A. B. Ages, 1971: Oceanographic records from twelve cruises in the Strait of Georgia and Juan de Fuca Strait, 1968. Department of Energy, Mines and Resources, Marine Sciences Branch, Vol. I-5.

Crean, P. B., 1976: Numerical model studies of the tides between Vancouver Island and the mainland coast. J. Fish. Res. Board Can., 33, 2340-2344.

_____, 1978: A numerical model of barotropic mixed tides between Vancouver Island and the mainland and its relation to studies of the estuarine circulation. Hydrodynamics of Estuaries and Fjords, edited by J. C. J. Nihoul, pp. 283-313. Elsevier Scientific Publishing Co., Amsterdam.

Csanady, G. T., 1976: Topographic waves in Lake Ontario. J. Phys. Oceanogr., 6, 93-103.

_____, 1978: The arrested topographic wave. J. Phys. Oceanogr. 8, 47-62.

Department of the Environment, 1972a: Data record of current observations, Strait of Georgia, Section 4, Gabriola Island to Gower Point, 1969-1972. Water Management Service, Marine Sciences Directorate, Pacific Region, Manuscript Report Series, Vol. 10, 153 pp.

_____, 1972b: Data record of current observations, Strait of Georgia, Section 5, Porlier Pass to Sand Heads, 1969-1972. Water Management Service, Marine Sciences Directorate, Pacific Region, Manuscript Report Series, Vol. 11, 124 pp.

_____, 1973a: Data record of current observations, Strait of Georgia, Section 6, Samuel Island to Point Roberts, 1969-1970. Water Management Service, Marine Sciences Directorate, Pacific Region, Manuscript Report Series, Vol. 12, 96 pp.

_____, 1973b: Data record of current observations, Strait of Georgia, Section 3, Northwest Bay to McNaughton Point, 1968-1969. Water Management Service, Marine Sciences Directorate, Pacific Region, Manuscript Report Series, Vol. 13, 106 pp.

de Szoeke, R. A., 1975: Some effects of bottom topography on baroclinic stability. J. Mar. Res., 33, 93-122.

Düing, W., 1973: Some evidence for long-period barotropic waves in the Florida Current. J. Phys. Oceanogr. 3, 343-346.

_____, 1975: Synoptic studies of transients in the Florida Current. J. Mar. Res., 33, 53-73.

Düing, W., C. N. K. Mooers, and T. N. Lee, 1977: Low-frequency variability in the Florida Current and relations to atmospheric forcing from 1972 to 1974. J. Mar. Res., 35, 129-161.

Eady, E. T., 1949: Long waves and cyclone waves. Tellus, 1, 33-52.

Fissel, D. E., and W. S. Huggett, 1976: Observations of currents, bottom pressures, and densities through a cross section of Juan de Fuca Strait. Pacific Marine Science Report 76-6, Institute of Ocean Sciences, Patricia Bay, Victoria, B. C., Unpublished manuscript, 68 pp.

Gill, A. E., and E. H. Schumann, 1973: The generation of long waves by the wind. J. Phys. Oceanogr., 4, 83-90.

Godin, G., 1972: The Analysis of Tides. University of Toronto Press, Toronto. 264 pp.

Grimshaw, R., 1976: The stability of continental shelf waves in the presence of a boundary current shear. Res. Rep. No. 43, School of Mathematical Sciences, University of Melbourne, 19 pp.

Heaps, N. S., 1978: Linearized vertically integrated equations for residual circulation in tidal seas. Unpublished manuscript, 39 pp.

Helbig, J. A., and L. A. Mysak, 1976: Strait of Georgia oscillations: low-frequency waves and topographic planetary waves. J. Fish. Res. Board Can., 33, 2329-2339

Helbig, J. A., 1977: Low-frequency current oscillations and topographic waves in the Strait of Georgia. M.Sc. thesis, University of British Columbia, 81 pp.

Herlinveaux, R. H., 1957: On tidal currents and properties of the sea water along the British Columbia coast. Fish. Res. Board Can., Pacific Progress Report No. 108.

Herlinveaux, R. H., and L. F. Giovando, 1969: Some oceanographic features of the inside passage between Vancouver Island and the mainland of British Columbia. Fish. Res. Board Can., Technical Report No. 142, 48 pp.

Howe, M. S., 1971: Wave propagation in random media. J. Fluid Mech., 45, 769-783.

Huyer, A., B. M. Hickey, J. D. Smith, R. L. Smith, and R. D. Pillsbury, 1975: Alongshore coherence at low frequencies in currents observed over the continental shelf off Oregon and Washington. J. Geophys. Res., 80, 3495-3505.

Jenkins, G. M. and D. G. Watts, 1968: Spectral Analysis and Its Applications. Holden-Day, San Francisco, 525 pp.

Keller, J. B., 1967: The velocity and attenuation of waves in a random medium. Electromagnetic Scattering, R. L. Bowell and R. S. Stein, Eds., Gordon and Breach, 823-834.

Keller, J. B., and G. Veronis, 1969: Rossby waves in the presence of random currents. J. Geophys. Res., 74, 1941-1951.

Kendrew, W. G., and D. Kerr, 1955: The climate of British Columbia and the Yukon territory, Queen's Printer, Ottawa.

Kundu, P. K., and J. S. Allen, 1976: Some three-dimensional characteristics of low-frequency current fluctuations near the Oregon coast. J. Phys. Oceanogr., 6, 181-199.

Kuo, H.-L., 1949: Dynamic instability of two-dimensional non-divergent flow in a barotropic atmosphere. J. Meteor., 6, 105-122.

_____, 1973: Dynamics of quasi-geostrophic flows and instability theory. Adv. Appl. Mech., 13, 248-330.

LeBlond, P. H., and L. A. Mysak, 1977: Trapped coastal waves and their role in shelf dynamics. The Sea, vol. 6, edited by E. D. Goldberg, I. N. McCave, J. J. O'Brien, and J. H. Steele, pp. 459-495, John Wiley and Sons, New York.

_____, 1978: Waves in the Ocean, Elsevier Scientific Publishing Co., Amsterdam.

Lee, T. N., 1975: Florida Current spin-off eddies. Deep-Sea Res., 22, 753-765.

Lee, T. N., and D. Mayer, 1977: Low-frequency current variability and spin-off eddies along the shelf off Southeast Florida. J. Mar. Res., 35, 193-220.

Lin, C. C., 1945: On the stability of two-dimensional parallel flows. Part II--Stability in an inviscid fluid. Quart. Appl. Math., 3, 218-234.

_____, 1961: Some mathematical problems in the theory of the stability of parallel flows. J. Fluid Mech., 10, 430-438.

Manton, M. J., and L. A. Mysak, 1976: The stability of inviscid plane Couette flow in the presence of random fluctuations. J. Engineering Math., 10, 231-241.

McKee, W. D., 1977: Continental shelf waves in the presence of a sheared geostrophic current. Lecture Notes in Physics, vol. 64, edited by D. G. Provis and R. Radok, pp. 173-183, Australian Academy of Sciences, Canberra, Springer-Verlag, Berlin.

Mooers, C. N. K., 1973: A technique for the cross spectrum analysis of pairs of complex-valued time series, with emphasis on properties of polarized components and rotational invariants. Deep-Sea Res., 20, 1129-1141.

Mooers, C. N. K., and D. A. Brooks, 1977: Fluctuations in the Florida Current, summer 1970. Deep-Sea Res., 24, 399-425.

Mysak, L. A., and F. Schott, 1977: Evidence for the baroclinic instability of the Norwegian current. J. Geophy. Res., 82, 2087-2095.

Mysak, L. A., 1977: On the stability of the California undercurrent off Vancouver Island. J. Phys. Oceanogr., 7, 904-917.

_____, 1978: Wave propagation in random media, with oceanic applications. Rev. Geophys. Space Phys., 16, 233-261.

Niiler, P. P., and L. A. Mysak, 1971: Barotropic waves along an eastern continental shelf. Geophys. Fluid Dyn., 2, 273-288.

Niiler, P. P., and W. S. Richardson, 1973: Seasonal variability of the Florida Current. J. Mar. Res., 31, 144-167.

Pedlosky, J., 1964: The stability of currents in the atmosphere and the ocean: Part I. J. Atmos. Sci., 21, 201-219.

Rhines, P., 1975: Waves and turbulence on a β-plane. J. Fluid Mech., 69, 417-443.

Schott, F., and W. Düing, 1976: Continental shelf waves in the Florida Straits. J. Phys. Oceanogr., 6, 451-460.

Singleton, R. C., 1969: An algorithm for computing the mixed radix Fast Fourier Transform. IEEE Transactions on Audio and Electroacoustics, AU-17, 93-103.

Stone, J. M., 1963: Radiation and Optics, McGraw-Hill, New York.

Stronach, J. A., 1977: Observational and modelling studies of the Fraser River Plume. Ph.D. thesis, University of British Columbia, 260 pp.

Tabata, S., and J. A. Stickland, 1972a: Summary of oceanographic records obtained from moored instruments in the Strait of Georgia, 1969-1970: Current velocity and seawater temperature from Station H-06. Environment Canada, Water Management Service, Marine Sciences Branch, Pacific Region, Pacific Marine Science Report No. 72-7, 132 pp.

_____, 1972b: Summary of oceanographic records obtained from moored instruments in the Strait of Georgia, 1969-1970: Current velocity and seawater temperature from Station H-16. Environment Canada, Water Management Service, Marine Sciences Branch, Pacific Region. Pacific Marine Science Report No. 72-8, 144 pp.

_____, 1972c: Summary of oceanographic records obtained from moored instruments in the Strait of Georgia 1969-1970: Current velocity and seawater temperature from Station H-26. Environment Canada, Water Management Service, Marine Sciences Branch, Pacific Region, Pacific Marine Science Report No. 72-9, 141 pp.

Tabata, S., J. A. Stickland, and B. R. de Lange Boom, 1971: The program of current velocity and water temperature observations from moored instruments in the Strait of Georgia, 1969-1970, and examples of records obtained. Fisheries Research Board of Canada, Technical Report No. 253, 222 pp.

Tatarskii. V. I., and M. E. Gertsenshtein, 1963: Propagation of waves in a medium with strong fluctuations of the refractive index. Soviet Physics JETP, 17, 458-463.

Veronis, G., and H. Stommel, 1956: The action of a variable wind stress on a stratified ocean, J. Mar. Res., 15, 43-75.

Waldichuk, M., 1957: Physical oceanography of the Strait of Georgia, British Columbia. J. Fish. Res. Board Can., 14, 321-486.

Wang, D.-P., and C. N. K. Mooers, 1977: Long coastal-trapped waves off the west coast of the United States, summer 1973. J. Phys. Oceanogr., 7, 856-864.

Webster, I., and D. M. Farmer, 1977: Analysis of lighthouse station temperature and salinity data--Phase II. Pacific Marine Science Report 77-21, Institute of Ocean Sciences, Patricia Bay, Sidney, B. C., Unpublished manuscript.

Wright, D. G., 1978: Mixed baroclinic-barotropic instability with ocean applications. Ph.D. thesis, University of British Columbia, 201 pp.

Wunsch, C., and M. Wimbush, 1977: Simultaneous pressure, velocity and temperature measurements in the Florida Straits, J. Mar. Res., 35, 75-104.

Appendix A: Order of Magnitude Estimates of the Integral Terms in (3.25)

In this appendix it is shown that the integral terms in (3.25) are all of order unity. It is convenient to rewrite (3.25) as

$$H\psi = \varepsilon^2\{Q_x I_1 + (h'/h^2)(V - c)I_2 - h^{-1}(V - c)I_3\} \tag{A.1}$$

where

$$H = [(V - c)^2 - \varepsilon^2]\mathcal{D} - (V - c)Q_x - \varepsilon^2\sigma^2 h^{-1} \tag{A.2}$$

and I_1 , I_2 , and I_3 are integrals defined, for example, by

$$\begin{aligned} I_1 = \int_0^{\ell} (V - c)^{-1} G(x,\xi)\,[&R(x - \xi)\mathcal{D}\psi \\ &- (h'/h^2)R'(x - \xi)\psi - h^{-1}R''(x - \xi)\psi]d\xi. \end{aligned} \tag{A.3}$$

It suffices to consider only I_1 since the other integrals are similar in form. There are two types of points in the range of integration that must be dealt with, namely points x_c at which $c = V(x_c)$ and the integrand is singular and points $x_\pm$ where $c = V(x_\pm) \pm \varepsilon$. At all other points the integrands are continuous and are assumed to be of unit order. To isolate the singularities we partition the integral as

$$\begin{aligned} I_1 \sim &\int_0^{x_- - \delta} + \int_{x_- - \delta}^{x_- + \delta} + \int_{x_- + \delta}^{x_c - \delta} + \int_{x_c - \delta}^{x_c + \delta} + \int_{x_c + \delta}^{x_+ - \delta} + \int_{x_+ - \delta}^{x_+ + \delta} + \int_{x_+ + \delta}^{\ell} \\ &= J_1 + J_2 + J_3 + J_4 + J_5 + J_6 + J_7 , \end{aligned} \tag{A.4}$$

where δ is some small positive number which we will later let tend to zero. We need determine only J_2, J_4, and J_6.

Consider J_2 and J_6 first; since they are of the same form we examine only J_2. Since ψ is proportional to the cross-stream velocity it must be continuous, and, therefore, ψ'' can have, at worst, a δ-function-like singularity. We require a somewhat sharper result, however. Ordinarily, one could find a Frobenius-type solution to (A.1) in order to determine the behaviour of ψ at x_-, but the presence of the integral terms prevents this. We therefore look for an iterative solution to (A.1) of the form

$$H\psi_0 = 0 \tag{A.5}$$

$$H\psi_1 = \varepsilon^2\{Q_x I_1(\psi_0) + (h'/h^2)(V - c)I_2(\psi_0) - h^{-1}(V - c)I_3(\psi_0)\}, \tag{A.6}$$

etc. A series expansion of (A.5) about $x = x_-$ indicates that the two linearly independent solutions are of the form

$$\psi_0^{(1)} = (x - x_-)[1 + \sum_{n=1}^{\infty} a_n(x - x_-)^n] \tag{A.7}$$

$$\psi_0^{(2)} = \sum_{n=0}^{\infty} b_n(x - x_-)^n + a\psi_0^{(1)} \ell n|x - x_-|. \tag{A.8}$$

That is, ψ_0 behaves no worse than $(x - x_-)\ell n|x - x_-|$; since ψ_1 is determined by the integrated value ψ_0, it can be no more singular than ψ_0. The same argument holds for higher ψ_n, and we conclude that ψ

shares this quality. We are now ready to estimate J_2,

$$J_2 < (1/\varepsilon)\max[G(x,\xi)]\left\{R(\varepsilon)\int_{x_-\delta}^{x_-+\delta} \mathcal{D}\psi - h^{-1}[R'(\varepsilon)h'/h + R''(\varepsilon)]\int_{x_-\delta}^{x_-+\delta}\psi\right\}. \tag{A.9}$$

Since ψ is continuous, the last term vanishes in the limit $\delta \to 0$, and the first term gives the jump in ψ'/h and therefore also vanishes since ψ' is of the form $\ell n|x - x_-|$ near $x = x_-$. We conclude that J_2, and hence J_6, both vanish as $\delta \to 0$.

Evaluation of J_4 is more straightforward. We have

$$J_4 < \max[G(x,\xi)][R(\delta)\mathcal{D}\psi - (h'/h^2)R'(\delta)\psi - h^{-1}R''(\delta)\psi]\int_{x_c-\delta}^{x_c+\delta}(V - c)^{-1}d\xi. \tag{A.10}$$

Consider only the integral and put $\zeta = V(\xi)$ to obtain

$$I = \int_{x_c-\delta}^{x_c+\delta}(V - c)^{-1}d\xi = \int_{c-\delta'}^{c+\delta'}[F'(\zeta)(\zeta - c)]^{-1}d\zeta$$

where $F(\zeta)$ is the function inverse to $V(\xi)$, and δ' is an appropriately defined constant which tends to 0 with δ. Now (A.7) is a Cauchy integral and is readily evaluated by allowing c to have a small imaginary part c_i. In the limit of $c_i \to 0$, we find

$$I = \mathrm{sgn}(c_i)/[2F'(c)] + PV \int_{c-\delta'}^{c+\delta'} [F'(\zeta)(\zeta - c)]^{-1} d\zeta. \qquad (A.11)$$

Here PV denotes the Cauchy principle value, and therefore in the limit of $\delta \to 0$, I reduces to $\pm (1/2F'(c))$ which is an $0(1)$ quantity. It follows then that J_4 is $0(1)$ and hence that the integral terms in (A.1) are also $0(1)$.

Appendix B: The First-Order Solutions

In this section we specify the first-order solutions for the channel and shelf models. For the channel case we find:

$$\psi_1 = \begin{cases} A_{11}\psi_0 + iA_0P_1 & 0 \le x \le 1 \\ A_{12}\psi_0 + iA_0P_2 & 1 \le x \le \ell \end{cases} \tag{B.1}$$

where

$$c_{i0} \sin \lambda P_1 = e^{b(x-1)}\{(G_1x - eD_1)\cos \lambda x + e^{1-x}[(A_1x + B_1)\sin \lambda x + (C_1x + D_1)\cos \lambda x]\}, \tag{B.2}$$

$$c_{i0} \sin \alpha(1 - \ell)P_2 = [G_2(x - \ell) - e^{1-\ell}D_2]\cos \alpha(x - \ell) + e^{1-x}\{[A_2(x - \ell) + B_2]\sin \alpha(x - \ell) + [C_2(x - \ell) + D_2]\cos \alpha(x - \ell) \tag{B.3}$$

$$A_1 = a_1/\gamma_1$$

$$B_1 = (p_1 + 2a_1/\gamma_1)/\gamma_1$$

$$C_1 = 2\lambda a_1/\gamma_1$$

$$D_1 = 2\lambda[p_1 + a_1(1 + 2/\gamma_1)]/\gamma_1$$

$$G_1 = - q_1/2\lambda$$

$$a_1 = 2\varepsilon^2/c_{i0}^2 + 1 + 2b$$

$$p_1 = -2(1 + b)$$

$$q_1 = -2(\varepsilon^2 c_{r0}/c_{i0}^2 + b)$$

$$\gamma_1 = 1 + 4\lambda^2$$

$$A_2 = a_2/\gamma_2$$

$$B_2 = -2(1 - a_2/\gamma_2)/\gamma_2$$

$$C_2 = 2\alpha a_2/\gamma_2$$

$$D_2 = -2\alpha[2 - a_2(1 + 2/\gamma_2)]/\gamma_2$$

$$G_2 = -q_2/2\alpha$$

$$a_2 = 2\varepsilon^2/c_{i0}^2 + 1$$

$$q_2 = -2\varepsilon^2 c_{r0}/c_{i0}^2$$

$$\gamma_2 = 1 + 4\alpha^2.$$

For the shelf case we find

$$\psi_1 = \begin{cases} A_{11}\psi_0 + iA_0 P_1 & 0 \le x \le 1 \\ \\ A_{12}\psi_0 + iA_0 P_2 & x \ge 1 \end{cases} \qquad \text{(B.4)}$$

where P_1 is given as above and

$$P_2 = u_1(x) J_\nu(\rho\zeta) + u_2(x) Y_\nu(\rho\zeta) \qquad \text{(B.5)}$$

$$u_1(x) = -\pi[2\mu^2 c_{i0} J_\nu(\rho)]^{-1} \int_0^{e^{(1-x)}} J_\nu(\rho\xi) Y_\nu(\rho\xi) F(\xi) d\xi \qquad (B.6)$$

$$u_2(x) = \pi[2\mu^2 c_{i0} J_\nu(\rho)]^{-1} \int_0^{e^{1-x}} J_\nu^2(\rho\xi) F(\xi) d\xi \qquad (B.7)$$

$$F(\xi) = (2\rho^2\xi^2 + 1)(1 - \mu^{-1}\ell n\xi) - 2\rho^2 c_{r0}\xi - 2. \qquad (B.8)$$

Appendix C: Evaluation of the Integral Terms for a Simple Flow Model

The purpose of this appendix is to estimate the size of the integral terms in the mean vorticity equation for the case of large σ. To do so we choose the simplest possible model, a parabolic zonal flow on the β-plane. The equation equivalent to (3.25) is

$$[(U - c)^2 - \varepsilon^2]F\psi + (U - c)Q_y\psi - \varepsilon^2\sigma^2\psi$$

$$= -\varepsilon^2 Q_y \int_0^1 (U - c)^{-1} G(y,\xi)\,[R(y - \xi)F\psi - R''(y - \xi)\psi]\,d\xi \qquad (C.1)$$

$$- (U - c) \int_0^1 (U - c)^{-1} G(y,\xi)\,[R''(y - \xi)F\psi - R^{iv}(y - \xi)\psi]\,d\xi,$$

where $F = d^2/dx^2 - k^2$. Although (C.1) is somewhat less complicated than (3.25), the integrals are of the same form. In order to evaluate these terms two obstacles must be surmounted. First $G(y,\xi)$ must be determined, and second, a form for $R(y - \xi)$ must be specified. To obtain an analytical solution for $G(y,\xi)$ we choose U such that $Q_y = \beta - U''$ vanishes, namely

$$U(y) = \beta y(y - 1)/2; \qquad (C.2)$$

then $G(y,\xi)$ is given by

$$G(y,\xi) = \begin{cases} \sinh ky \sinh k(1 - \xi)/k \sinh k & 0 \le y \le \xi \le 1 \\ \\ \sinh k\xi \sinh k(1 - y)/k \sinh k & 0 \le \xi \le y \le 1. \end{cases} \qquad (C.3)$$

We select $R(y)$ to be Gaussian,

$$R(y) = \exp(-y^2\sigma^2/2). \tag{C.4}$$

We now take the solution $\psi = \psi_0 + \sigma^{-1}\psi_1$ as determined from the perturbation expansion outlined in Section 7, substitute it into (C.1), and determine the relative values of the various terms in the real and imaginary parts of the resulting expression. Specifically, we find

$$\psi_0 = A_0 \sin n\pi y \tag{C.5}$$

$$\psi_1 = iA_0(\beta K^2/2n\pi c_{i0})\{(y^2 - y)\sin n\pi y/n\pi - [y^3/3 - y^2/2 - (2c_{r0}/\beta + 1/2n^2\pi^2)y]\cos n\pi y]\} \tag{C.6}$$

$$c_{i0} = \varepsilon/K \tag{C.7}$$

$$c_{r0} = -(\beta/4)(1/n^2\pi^2 + 1/3), \tag{C.8}$$

where $K^2 = k^2 + n^2\pi^2$. The real and imaginary parts of (C.1) are

$$[(U - c_r)^2 - c_i^2 - \varepsilon^2]F\psi_0 + 2(U - c_r)c_i\sigma^{-1}F\psi_1 - \varepsilon^2\sigma^2\psi_0 = -(U - c_r)(I_1 - I_4) - c_i(I_2 + I_3) \tag{C.9}$$

$$\sigma^{-1}[(U - c_r)^2 - c_i^2 - \varepsilon^2]F\psi_1 - 2(U - c_r)c_iF\psi_0 - \varepsilon^2\sigma\psi_1 = -(U - c_r)(I_2 + I_3) + c_i(I_1 - I_4) \tag{C.10}$$

where

$$I_1 = \int_0^1 |U - c|^{-2}(U - c_r)G(y,\xi)[R''(y - \xi)F\psi_0 - R^{iv}(y - \xi)\psi_0]d\xi \tag{C.11}$$

$$I_2 = 1/\sigma \int_0^1 |U - c|^{-2}(U - c_r)G(y,\xi)[R''(y - \xi)F\psi_1 - R^{iv}(y - \xi)\psi_1]d\xi \tag{C.12}$$

$$I_3 = c_i \int_0^1 |U - c|^{-2}G(y,\xi)[R''(y - \xi)F\psi_0 - R^{iv}(y - \xi)\psi_0]d\xi \tag{C.13}$$

$$I_4 = c_i/\sigma \int_0^1 |U - c|^{-2}G(y,\xi)[R''(y - \xi)F\psi_1 - R^{iv}(y - \xi)\psi_1]d\xi. \tag{C.14}$$

The relative magnitudes of the terms in (C.9) and (C.10) are presented in Table V for selected values of ε, σ, and k. The ratio T4/T3 determines whether or not neglect of the integral terms is justified. One sees that the validity of this approximation improves as k increases and σ decreases. This effectively puts an upper bound on the choice of σ. There is relatively little dependence on ε. Only in the case of $\varepsilon = .5$, $\sigma = 10$, and $k = \pi/5$ is the rhs of (C.1) of greater magnitude than the lhs and then, only by 16 percent. The approximation is very good for the two cases of $\varepsilon = .5$, $\sigma = 10$, $k = 2\pi$ and $\varepsilon = .5$, $\sigma = 5$, $k = \pi$.

Table V. Relative magnitudes of the terms in (C.9) and (C.10). Here T12, T3, and T4 refer, respectively, to the absolute value of the sum of terms 1 and 2, and the absolute value of terms 3 and 4 in (C.9) and (C.10). The values given here are symmetrical about $y = 0.5$.

$\varepsilon = .5, \sigma = 10, k = \pi/5$

	(C.9)		(C.10)	
y	T4/T3	T12/T3	T4/T3	T12/T3
0.1	0.26	0.91	1.52[1]	0.95
0.2	0.89	0.91	1.22[2]	0.92
0.3	1.13	0.91	0.70	0.91
0.4	1.16	0.91	0.53	0.90
0.5	1.16	0.91	0.63	0.90

$\varepsilon = .5, \sigma = 10, k = \pi$

	(C.9)		(C.10)	
y	T4/T3	T12/T3	T4/T3	T12/T3
0.1	0.21	0.85	0.21	0.92
0.2	0.85	0.84	0.61	0.86
0.3	0.94	0.84	0.64	0.84
0.4	0.93	0.84	0.67	0.83
0.5	0.92	0.83	0.72	0.83

$\varepsilon = .5, \sigma = 10, k = 2\pi$

	(C.9)		(C.10)	
y	T4/T3	T12/T3	T4/T3	T12/T3
0.1	0.30	0.76	0.02	0.97
0.2	0.60	0.75	0.41	0.80
0.3	0.61	0.74	0.50	0.74
0.4	0.61	0.73	0.53	0.72
0.5	0.62	0.72	0.55	0.72

$\varepsilon = .1, \sigma = 10, k = \pi$

	(C.9)		(C.10)	
y	T4/T3	T12/T3	T4/T3	T12/T3
0.1	0.08	1.00	0.17	0.48
0.2	0.74	0.86	0.66	0.73
0.3	0.89	0.76	0.69	0.75
0.4	0.92	0.69	0.66	0.75
0.5	1.00	0.64	0.69	0.74

$\varepsilon = .5, \sigma = 5, k = \pi$

	(C.9)		(C.10)	
y	T4/T3	T12/T3	T4/T3	T12/T3
0.1	0.11	0.83	2.17[3]	2.44
0.2	0.27	0.83	0.70[4]	1.23
0.3	0.51	0.83	0.28	0.87
0.4	0.67	0.83	0.13	0.75
0.5	0.75	0.82	0.27	0.75

[1,2,3,4] If the ratio T4/T1, where T1 refers to the first term in either (C.9) or (C.10), is formed the resulting values are 0.28, 0.60, 0.73, and 0.51, respectively.

We conclude, then, that the neglect of the integrals is a good approximation, but that in some cases, namely very large σ or small k, the perturbation solutions are best regarded as representing a first-order iterative solution to the complete integro-differential equation.

The value of T12/T3 indicates how well the two-term perturbation solution satisfies the simplified vorticity equation (7.7). Since the terms represented by T12 and T3 are generally of opposite sign, this solution represents a good approximation to the solution of (7.7) in most cases.

Appendix D: Baroclinic Instability in a 2-Layer System

In this appendix, the equations governing the model described in Section 11 are derived. Proceeding from the full nonlinear equations of motion (see, e.g., Veronis and Stommel, 1964, or Helbig, 1977), we essentially follow the procedure developed by Pedlosky (1964) although the two approaches differ in some respects. The principal assumption made in the derivation of the 2-layer equations is that the horizontal components of velocity are z-independent within each layer.

Consider then this set of equations:

upper layer

$$u_{1t} + \underline{u}_1 \cdot \nabla_H u_1 - fv_1 = - g\eta_{1x} \tag{D.1}$$

$$v_{1t} + \underline{u}_1 \cdot \nabla_H v_1 + fu_1 = - g\eta_{1y} \tag{D.2}$$

$$(\eta_1 - \eta_2)_t + \underline{u}_1 \cdot \nabla_H(\eta_1 - \eta_2) + (h_1 + \eta_1 - \eta_2)\nabla_H \cdot \underline{u}_1 = 0 \tag{D.3}$$

lower layer

$$u_{2t} + \underline{u}_2 \cdot \nabla_H u_2 - fv_2 = - g\eta_{1x} - g\delta(\eta_2 - \eta_1)_x \tag{D.4}$$

$$v_{2t} + \underline{u}_2 \cdot \nabla_H v_2 + fu_2 = - g\eta_{1y} - g\delta(\eta_2 - \eta_1)_y \tag{D.5}$$

$$\eta_{2t} + \underline{u}_2 \cdot \nabla_H \eta_2 + (h_2 + \eta_2)\nabla_H \cdot \underline{u}_2 + \underline{u}_2 \cdot \nabla h_2 = 0. \tag{D.6}$$

Here the subscript $i = 1,2$ refers to the upper or lower layer, respectively; η_1 and η_2 are the sea surface and interfacial displacements

(see Figure 11.1); h_1 and h_2 are the mean layer thicknesses; $\delta = (\rho_2 - \rho_1)/\rho_2$ expresses the density difference between the two layers, and ∇_H refers to the two-dimensional Laplacian operator.

As before, it is convenient to non-dimensionalize these equations. The following scale factors are chosen: the shelf width L for the horizontal coordinates (x,y), a typical speed U for the velocities, and an advective time L/U for t. In addition, we write the lower-layer depth as $h_2 = h_{20}b(x,y)$ where h_{20} is the maximum depth of the lower layer, and $b(x,y)$ is an $O(1)$ quantity. The elevations are scaled geostrophically by (fUL/g) and $(fUL/g\delta)$, respectively. In non-dimensional form the equations of motion are:

upper layer

$$Ro(u_{1t} + \underline{u}_1 \cdot \nabla_H u_1) - \hat{f}v_1 = - \eta_{1x} \tag{D.7}$$

$$Ro(v_{1t} + \underline{u}_1 \cdot \nabla_H v_1) + \hat{f}u_1 = - \eta_{1y} \tag{D.8}$$

$$Ro[(\eta_2 - \delta\eta_1)_t + \underline{u}_1 \cdot \nabla_H(\eta_2 - \delta\eta_1)] = [B_1 - Ro(\eta_2 - \delta\eta_1)]\nabla \cdot \underline{u}_1 \tag{D.9}$$

lower layer

$$Ro(u_{2t} + \underline{u}_2 \cdot \nabla_H u_2) - \hat{f}v_2 = - \eta_{2x} - (1 - \delta)\eta_{1x} \tag{D.10}$$

$$Ro(v_{2t} + \underline{u}_2 \cdot \nabla_H v_2) + \hat{f}u_2 = - \eta_{2y} - (1 - \delta)\eta_{2y} \tag{D.11}$$

$$Ro(\eta_{2t} + \underline{u}_2 \cdot \nabla\eta_2) = - [B_2 b + Ro\eta_2]\underline{\nabla} \cdot \underline{u}_2 - B_2\underline{u}_2 \cdot \nabla b. \tag{D.12}$$

Here $Ro = U/fL$ is the Rossby number, $\hat{f} = f/f = 1$ is retained temporarily to aid in the identification of the Coriolis term, and B_1 and B_2 are Burger numbers defined by $B_1 = g'h_1/f^2L^2$ and $B_2 = g'h_2/f^2L^2$ where $g' = g\delta$ is the reduced acceleration due to gravity. We will henceforth ignore the term of $0(\delta)$ on the rhs of (D.10) and (D.11) since $\delta << 1$. It will also be assumed that b is a function of x only.

The presence of the Rossby number in these equations, which for GS is approximately 4×10^{-2}, suggests a perturbation expansion of the form

$$(\underline{u}_i, \eta_i) = \sum_{n=0}^{\infty} Ro^n (\underline{u}_i^{(n)}, \eta_i^{(n)}) \tag{D.13}$$

The basic state must satisfy the zeroth-order equations,

$$\hat{f} v_1^{(0)} = \eta_{1x}^{(0)} \tag{D.14}$$

$$\hat{f} u_1^{(0)} = - \eta_{1y}^{(0)} \tag{D.15}$$

$$\nabla_H \cdot \underline{u}_1^{(0)} = 0 \tag{D.16}$$

$$\hat{f} v_2^{(0)} = (\eta_2^{(0)} + \eta_1^{(0)})_x \tag{D.17}$$

$$\hat{f} u_2^{(0)} = (\eta_2^{(0)} + \eta_1^{(0)})_y \tag{D.18}$$

$$\nabla_H \cdot \underline{u}_2^{(0)} - u_2^{(0)} b^{-1} \frac{db}{dx} = 0. \tag{D.19}$$

Equations (D.14), (D.15), (D.17) and (D.18) define stream functions for each layer. We note that while (D.16) is identically satisfied, (D.19)

requires that either $u_2^{(0)}$ vanish or that db/dx be $0(Ro)$. Although we will, in fact, choose $u_2^{(0)} = 0$, this problem again arises at the next level, and so we put $db/dx = - RoT(x)$. A minus sign is chosen so that the sign of T coincides with that of the bottom slope; i.e., if the bottom slopes upward to the east, $T > 0$. This choice also facilitates comparison with Mysak and Schott (1977). As a basic state we choose

$$\left.\begin{aligned} \underline{u}_i^{(0)} &= (0, V_i(x)) \\ \eta_i^{(0)} &= H_i(x) \end{aligned}\right\} \tag{D.20}$$

where V_i and H_i are related by (D.14)-(D.19). It is easy to show that this state actually satisfies the complete nonlinear set of equations (D.7)-(D.12).

The perturbation state is governed by the first-order equations

$$\hat{f}v_1^{(1)} = \eta_1^{(1)}{}_y \tag{D.21}$$

$$\hat{f}u_1^{(1)} = - \eta_1^{(1)}{}_x \tag{D.22}$$

$$\hat{f}v_2^{(1)} = - (\eta_1^{(1)} + \eta_2^{(1)})_x \tag{D.23}$$

$$\hat{f}u_2^{(1)} = - (\eta_1^{(1)} + \eta_2^{(1)})_y \tag{D.24}$$

which again define stream functions for each layer. As such (D.21)-(D.24) are indeterminate, and it is necessary to go to second order to obtain an equation for $\eta_1^{(1)}$ and $\eta_2^{(1)}$. To second order, one finds:

upper layer

$$(\partial_t + V_1\partial_y)u_1^{(1)} - \hat{f}v_1^{(2)} = -\eta_{1x}^{(2)} \tag{D.25}$$

$$(\partial_t + V_1\partial_y)v_1^{(1)} + u_1^{(1)}V'_1 + \hat{f}u_1^{(2)} = -\eta_{1y}^{(2)} \tag{D.26}$$

$$(\partial_t + V_1\partial_y)(\eta_2^{(1)} - \delta\eta_1^{(1)}) + u_1(H_2 - \delta H_1)_x = \underline{B_1\nabla} \cdot \underline{u_1}^{(2)} \tag{D.27}$$

lower layer

$$(\partial_t + V_2\partial_y)u_2^{(1)} - \hat{f}v_2^{(2)} = -(\eta_2^{(2)} + \eta_1^{(2)})_x \tag{D.28}$$

$$(\partial_t + V_2\partial_y)v_2^{(1)} - u_2^{(1)}V'_2 + \hat{f}u_2^{(2)} = -(\eta_2^{(2)} + \eta_1^{(2)})_y \tag{D.29}$$

$$(\partial_t + V_2\partial_y)\eta_2^{(1)} - u_2^{(1)}H'_2 = -B_2b\nabla \cdot \underline{u}_2^{(2)} + B_2u_2^{(1)}{}_oT. \tag{D.30}$$

Here a prime denotes differentiation with respect to x. By cross-differentiating the momentum equations and substituting for $\underline{\nabla} \cdot \underline{u}_i^{(2)}$ from the continuity equation we obtain the vorticity equations for the perturbation state,

$$[\partial_t + V_1\partial_y][v_{1x} - u_{1y} + \frac{\hat{f}}{B_1}(\eta_2 - \delta\eta_1)] + u_1V''_1 + \frac{\hat{f}}{B_1}u_1[H_2 - \delta H_1]_x = 0 \tag{D.31}$$

$$[\partial_t + V_2\partial_y][v_{2x} - u_{2y} - \frac{\hat{f}}{B_{2b}}\eta_2] + u_2V''_2 - \frac{\hat{f}}{B_{2b}}[u_2H'_2 + B_2u_2T] = 0. \tag{D.32}$$

Here we have dropped the superscript (1). A Taylor series expansion of $b(x)$ about the point x_0 where $b(x_0) = 1$ gives

$$b(x) = 1 + RoT(x_0)(x - x_0) + 0(R_0^2). \tag{D.33}$$

It follows then that to the present order of analysis, $1/b$ may be replaced by 1. In terms of the stream functions,

$$\left.\begin{aligned} \Phi_1 &= \eta_1 \\ \Phi_2 &= \eta_2 + \eta_1 \end{aligned}\right\}, \tag{D.34}$$

and the basic state velocities, (D.31)-(D.32) may be rewritten

$$[\partial_t + V_1\partial_y][\nabla^2\Phi_1 + F_1(\Phi_2 - \Phi_1)] - \Phi_{1y}[V''_1 - F_1(V_1 - V_2)] = 0 \tag{D.35}$$

$$[\partial_t + V_2\partial_y][\nabla^2\Phi_2 - F_2(\Phi_2 - \Phi_1)] - \Phi_{2y}[V''_2 + F_2(V_1 - V_2) + T] = 0, \tag{D.36}$$

where F_1 and F_2 are internal Froude numbers given simply by the reciprocals of B_1 and B_2, respectively. To obtain these, a term of $0(\delta)$ was dropped. This is the desired set of equations governing the perturbation state. Since they express the conservation of potential vorticity in the system, they could also have been developed directly from the full, nonlinear, vorticity equations.